UNIVERSITY GRANTS COMMISSION
BAHADUR SHAH ZAFAR MARG
NEW DELHI – 110 002

STATEMENT OF EXPENDITURE IN RESPECT OF MAJOR RESEARCH PROJECT

1. Name of Principal Investigator: **ANIMESH GHOSH**

2. Deptt. of Principal Investigator: **Department of Pharmaceutical Sciences and Technology**

University/College: **Birla Institute of Technology, Mesra, Ranchi -835215, Jharkhand**

3. UGC approval Letter No. and Date: **F. No.-41-708/2012 (SR) dated 23.07.2012**

4. Title of the Research Project: **"Improvement of Bioavailability of Poorly Water Soluble Drugs by micronization and establishment of Level 'A' In Vitro-In Vivo Correlation"**

5. Effective date of starting the project: **01.07.2012**

6. a. Period of Expenditure: **From 01.07.2012 to 30.06.2015**

b. Details of Expenditure:

S.No	Item	Amount Approved (Rs.)	Amount received (Rs)		Expenditure Incurred (Rs.)
i	Books & Journals	NIL	1st Installment	2nd Installment	NIL
ii	Equipment	5,00,000/-	577000/-	52000/-	5,00,000/-
iii	Contingency	20,000/-			13618/-
iv	Field Work/Travel (Give details in the proforma at Annexure-IV).	10,000/-			15308/-
v	Hiring Services	NIL			NIL
vi	Chemicals & Glassware	1,00,000/-			101356/-
vii	Overhead	12,000/-			12,000/-
viii	Any other items (Please specify)	NIL			NIL
	Total	**642000/-**	**629000/-**		**642282/-**

c. Staff: **Not Applicable**; Date of Appointment: **Not Applicable**

PRINCIPAL INVESTIGATOR   CO-INVESTIGATOR   ACCOUNTS OFFICER   REGISTRAR/PRINCIPAL

29.06.16   29/06/16

(SEAL)

Animesh Ghosh *Ph.D.*
Assistant Professor
Department of Pharmaceutical Science & Technology
Birla Institute of Technology, Mesra
Ranchi - 835215, Jharkhand, India

1

Mrs. A. Mukherjee
Dy. Finance Officer
Birla Institute of Technology
Mesra, Ranchi (Jharkhand)

Registrar
Birla Institute of Technology
Mesra, Ranchi

M.N - 410224

UNIVERSITY GRANTS COMMISSION
BAHADUR SHAH ZAFAR MARG
NEW DELHI - 110 002

UTILIZATION CERTIFICATE

Certified that out of the grant of **Rs 6,29,000/- (Six lakhs twenty nine thousand) only** received from the University Grants Commission under the scheme of support for Major Research Project entitled **"Improvement of Bioavailability of Poorly Water Soluble Drugs by micronization and establishment of Level A In Vitro-In Vivo Correlation"** vide UGC letter No. **F. No. 41-708/2012 (SR) dated 23.07.2012, Rs.6,42,282/- (Six lakhs forty two thousand two hundred and eighty two) only** has been fully utilized for the purpose for which it was sanctioned and in accordance with the terms and conditions laid down by the University Grants Commission.

PRINCIPAL INVESTIGATOR
Animesh Ghosh Ph.D.
Assistant Professor
Department of Pharmaceutical Science & Technology
Birla Institute of Technology, Mesra
Ranchi - 835215, Jharkhand, India

ACCOUNTS OFFICER Mrs. A. Mukherjee
Dy. Finance Officer
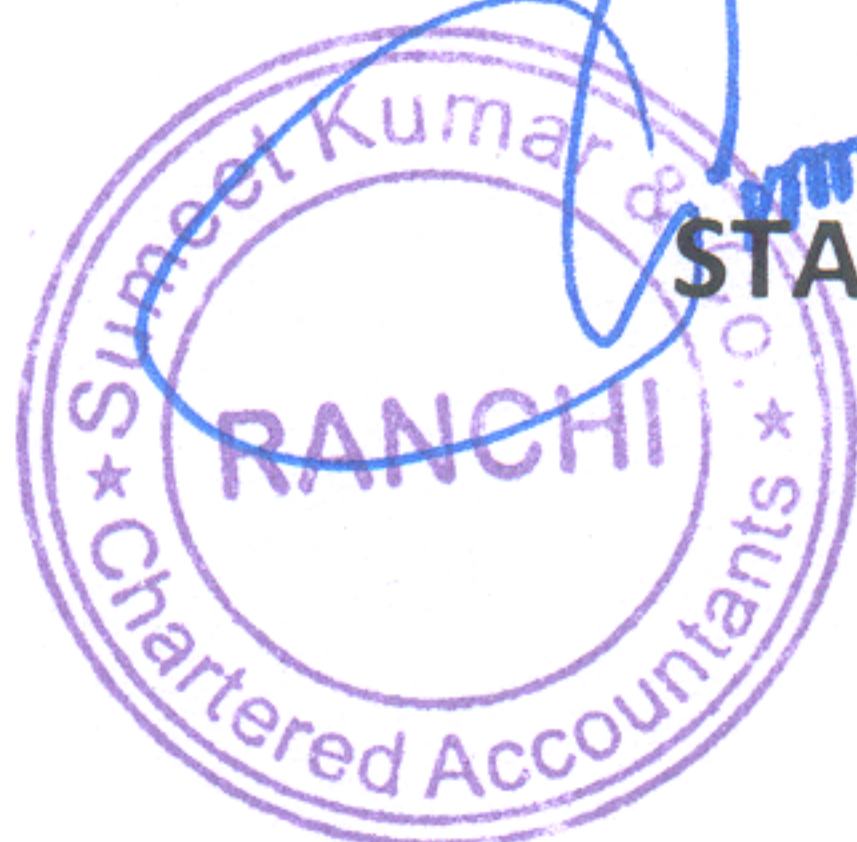Birla Institute of Technology
Mesra, Ranchi (Jharkhand)

REGISTRAR
(Seal) Registrar
Birla Institute of Technology
Mesra; Ranchi

CO-INVESTIGATOR
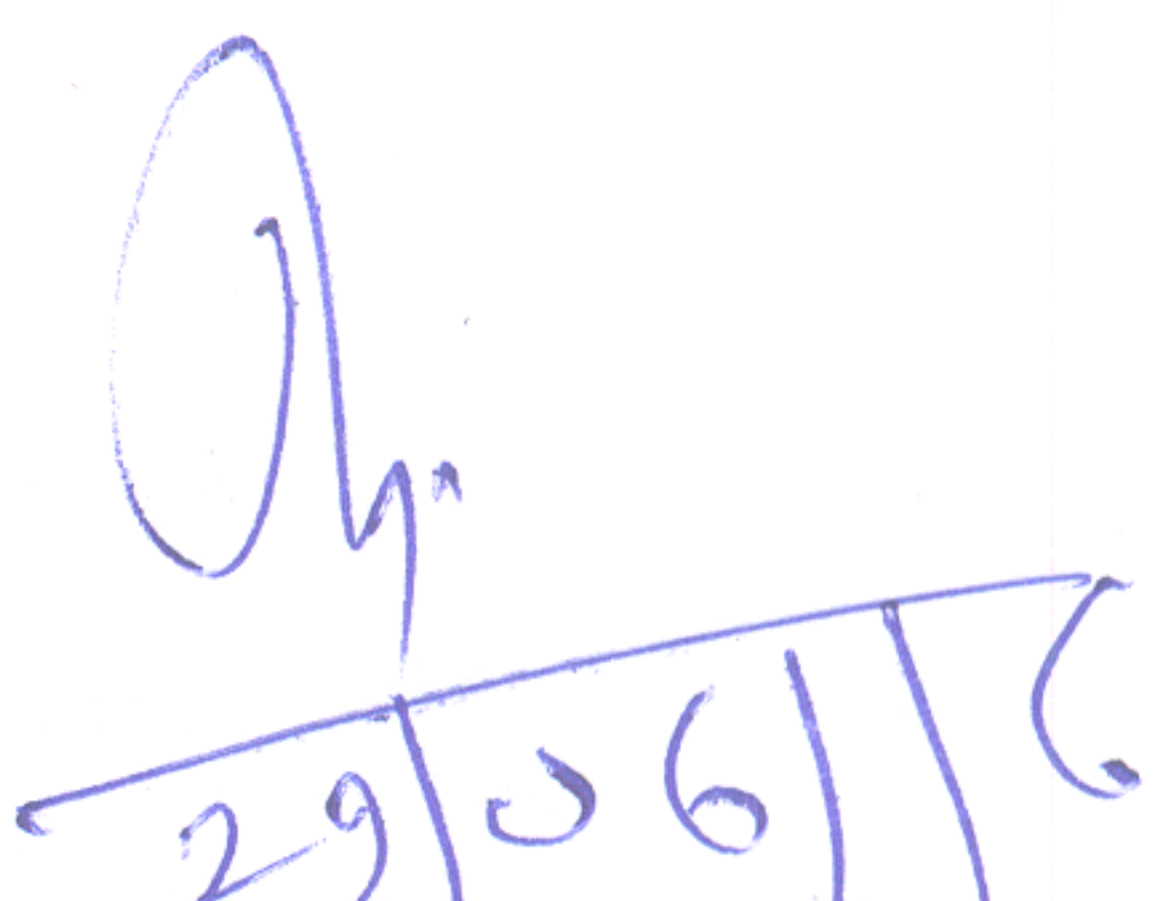
STATUTORY AUDITOR

(Seal)

2

UNIVERSITY GRANTS COMMISSION
BAHADUR SHAH ZAFAR MARG
NEW DELHI – 110 002.
Annual/Final Report of the work done on the Major Research Project.
(Report to be submitted within 6 weeks after completion of each year)

1. Project report No. 1st/2nd/3rd/Final: **Final**
2. UGC Reference No.F.: **F. No. 41-708/2012 (SR) dt.23.07.2012**
3. Period of report: **From 01.07.2012 to 30.06.2015**
4. Title of research project: **"Improvement of Bioavailability of Poorly Water Soluble Drugs by micronization and establishment of Level A In Vitro-In Vivo Correlation"**
5. (a) Name of the Principal Investigator: **Animesh Ghosh**
   (b) Department: **Department of Pharmaceutical Sciences and Technology**
   (c) University/College where work has progressed: **Birla Institute of Technology, Mesra**
6. Effective date of starting of the project: **01.07.2012**
7. Grant approved and expenditure incurred during the period of the report:
a) Total amount approved **Rs. 6,42,000/- (Six lakhs forty two thousand) only**
b) Total expenditure **Rs. 6,42,282/- (Six lakhs forty two thousand two hundred and eighty two) only**
c) Report of the work done: (Please attach a separate sheet): **Annexure I**
   I. Brief objective of the project:
   II. Work done so far and results achieved and publications, if any, resulting from the work (Give details of the papers and names of the journals in which it has been published or accepted for publication:
   III. Has the progress been according to original plan of work and towards achieving the objective? if not, state reasons:
   IV. Please indicate the difficulties, if any, experienced in implementing the project:
   V. If project has not been completed, please indicate the approximate time by which it is likely to be completed. A summary of the work done for the period (Annual basis) may please be sent to the Commission on a separate sheet:
   VI. If the project has been completed, please enclose a summary of the findings of the study. One bound copy of the final report of work done may also be sent to University Grants Commission:
   VII. Any other information which would help in evaluation of work done on the project. At the completion of the project, the first report should indicate the output, such as (a) Manpower trained (b) Ph. D. awarded (c) Publication of results (d) other impact, if any:

SIGNATURE OF THE PRINCIPAL INVESTIGATOR

Animesh Ghosh *Ph.D.*
Assistant Professor
Department of Pharmaceutical Science & Technology
Birla Institute of Technology, Mesra
Ranchi - 835215, Jharkhand, India

REGISTRAR
(Seal)
Registrar
Birla Institute of Technology
Mesra; Ranchi

SIGNATURE OF THE CO-INVESTIGATOR

3

UNIVERSITY GRANTS COMMISSION
BAHADUR SHAH ZAFAR MARG
NEW DELHI – 110 002

PROFORMA FOR SUBMISSION OF INFORMATION AT THE TIME OF SENDING THE
FINAL REPORT OF THE WORK DONE ON THE PROJECT

|		
1	TITLE OF THE PROJECT	"Improvement of Bioavailability of Poorly Water Soluble Drugs by micronization and establishment of Level A In Vitro-In Vivo Correlation"
2	NAME AND ADDRESS OF THE PRINCIPAL INVESTIGATOR	Animesh Ghosh Assistant Professor Department of Pharmaceutical Sciences and Technology Birla Institute of Technology, Mesra, Ranchi – 835215, Jharkhand
3	NAME AND ADDRESS OF THE INSTITUTION	Birla Institute of Technology, Mesra, Ranchi – 835215, Jharkhand
4	UGC APPROVAL LETTER NO. AND DATE	F. No. 41-708/2012 (SR) dt.23.07.2012
5	DATE OF IMPLEMENTATION	01.07.2012
6	TENURE OF THE PROJECT	3 Years
7	TOTAL GRANT ALLOCATED	Rs. 6,42,000/-
8	TOTAL GRANT RECEIVED	Rs. 6,29,000/-
9	FINAL EXPENDITURE	Rs. 6,42,282/-
10	TITLE OF THE PROJECT	"Improvement of Bioavailability of Poorly Water Soluble Drugs by micronization and establishment of Level A In Vitro-In Vivo Correlation"
11	OBJECTIVES OF THE PROJECT	To improve bioavailability of poorly water soluble drugs by micronization and establishment of Level A In Vitro-In Vivo correlation.
12	WHETHER OBJECTIVES WERE ACHIEVED (GIVE DETAILS)	Yes **(Annexure II)**
13	ACHIEVEMENTS FROM THE PROJECT	Two improved formulations were developed by utilizing two environment friendly techniques.
14	SUMMARY OF THE FINDINGS (IN 500 WORDS)	**Annexure III**
15	CONTRIBUTION TO THE SOCIETY (GIVE DETAILS)	**Annexure IV**
16	WHETHER ANY PH.D. ENROLLED/PRODUCED OUT OF THE PROJECT	No
17	NO. OF PUBLICATIONS OUT OF THE PROJECT (PLEASE ATTACH)	Two (attached)

(PRINCIPAL INVESTIGATOR)	(CO-INVESTIGATOR)	(REGISTRAR)
		(Seal)

29.06.16.

29/06/16

Registrar
Birla Institute of Technology
Mesra; Ranchi

Animesh Ghosh *Ph.D.*
Assistant Professor
Department of Pharmaceutical Science & Technology
Birla Institute of Technology, Mesra
Ranchi - 835215, Jharkhand, India

4

Sumeet Kumar & Co.
RANCHI
Chartered Accountants
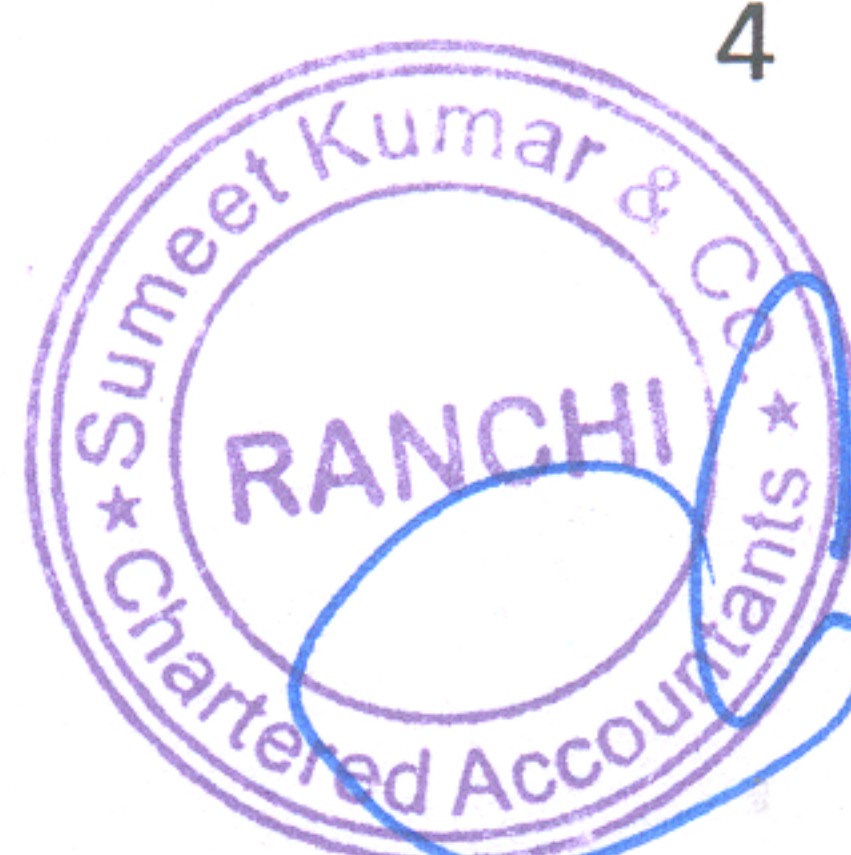
Solubility Enhancement of Ezetimibe by a Cocrystal Engineering Technique

Kumari Sugandha,[†] Santanu Kaity,[†] Samrat Mukherjee,[‡] Jinu Isaac,[†] and Animesh Ghosh*[,†]

[†]Department of Pharmaceutical Sciences and [‡]Department of Applied Physics, Birla Institute of Technology, Mesra Ranchi 835215, India

S *Supporting Information*

ABSTRACT: The present study illustrates the formation and characterization of three different cocrystals of ezetimibe using methyl paraben as a coformer, employing three different processes, namely, solution crystallization, liquid assisted grinding, and reaction crystallization. Thermal analysis by differential scanning calorimetry (DSC) and thermogravimetric analysis were used as a primary analytical tool, followed by spectroscopic and crystallographic study as a confirmatory analytical tool. Equilibrium aqueous solubility studies were performed for all cocrystals taking ezetimibe as the

control. The ideal solubility of drug and cocrystals was also calculated using data obtained from DSC (heat of fusion, ΔH, and transition melting temperature, T_m). The equilibrium aqueous solubility of ezetimibe was enhanced by about 2-fold in the case of cocrystal prepared by solution crystallization. Cocrystals prepared via reaction crystallization showed solubility that was almost the same as that of pure ezetimibe. The dissolution profile of all cocrystals, with pure ezetimibe as a control, was studied for 2 h in defined biorelevant media. Cocrystal II, prepared by a liquid assisted grinding method, showed significant improvement in solubility at 45 and 120 min, indicating a good dissolution profile. The study demonstrates that pharmaceutical cocrystallization of ezetimibe with methyl paraben can be a possible and potential alternative and effective approach for improving its solubility.
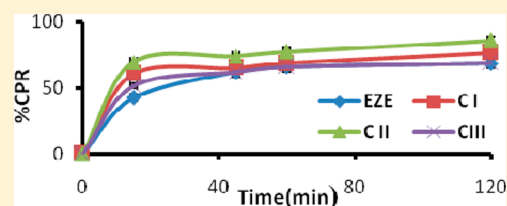
■ INTRODUCTION

The efficacy of active pharmaceutical ingredients (APIs) dramatically depends on the physical properties of their solid form. Dissolution rate, solubility, hygroscopic nature, and chemical stability are some of the most important factors that must be considered.[1] API can be polymorphic,[2] meaning that it can exist in two or more crystallographic forms. This may include solvation or hydration products (also known as pseudo polymorphs) and amorphous forms.[3] Cocrystals are like polymorphic solids, crystalline in nature and composed of two or more compounds in the same crystal lattice. Nevertheless, cocrystallization influences the same before mentioned properties, just like for different polymorphs.[4,5] A large range of intermolecular interactions including electrostatic interactions (ion−ion, ion-dipole, and dipole−dipole interactions), coordinate bonding (metal−ligand), hydrogen bonding, halogen bonding, π−π stacking, and van der Waals forces can be responsible when cocrystallization occurs.[6] While the intramolecular interactions bond the atoms in a molecule, the intermolecular forces minimize the energy of the molecules in the crystal and are primarily responsible for the formation of organic crystals.[7] The major attractive interactions in most pharmaceutical crystals are hydrogen bonds and van der Waals interactions.[8] The arrangement of molecules in a crystal determines its physical properties and, in some cases, its chemical properties also.[9] The physicochemical properties of the solid drug can affect its performance. Thus, an understanding of the crystalline state leads to an understanding of the

drug properties, which is crucial for preformulation and formulation in the pharmaceutical industry.

This class of pharmaceutical cocrystals has gained large interest over the past few years since they offer the potential to eliminate undesirable physicochemical properties without covalent modification of the API. Moreover, unlike salt forms of APIs, cocrystal formation is not restricted to an ionizable (acidic or basic) center on the API and can simultaneously address multiple functional groups on the API. A relatively large number of nontoxic compounds with hydrogen bonding functionalities exist on the generally regarded as safe (GRAS) list that may act as cocrystal formers in comparison to the limited number of salt forming counterions in use.[10]

The presence of multiple functional groups inherent to APIs affords the opportunity for the design of pharmaceutical cocrystals. In fact an analysis of the top 100 prescription drugs[11] reveals that 39% of pharmaceutically active ingredients contains at least one alcohol, and 30% contain at least one carboxylic acid; this is also consistent with the percentage alcohol and carboxylic acid moieties in the Merck Index.[12] Consequently addressing the ability of these functional groups to form supramolecular synthons would be of great interest. The crystal engineering approach for APIs based upon the use of reliable supramolecular heterosynthons is exemplified by several series of cocrystals involving carbamazepine (CBZ),[13,14]

ibuprofen,[15] iracetam,[16] fluoxetine hydrochloride,[17] and itraconazole.[18]

Ezetimibe (EZE) is a modern hypocholesterolemic drug used both as monotherapy and adjunctive therapy to diet for the reduction of elevated total cholesterol (total-C), low density lipoprotein cholesterol (LDL-C), and apoprotein B (apo B) in patients with primary hypercholesterolemia (heterozygous familial and nonfamilial).[19] However, this API as per Biopharmaceutics Classification System, class II drug,[20] has poor water solubility (0.012 mg/mL at 25 °C),[21] which leads to its limited dissolution resulting in poor bioavailability (35−65%).[22]

Several researchers have reported the improvement in solubility/dissolution properties of ezetimibe by complexation with cyclodextrin,[23] solid dispersion,[24] and preparing liquid−solid compacts.[25] From the literature, it has been found that a cocrystal technique is an alternative approach to manipulate the physicochemical properties of the drug such as solubility, dissolution rate, stability, and compressibility and to improve overall performance of APIs without affecting the pharmacological properties. Ezetimibe has rarely been investigated for its cocrystallization tendencies. This motivated us to explore the potential of ezetimibe to cocrystallize in order to improve its solubility.

The present study is aimed at enhancing the solubility of ezetimibe by the cocrystal engineering technique. After a suitable coformer was selected, cocrystals of EZE were prepared by solution crystallization method (CI), liquid assisted grinding (LAG) method (CII), and reaction crystallization method (CIII). The product thereof was characterized by differential scanning calorimetry (DSC), thermogravimetric analysis (TGA), Fourier transform infrared spectroscopy (FTIR), Raman spectroscopy, and powder X-ray diffraction (PXRD). After that, the cocrystals were subjected to a solubility and dissolution study.

■ EXPERIMENTAL SECTION

Materials. Ezetimibe was obtained as a gift sample from Dr. Reddy's Laboratory Ltd. Hyderabad, India. Methyl paraben (99%) was purchased from CDH, New Delhi, India, and the solvents used for crystallization including methanol were of HPLC grade (Rankem, India). Analytical chemicals such as acetonitrile and potassium dihydrogen ortho phosphate were purchased from Rankem, India. All of these were used as received.

Sample Preparation. *Selection of Coformers.* Various coformers such as benzoic acid, salicylic acid, L-proline, valine, glycine, and methyl paraben were selected from the GRAS list generated by the U.S. FDA (generally regarded as safe additive chemicals by the Food and Drug Administration)[26]

Cocrystal Preparation and Preliminary Screening. Solution crystallization,[27,28] and slurry[29] methods were opted to prepare cocrystals. The first hand information about the existence of new solid phases was obtained by melting point, as it is a fundamental physical property of a compound. Digital melting point apparatus (OPTIMELT, SRS, Germany) was used to determine the melting points of pure API, coformer, and the solid phase obtained.

The following three methods were used to prepare cocrystal of ezetimibe with the selected coformer (from the preliminary screening based on melting point).

Solution Crystallization Method (CI). This is the simplest technique for air stable samples. Solution crystallization can yield large, well-formed single crystals, from which one may easily evaluate crystal habit and surface features. Analysis of the diffraction pattern of a single crystal is typically the best means of obtaining an absolute crystal structure determination.[30] A molar ratio of 1:1 mixture of ezetimibe (204.7 mg, 0.5 mmol) and methyl paraben (76.075 mg, 0.5

mmol) was dissolved in a 10 mL solution of methanol in a 20 mL conical flask. The resulting solution was placed in a water bath (REMI RSB-12) maintained at a temperature of 35 °C for slow evaporation. After 2 days, white, very fine needle-shaped crystals were recovered, filtered, and air-dried.[27,28] The crystal size was not sufficient for single crystal X-ray diffraction analysis.

Liquid Assisted Grinding (LAG) Method (CII). This is a solvent-free solid state grinding method where the relative solubility of ingoing component in a particular solvent is not a concern unlike in the case of the solution crystallization method. Further, the absence of solvent makes this an inherently "green" approach to form cocrystals by eliminating large volumes of solvent waste; the minimization of excess crystallization solvent could help achieve corporate green chemistry targets.[30] A mixture of a 1:1 molar ratio of ezetimibe and methyl paraben at a total of 1 g was placed in the grinding jar (45 mL) in a planetary micromill (Fritsch, Germany) with 10 stainless steel balls (5 mm dia). A total of 50 μL of methanol was added in the mixture and milled for 30 min at an operating frequency of 600 rpm.[31]

Reaction Crystallization Method (CIII). This is a method for rapid generation of cocrystals at microscopic and macroscopic scale at ambient temperature, where nucleation and cocrystallization are initiated by the effect of the cocrystal components on reducing the solubility of the molecular complex to be crystallized.[31] The saturated solution of the lesser soluble component (drug) was made in 10 mL of methanol and filtered, and then the more soluble component (methyl paraben) was added in an amount just under its solubility limit. The goal was not to have any excess drug or coformer in the starting solutions that could be confused as a cocrystal. Furthermore, by not exceeding the solubility limits of the components, the cocrystal that precipitated out of solution was pure. Solution concentrations were monitored by HPLC throughout the crystallization process to evaluate whether the solid observed appeared to be a complex of the reactants (cocrystals). The solid precipitate was also collected and analyzed by HPLC to determine the stoichiometry of the complex. If the solid appeared to be a cocrystal based on the HPLC results, it was further characterized by DSC, TGA, and PXRD.[32]

Differential Scanning Calorimetry (DSC). DSC of all the samples were conducted using DSC Q10 (TA Instruments, USA) which was calibrated for temperature and enthalpy using indium. Samples (3−5 mg) were crimped in nonhermetic aluminum pans and scanned from 25 to 200 °C at a heating rate 10 °C/min under a continuously purged dry nitrogen atmosphere (flow rate 50 mL/min).The data were managed by TA Explorer software.

Thermogravimetric Analysis (TGA). TGA was performed by a DTG-60 (Shimadzu, Japan) analyzer. The samples (approximately 5 mg) were placed into aluminum pans and heated from 25 to 500 °C at the rate of 10 °C/min under nitrogen purge at a flow rate of 50 mL/min. The data were managed by TA-60WS acquisition software.

Fourier Transform Infrared Spectroscopy (FTIR). A FTIR-8400 S spectrophotometer (Shimadzu, Japan) was employed to collect the infrared spectrum of drug, coformer, and cocrystals. The IR absorption spectra of samples were measured over the range of 4000−600 cm^{-1}. A few milligrams of sample was mixed with 10 times of its weight of potassium bromide (KBr) and pressed to form a pellet. The data were analyzed using IR solution software.

Raman Spectroscopy. Raman spectra of pure drug, coformer, and cocrystals were obtained using a Raman spectrometer (Renishaw plc.) with 514 nm stabilized diode laser excitation. The laser power at the sample was approximately 10 mW. A 50× objective lens was used, giving a laser spot diameter (footprint) of 2 μm at the sample. Spectra were obtained for a 10 s exposure of the argon detector in the region 3200−100 cm^{-1} using the extended scanning mode of the instrument.

Powder X-ray Diffraction (PXRD). PXRD patterns were collected on Bruker AXS D8 Advance Diffractometer system with a Cu Kα radiation (1.5406 Å). The tube voltage and current were set at 40 kV and 35 mA, respectively. Each sample was placed on an aluminum sample holder and measured by a continuous scan between 3 and 80° in 2θ with a step size of 0.020° and step time 31.2 s. The experimental PXRD patterns were refined using Diffrac plus software.

Scanning Electron Microscopy (SEM). The surface morphology and topography of all three cocrystals were evaluated by scanning electron microscopy (JSM-6390LV, Jeol, Japan). Before examination, the samples were mounted onto stubs using double-sided dried adhesive carbon tape and vacuum coated with gold palladium film (thickness 2 nm) by sputter coater (Edward S-150, U.K.) to make them electrically conductive. Representative sections were photographed.

Solubility Studies. *Determination of Cocrystal Stoichiometry. Stoichiometry via PXRD.* The stoichiometry of ezetimibe and methyl paraben were calculated from the X-ray diffractograms of CI, CII, and CIII. The peaks with highest intensity of ezetimibe and methyl paraben were identified. Peaks of cocrystals were fitted with Gaussian line shapes, and the area under the peak at their respective 2θ value (highest peak intensity of the virgin crystals) was calculated by integration.[33]

Stoichiometry via HPLC Results in the Case of CIII. In the case of cocrystal prepared through reaction crystallization method (RCM), the stoichiometry was calculated through analysis of the solid precipitate left after attainment of equilibrium position [transition concentration (C_{tr})] in the RCM experiment.

Determination of transition concentration (C_{tr}): Transition concentration (C_{tr}) is the solution concentrations ($[drug]_{tr}$ and $[ligand]_{tr}$) which separates the region where either the solid cocrystal or drug are thermodynamically stable.[34−39]

The measurement of cocystal C_{tr} values was performed by precipitating cocrystal as a result of stirring excess solid coformer in a presaturated drug solution wherein cocrystal occurs though RCM.

A saturated solution of drug (ezetimibe) was prepared in methanol and to it a known excess amount of coformer (methyl paraben) was added. The amount of coformer added was based on its solubility limit in methanol. The solution was stirred on a water bath shaker, maintained at a temperature of 25 °C for 24 h, and checked for precipitation of cocrystals. The solid precipitate so obtained was separated and dried.

Stoichiometry calculation: For calculating, the stoichiometry, a known concentration (5 μg/mL) of the solid was prepared in methanol, and the concentration of both the drug and the coformer was measured by HPLC. The concentrations were determined in molality units, and their ratio gave the stoichiometry of the cocrystal. The whole process was performed in triplicate.

Theoretical Calculations. For cocrystal $A_\alpha B_\beta$, where A is drug and B is ligand, solubility is described by the chemical equilibrium of solid cocrystal with solution and the corresponding equilibrium constant given by[40,41]

$$A_\alpha B_\beta \leftrightharpoons \alpha A_{(solution)} + \beta B_{(solution)}$$

$$K = \frac{a_{A(solution)}^\alpha a_{B(solution)}^\beta}{a_{A_\alpha B_\beta (s)}}$$

Defining solid cocrystal activity as unity ($a_{A_\alpha B_\beta (s)} = 1$) and assuming the activity coefficients (γ) of A and B equal unity for low solute levels, the above equation reduces to

$$K_{sp} = [A]^\alpha [B]^\beta \qquad (1)$$

where K_{sp} is the solubility product of the cocrystal. The cocrystal solubility ($S_{A_\alpha B_\beta}$) is given as

$$S_{A_\alpha B_\beta} = \sqrt[\alpha+\beta]{K_{sp}/\alpha^\alpha \beta^\beta} \qquad (2)$$

The saturation solubility of pure drug (ezetimibe), CI, CII, and CIII in water was determined by suspending an excess amount of material in water. The solutions were shaken on a water bath shaker at a temperature of 25 ± 2 °C for approximately 24 h. Samples were then filtered using a 0.2 μm nylon filter (AXIVA) and analyzed by HPLC. If necessary, samples were diluted in methanol prior to analysis. Ezetimibe and methyl paraben solubility was also measured as a

control. The solubility of the cocrystals was calculated using eqs 1 and 2.

High Performance Liquid Chromatography (HPLC). Solution concentration of ezetimibe and methyl paraben was analyzed by HPLC (Waters USA) equipped with a UV/vis detector. A C18 Nova-Pak column 4 μm, 4.6 × 150 mm (Waters, USA) at ambient temperature with a flow rate of 1 mL/min was used to separate ezetimibe and methyl paraben. An isocratic method with water (pH 3.0) and acetonitrile mixed in a ratio of 55:45(v/v), respectively, was opted for quantitative determination of ezetimibe and methyl paraben, at an optimum wavelength of 248 nm. Sample injection volume was 20 μL. Empower software from Waters was used to collect and process the data. All concentrations are reported in molality.

Determination of Ideal Solubility from Thermal Behavior. For an ideal solution, the solute solubility, x (mole fraction), is a function of the heat of fusion (ΔH_m or ΔH_s^{ideal}), melt temperature (T_m), solution temperature (T) and universal gas constant (R). It is expressed by the following equation[42]

$$\ln \chi_{solute}^{ideal} = \frac{-\Delta H_m}{R} \frac{(T_m - T)}{T_m T} \qquad (3)$$

where

$$\Delta H_m \cong \Delta H_s^{ideal}$$

Melting temperature and enthalpy of all the samples including drug and coformer were obtained from DSC data and put into the above equation to get the ideal solubility value. To determine the ideal solubility of cocrystals using the same equation, the melting enthalpy was first normalized by the cocrystal stoichiometry. The enthalpy of melting of the cocrystals was the measured value divided by the number of moles of reactant per mole of cocrystal.

Dissolution Study. The dissolution studies were conducted in 500 mL of 0.45% sodium lauryl sulfate (SLS) in 0.05 M acetate buffer (pH 4.5) in a USP type II dissolution apparatus (Electrolab, India). Paddle rotation speed was 50 rpm. Ten micrograms of drug or its equivalent amount of cocrystal was added to the dissolution medium. Time points were collected for 2 h, and the concentrations of ezetimibe were analyzed by HPLC. The dissolution profile of the cocrystals was then statistically analyzed by applying one-way ANOVA followed by Tukey's post hoc test.

RESULTS AND DISCUSSION

Cocrystal Preparation. The detailed methodology opted for preparing cocrystals of ezetimibe using selected coformers, along with the results obtained, is presented in Supporting Information (Table S1).

A total of nine formulations were prepared, using seven coformers. It was observed that the melting point of multicomponent solid form of ezetimibe prepared with methyl paraben was 109.97 °C, indicating a lower melting point than either ezetimibe or methyl paraben. The chemical structure of ezetimibe and methyl paraben is given in Figure 1. The multicomponent solid form of ezetimibe with L-proline displayed a melting point of 173.1 °C, which was in agreement with the findings of Scott et al. (2012).[19] These observations clearly indicated the formation of stable interaction between ezetimibe and the coformer. After an analysis of 50 cocrystalline samples, it was documented earlier that 51% cocrystals had melting points between the API and coformer, 39% were lower than either the API or coformer, 6% were higher, and 4% had the same melting point as either the API or coformer.[43] The altered melting points in multicomponent solid forms might be attributed to noncovalent bonding interaction between API and coformers, altered packing arrangements, and change in crystallinity of molecules in the cocrystals. Therefore, methyl
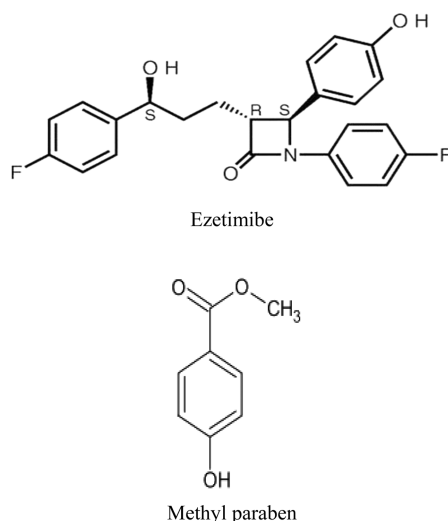
Ezetimibe

Methyl paraben

Figure 1. Chemical structure of ezetimibe and methyl paraben.

paraben was selected as a coformer for preparing cocrystals of ezetimibe by different methods.

Ezetimibe Cocrystal Preparation with Methyl Paraben As a Coformer. The melting points of CI, CII, and CIII prepared by solution crystallization, liquid assisted grinding, and reaction crystallization were 109.97, 111.27, and 109.12 °C, respectively. In all three cases, a melting point lower than that of pure ezetimibe or methyl paraben was obtained. Ghosh et al. reported that the cocrystals of sulfamethazine/3,4-dichloroben-zoic acid (1:1), sulfamethazine/fumaric acid/acetonitrile (2:1:1), sulfamethazine/1-hydroxy-2-napthoic acid (1:1), and sulfamethazine/3-hydroxy-2-napthoic acid (1:1) had a melting

point lower than the melting point of pure drug and respective coformers.[44] In another recent report, Bucar et al. obtained different cocrystals of caffeine having a lower melting point than that of pure drug and respective coformers.[45]

Thermal Analysis (DSC and TGA). Thermal analysis by DSC and TGA are the primary analytical tools for getting first-hand information about the existence of a new solid phase. The DSC thermograms of pure ezetimibe, methyl paraben, and the cocrystals (CI, CII, and CIII) are shown in Figure 2. The corresponding TGA patterns of the same are depicted in Figure 3.

The DSC thermograms of pure ezetimibe and methyl paraben showed single melting endotherm (T_m) at 164.36 and 127.34 °C, respectively. In all three cocrystals, melting endotherm was lower than that of either drug or cocrystal. From the TGA study of methyl paraben, it was observed that a negligible mass loss (2.66%) was obtained in the range of 25−130 °C, followed by a major mass loss of 96.99% in the range of 130−200 °C. This major mass loss was due to its degradation.

CI showed a single and sharp melting endotherm at a temperature of 109.97 °C. Further, negligible mass loss (3.51%) was observed in the TGA scan of CI in the range of 25−130 °C, suggesting that there was no degradation; rather it was only phase transformation. So it may be concluded that it is an anhydrous and pure cocrystal phase.

CII showed two melting endotherms at 81.1 and 111.27 °C, where first peak was broadened with very less intensity. From TGA study, a negligible mass loss (2.70%) in the range of 30−100 °C does not correspond to mass loss due to solvent. Another negligible mass loss (1.84%) seen in the range of 100−130 °C does not correspond to any degradation of cocrystal suggesting phase transformation. To check whether two endotherms correspond to two different polymorphic crystals,
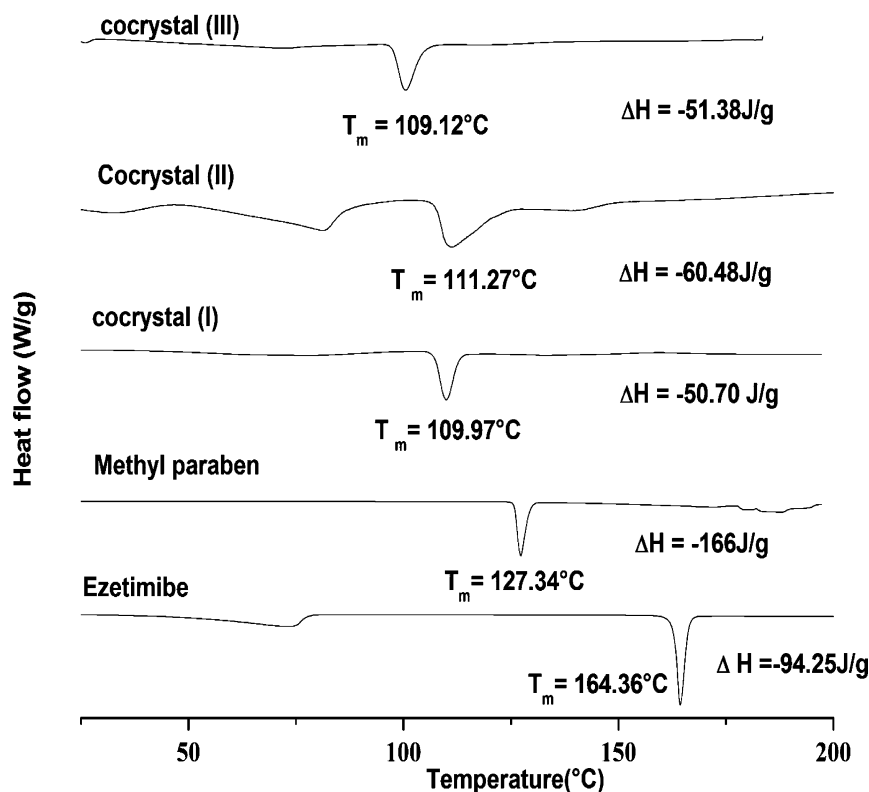

Figure 2. DSC scans of ezetimibe, methyl paraben, cocrystal I, cocrystal II, and cocrystal III.
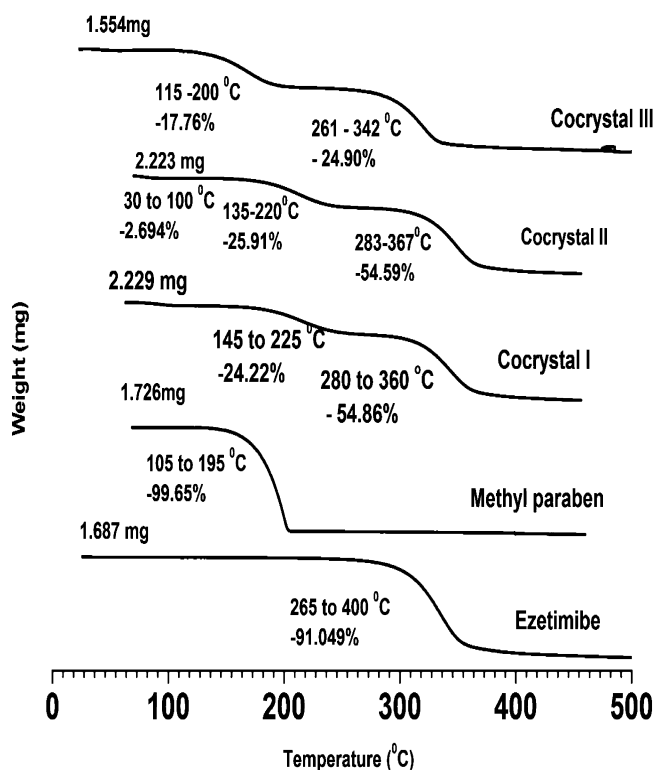
Figure 3. TGA of curve of ezetimibe, methyl paraben, cocrystal I, cocrystal II, and cocrystal III.

the cocrystal (CII) was heated at 10 °C/min up to 125 °C and then cooled at 10 °C/min up to ambient temperature then again reheated up to 250 °C at a same heating rate as shown in Supporting Information (Figure S1). One exothermic peak corresponding to recrystallization was observed at 72.73 °C during cooling cycle. However, in the reheating cycle, the first endotherm disappeared (81.1 °C) but the second endothermic peak appeared at the same temperature. It is clear that the exothermic peak observed at 72.73 °C is not due to the recrystallization of the polymorphic form I; rather it is due to the recrystallization of polymorphic form II. Upon heating polymorphic form I transforms to polymorphic form II as confirmed by the endothermic peak during reheating cycle. Similar findings were reported in the case of sulfamethazine/hydroxy benzoic acid cocrystal and ethenzamide/gentisic acid cocrystal (solvent system was toluene-acetonitrile 1:1) by Ghosh et al. and Aitipamula et al., respectively.[44,46]

CIII showed a single and sharp melting endotherm at 109.12 °C free of any eutectic melting, thus establishing the existence of pure cocrystal phase. A very negligible mass loss confirmed the phase transformation of cocrystal.

The heat of fusion (ΔH) of all cocrystals (Figure 2) was less than that of pure ezetimibe as well as methyl paraben, which indicates the probability of increased entropy and subsequent higher solubility of all cocrystals compared to pure ezetimibe. The mass loss occurred in all cocrystals in two stages. The first mass loss at a range of 130−200 °C was 19.69%, 22.06%, and 16.24% for CI, CII, and CIII, respectively, which is similar to mass loss pattern of methyl paraben. The second mass loss at a range of 250−380 °C was 54.86%, 54.59%, and 24.90% for CI,
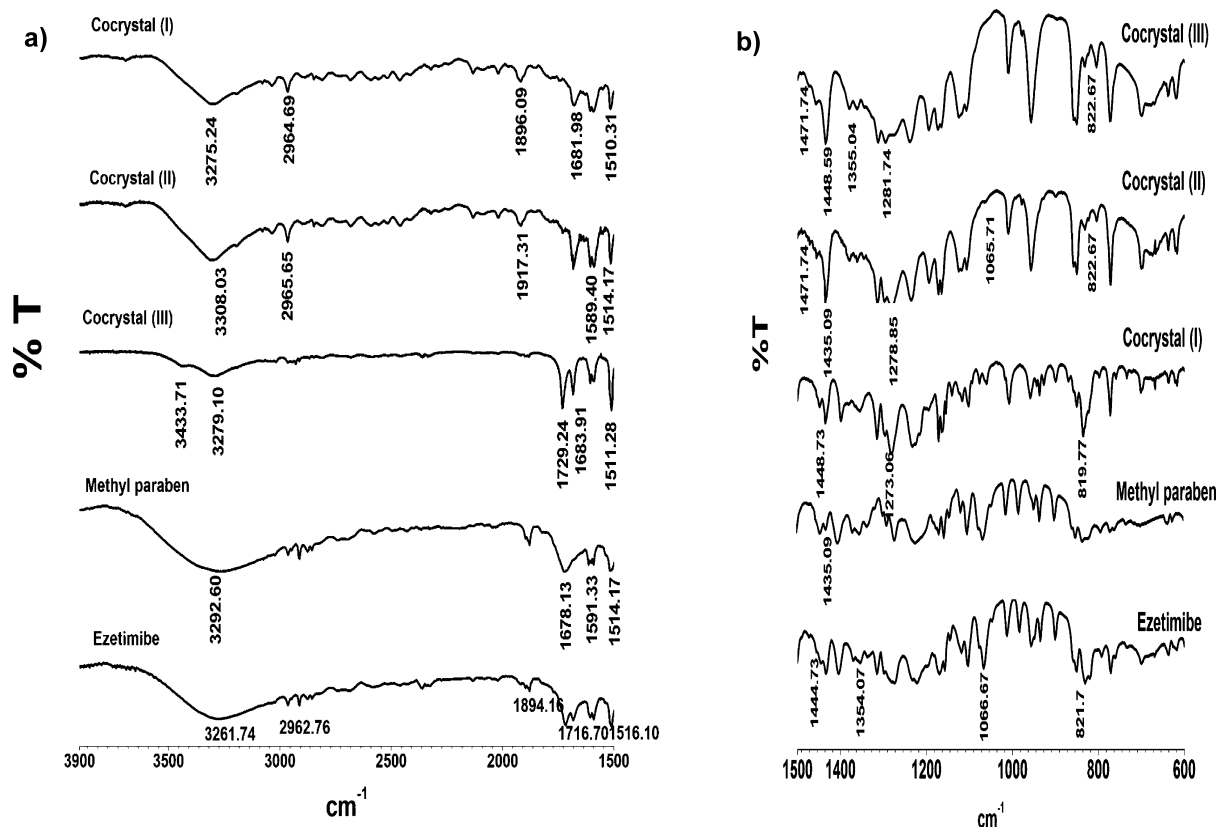

Figure 4. (a) FTIR spectra (1500−3900 cm^{-1}) obtained for ezetimibe, methyl paraben, and cocrystals. (b) FTIR spectra (600−1500 cm^{-1}) obtained for ezetimibe, methyl paraben, and cocrystals.

Table 1. Assignments of Major Bands of Raman Spectra of Ezetimibe, Methyl Paraben, and Their Cocrystal Products[a]

ezetimibe	methyl paraben	cocrystal I	cocrystal II	cocrystal III	assignment[48−52]
1760.22m		1761.43m	1761vw	1761.38vw	$v(C\!\!=\!\!O)$ lactam
1716.28m		1715.45w	1716.7vw	1716.38vw	$v(C\!\!=\!\!O)$ lactam
1613.64s	1676.15	1675.31	1675.47	1675.47	$v(C\!\!=\!\!O)$
	1606.83s	1611.09s	1611.63vs	1610.61s	$v(CC)$ar chain vibrations
	1588.92s	1588.92s	1587.16m	1588.18s	$v(C\!\!=\!\!C)$
1510.56m	1517.7m	1510.56m	1510.12m	1509.09w	$v(C\!-\!O)$ phenolic
1431.84s		1432.72vw	1431.2m	1434.33vvw	$v(C\!-\!N)$
1403.55w		1404.43s	1402.95s	1402.95vvw	$\delta(CH2)$
1370.64w		1369.75	1370.37	1369.32	(O−H) i.p. bend
1341.11w		1338.42vvw	1342.94vw	1341.88vw	$\beta(O\!-\!H)$
1316.83m	1311.42m	1311.42w	1312.22w	1311.16m	$v(C\!-\!O)c$
1292.43m			1292.02	1287.76	(CC)ar
	1281.54s	1281.54vvw	1281.36w	1282.43m	$v(C\!-\!O)$
1272.46w			1272.83w	1272.83w	$v(C\!-\!O)$
	1234.12w	1232.29w	1232.15w	1234.3w	$v(C\!-\!O)$
1214.85s		1214.85w	1214.96s	1216.03vw	$v(C\!-\!F)$
1183.49w		1182.56w			vC−O (H)
1168.66		1167.74			
1158.45s	1159.38s	1159.38s	1159.87s	1159.87s	$v(CC)$ar chain vib.
	1121.13w	1118.32vvw	1121.83vvw	1121.83vw	$v(C\!-\!O\!-\!C)$ asym
948.913m		948.913w	947.62w	949.851vw	$\beta(C\!-\!H)$
860.186s	856.252s	857.236m	857.839m	860.097m	$v(C\!-\!C)$
838.515s		836.54vw	838.622m	837.49vvw	$v(C\!-\!C)$
821.709w		821.709w	821.626m	822.76vvw	$v(\!\!=\!\!(C\!-\!H))$
	829.624w	828.63w		829.562w	
734.886w		734.886vw	737.214vw	734.92vw	CH2 rock
699.565m		700.578	700..421	700.421	$v(CC)$ al. chain vib.
635.413m		636.437m	636.167m	636.167w	
397.95m		397.95	397.199	397.199	$\delta(CC)$ aliphatic chains

[a]s, strong; m, medium; w, weak; vw, very weak; vvw, very very weak; v, stretching; β, in plane deformation; δ, bending; ϕ, phenyl; i.p., in plane; ar, aromatic; asym, asymmetric; vib, vibration; def, deformation.

CII, and CIII, respectively, which is also similar to the mass loss pattern of ezetimibe. So, it is clear that the amount of ezetimibe present in CIII is less as compared to other cocrystals, which may be reflected in stoichiometric ratio calculation by PXRD.

Fourier Transform Infrared Spectroscopy (FTIR). Vibrational spectroscopy is an excellent technique to characterize and study cocrystallization. The characteristic peaks and their shift of pure ezetimibe, methyl paraben, CI, CII, and CIII are tabulated in (Supporting Information (Table S2). The FTIR spectra of ezetimibe, methyl paraben, CI, CII, and CIII in the regions of 3900 to 1500 and 1500 to 600 cm^{-1} are presented in Figure 4 panels a and b, respectively.

A comparison of spectra reveals that there were several band shifts occurring between the starting components and CI. The FTIR spectra for pure ezetimibe and methyl paraben in the starting material have bands at 3261.74 and 3292.00 cm^{-1}, corresponding to $v(O\!-\!H)$, respectively. The bands at 1716.70 and 1678.13 cm^{-1}, corresponding to $v(C\!\!=\!\!O)$, was for ezetimibe and methyl paraben, respectively. In the case of CI, bands corresponding to v (O−H) of both molecules, shifted to 3275.24 cm^{-1}. The band corresponding to $v(C\!\!=\!\!O)$ of methyl paraben shifted to 1681.98 cm^{-1}, indicating the formation of the hydrogen bond between the phenolic hydroxyl group and carbonyl group (lactum) of ezetimibe with the *p*-hydroxy group of methyl paraben.[47] The peak at 1435.09 cm^{-1} ($v(C\!-\!O)$ enolic) of methyl paraben and the peak at 1444.73 cm^{-1} of ezetimibe shifted and then merged with the peak at 1448.73 cm^{-1} of CI with a relatively higher intensity. The peak at

1444.73 cm^{-1} [v (C−N)] of ezetimibe shifted to 1448.59 cm^{-1}, which is likely due to charge transfer interaction between tertiary nitrogen of ezetimibe with methyl paraben molecule. These peak shifts strongly indicated the formation of hydrogen bond and other weak interactions between ezetimibe and methyl paraben.

During formation of ezetimibe-methyl paraben cocrystal via the liquid assisted grinding method (CII), the OH band of ezetimibe and methyl paraben shifted to a higher wavenumber by 47 and 16 cm^{-1}, respectively, which was a very significant shift clearly depicting participation of OH group of both molecules in hydrogen bond formation. This peak was found to be sharper than the pure ezetimibe peak. Further, the band at 1354.07 cm^{-1}, corresponding to $\beta(O\!-\!H)$ of pure ezetimibe, shifted to 1361.79 cm^{-1}. The FTIR spectrum of pure ezetimibe has strong bands at 1716.70 cm^{-1}, which correspond to $v(C\!\!=\!\!O)$ lactam. During crystallization, its intensity was drastically reduced. In CII, the C−F stretching band shifted to a higher wavenumber by 13 cm^{-1}, which indicates that the fluorine (F) atom might be also engaged in formation of a hydrogen bond.

The cocrystal (CIII) of ezetimibe and methyl paraben prepared by the reaction crystallization process showed the maximum number of significant changes in FTIR spectrum. The FTIR spectrum of pure ezetimibe showed a broad peak at 3261.74 cm^{-1} of strong intensity, corresponding to stretching of OH group. This peak became narrow and weak in intensity with a shift toward a higher wavenumber by 18 cm^{-1}. Further, the carbonyl group (lactam) of ezetimibe and the carbonyl
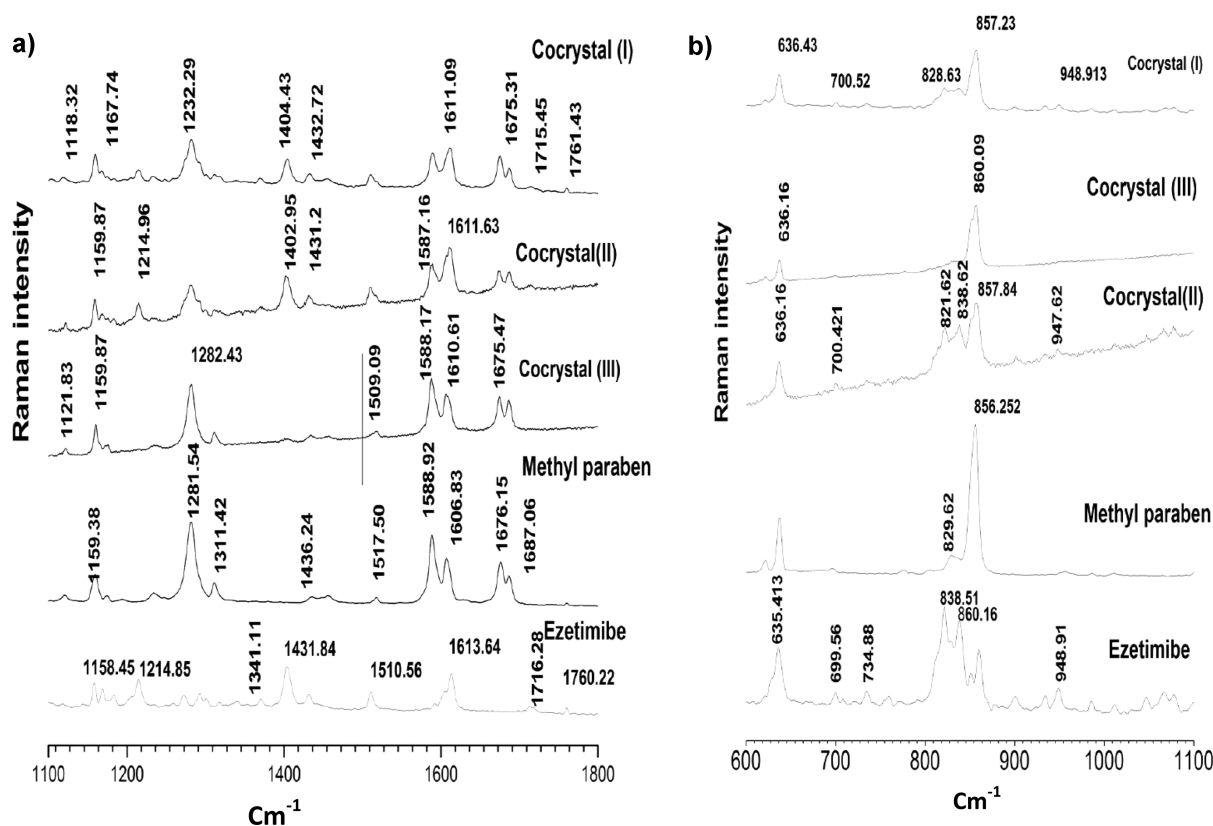
Figure 5. (a) Raman spectra (1100−1800 cm^{-1}) obtained for ezetimibe, methyl paraben and cocrystals. (b) Raman spectra (600−1100 cm^{-1}) obtained for ezetimibe, methyl paraben and cocrystals.

group of methyl paraben showed a shift to higher wavenumber by 14 and 5 cm^{-1}, respectively. It indicates that there is a electrostatic repulsion between the lone pair of electrons present in carbonyl group of both the drug and coformer. In this cocrystal (CIII) only, the band at 1444.73 cm^{-1} corresponding to v (C−N) got shifted to 1448.59 cm^{-1}, which is similar to CI.

Raman Spectroscopy. FTIR and Raman spectroscopy are complementary techniques for characterizing of solid forms of drugs.[43] Solid samples isolated from screening experiments can be mixtures and have poor crystal quality. Relying only on one technique may not provide enough evidence to confirm a potential hit. However, by comparing data for the screening samples from spectroscopic tools, a more informed determination may be achieved. These spectroscopic techniques can provide evidence for cocrystal formation by evaluating the intermolecular interactions. Additionally, Raman spectroscopy may be used in the identification of polymorphism, since different vibration modes can be associated with modifications in molecular packing in crystalline solids.[43] These differences are observed mainly in low-frequency, which may arise due to lattice vibration that is more sensitive to structural changes in solid state.[48] The assignment for the most prominent vibrational bands of ezetimibe, methyl paraben, CI, CII, and CIII are listed in Table 1 presented in Figure 5a,b.

The molecular interaction between ezetimibe and methyl paraben was examined by Raman spectroscopy, and the vibrational wavenumbers and assignments are listed in Table 1. The Raman spectra of pure ezetimibe in the starting material have bands at 1760.22, 1716.28, and 1431.84 cm^{-1}, corresponding to v(C=O) lactam, v(C=O) lactam, and

v(C−N), respectively. During the cocrystallization of ezetimibe and methyl paraben, these bands in the cocrystal (CI) were shifted to 1761.43, 1715.45, and 1432.72 cm^{-1}. A significant decrease in the intensity was observed in v(C−N). Similarly, intensity of v(C=O) lactam also decreased. Further, the peak of carbonyl stretching in methyl paraben also shifted, suggesting that C=O is participating in hydrogen bonding. The hydroxyl group also seemed to be participating in hydrogen bonding. The band for β(O−H) of pure ezetimibe showed a shift to a lower wavenumber by 4 cm^{-1}.

A comparison of the spectra reveals that there are several band shifts occurring between the individual components and the cocrystal (CII). During the formation of cocrystals, the bands at 1341.11 and 1234.12 cm^{-1} depicting β(O−H) and v(C−O)h shifted to 1342.94 and 1232.15 cm^{-1}, respectively with decreased intensity. It depicts that the hydroxyl group is engaged in hydrogen bonding.

CIII, prepared by reaction crystallization, showed the maximum number of band shifts as compared to other two cocrystals. It is in agreement with the FTIR results, thereby giving strong evidence of formation of new supramolecular synthon in cocrystal. The Raman spectra of pure ezetimibe showed band at 1431.84 cm^{-1} of strong intensity corresponding to stretching of C−N of lactam ring. This band showed a shift of 3 cm^{-1} with a significant decrease in its intensity, indicating possible Coulombic interaction between the nitrogen atom of ezetimibe and oxygen atom of methyl paraben. The band corresponding to stretching of C−F in ezetimibe got shifted to higher wavenumber by 2 cm^{-1}. The peak obtained was very weak, as compared to strong intense peak in pure ezetimibe,

indicating that fluorine is also participating in hydrogen bonding.

Powder X-ray Diffraction (PXRD). Powder X-ray diffraction is a fingerprint characterization method for cocrystals. If the resulting PXRD of the solid product obtained after cocrystallization experiment is different from that of the reactants, then it may be inferred that a new solid phase has formed. PXRD is a powerful technique for determining the presence of polymorphs, crystal habit modifications in drug crystals, and/or generation of new crystal form during cocrystallization process.[53]

The PXRD pattern of ezetimibe exhibited characteristic reflections at about 2θ 15.70°, 17.11°, 18.56°, 19.24°, 21.63°, 22.67°, 23.24°, 24.19°, 25.10°, 28.04°, and 32.76°. Similarly, the PXRD pattern of methyl paraben exhibited characteristic reflections at about 2θ 21.23°, 23.23°, 25.08°, and 36.56°. The major peak with 100% intensity had reflections at 2θ of 19.24° and 25.08° in ezetimibe and methyl paraben, respectively. As shown in Figure 6, unique PXRD patterns of the cocrystals distinguishable from the host (drug) and the guest (coformer) were noted.
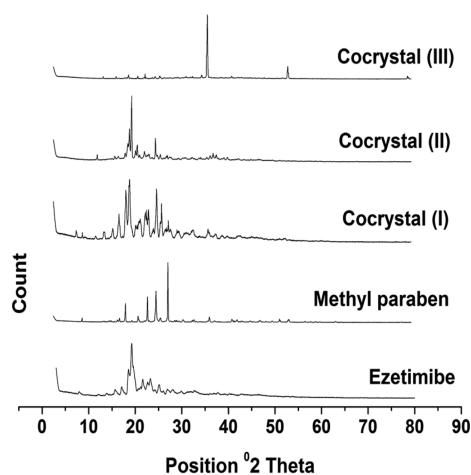

Figure 6. PXRD patterns of ezetimibe, methyl paraben, and cocrystals.

The PXRD pattern of CI exhibited characteristic reflections at about 2θ 13.91°, 15.77°, 17.11°, 18.60°, 19.34°, 20.74°, 21.66°, 22.77°, 23.44°, 24.50°, 26.25°, 27.71°, 28.15°, 29.78°, 31.18°, 33.40°, and 36.28°. The most intense peak was at reflection 2θ 19.34°. These peaks were significantly different from the parent components, which indicated that CI is a unique with respect to pure ezetimibe. Major peaks at 25.11° and 32.76° of pure ezetimibe were missing in the cocrystal phase, whereas, peaks at 31.18° and 39.31° were observed.

The PXRD pattern of CII exhibited characteristic reflections at about 2θ 18.99°, 19.33°, 19.79°, 19.80°, 20.63°, 21.04°, 22.60°, and 24.97°, which were significantly different from either of ezetimibe or methyl paraben. The absence of peaks, characteristic of pure ezetimibe and methyl paraben in the PXRD pattern of CII implies it to be pure and homogeneous cocrystal sample. Newer peaks, with significant intensities were observed at 18.99° and 20.64°. The most intense peak was obtained at 19.80°.

The PXRD pattern of CIII exhibited characteristic reflections at about 2θ 13.70°, 16.50°, 19.15°, 21.14°, 22.71°, 24.90°, 25.92°, 26.86°, 34.90°, 36.12°, 41.39°, and 53.45°. The PXRD pattern so obtained was very unique compared to the two

earlier cocrystals. The intensities of all the peaks were reduced drastically. No major peaks were seen except the most intense peak at 36.12°. The absence of characteristics peaks of ezetimibe and methyl paraben clearly indicates the cocrystal's uniqueness and purity.

It can be seen that the cocrystals exhibited spectra with different peak positions (patterns) from their respective host and guest crystals possessing different crystallographic structures with significant habit modification. Further, the relative intensities of their PXRD peaks were modified, which might be attributed to the different crystal habits[14] and arrangement of molecules indicating formation of new crystal forms. This was also strongly supported by the melting points observed for the cocrystals, which were completely different from their respective host and guest crystals as discussed earlier.

Scanning Electron Microscopy (SEM). Figure 7a–c shows the SEM overview of all the three cocrystal samples CI, CII, and CIII. The particles of sample CI appear to be mainly tetragonal and rod-shaped. The particles of CII on the other hand have no fixed geometry, although it is clear that the average particle size of the sample CII is quite less than that of CI. An important point worth noting here is that particles of both the samples CI and CII have nonspherical geometries and hence a larger surface compared to spherical particles. This may be because sample CII was prepared by high energy ball milling, which is a very high entropy synthesis route, and hence particles formed are mostly nonspherical and quite small. The particles of sample CIII are much bigger in size with average size of about 12 μm. The particle sizes and shapes seen in the electron micrographs completely complement the results of our dissolution study. We have determined in our dissolution study that the rate of dissolution for sample CII is highest, and for the sample CIII, it is lowest. This can be easily understood by examining the electron micrographs of CII. The particle size of CII is the smallest among the all three cocrystals. Further due to nonsphericity, the surface to volume ratio is much higher than the sample CIII. Both these factors add up in increasing its dissolution rate. Further, due to a larger particle size of the sample CIII, its dissolution rate is lowest among the three cocrystals.

Solubility Studies. *Determination of Cocrystal Stoichiometry. Stoichiometry of Cocrystals via PXRD.* The stoichiometry of ezetimibe and methyl paraben were calculated from the X-ray diffractograms of CI, CII, and CIII. The most intense peak of ezetimibe and methyl paraben was obtained at a reflection of 2θ, 19.24° and 25.08°, respectively. Stoichiometric (ezetimibe/methyl paraben) ratios were 1.35, 2.70, and 1.0 for CI, CII, and CIII, respectively, as given in Supporting Information (Table S3). The amount of ezetimibe present in CIII is less as compared to other two cocrystals. It may be confirmed from the mass loss data (24.90%) of CIII in the range of 250−380 °C, which corresponds to the mass loss of ezetimibe as shown in TGA data (Figure 3).

Stoichiometry via HPLC Results in the Case of CIII. The transition concentration values of drug and the coformer measured at the invariant point where two solid phases (drug and cocrystal) are in equilibrium with organic solution. The stoichiometric ratio of ezetimibe and methyl paraben in cocrystal III was 0.97:1. This result was found to be in good agreement with the stoichiometry obtained from PXRD quantification.

Measurement of Equilibrium Cocrystal Solubility. The equilibrium solubility ($[\text{drug}]_{Scc}/S_{drug}$) values of ezetimibe and
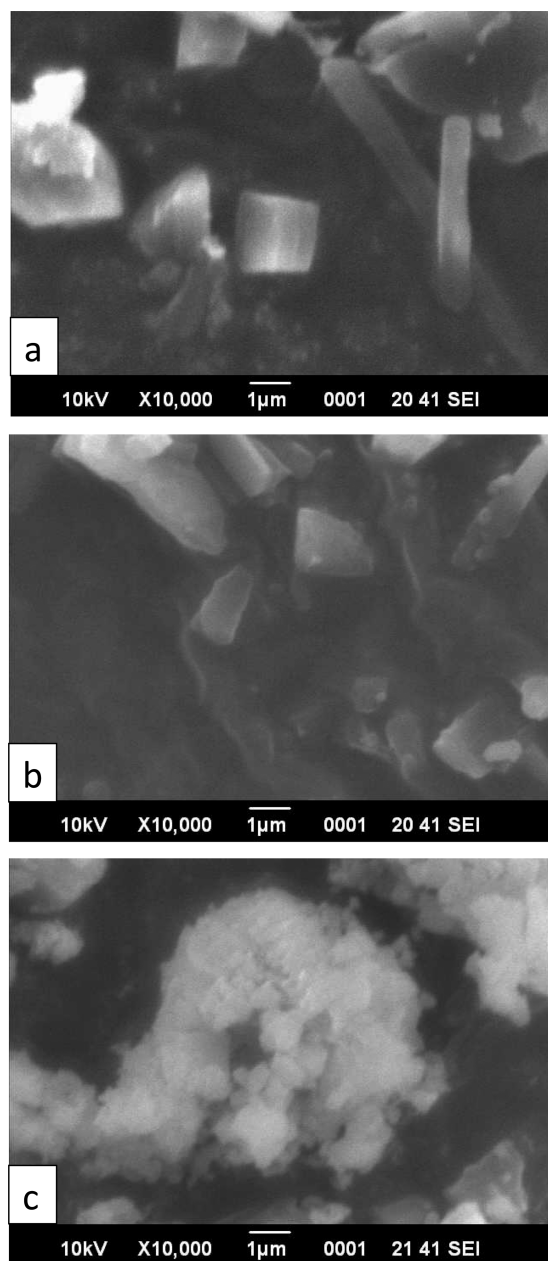
Figure 7. Scanning electron microscopy images of (a) cocrystal I (CI), (b) cocrystal II (CII), and (c) cocrystal III (CIII).

its cocrystals is shown in Table 2. Solubility product of cocrystal (K_{sp}), and equilibrium solubility values of cocrystals, that represent nonionized drug and coformer in solution, was calculated according to eqs 1 and 2, respectively. Solubility of

cocrystals were multiplied by the stoichiometric coefficient to provide the associated drug concentration and normalized with the relevant stable crystalline drug solubility to provide solubility ratios $[drug]_{Scc}/S_{drug}$. Solubility ratios emphasize the magnitude of change in solubility achieved by various cocrystals and facilitate comparisons between different cocrystals.

The cocrystals of ezetimibe and methyl paraben studied showed a maximum of about a 2-fold increase. The solubility ratios were 1.78, 1.42, and 0.94 for CI, CII, and CIII, respectively. The solubility of the cocrystals may be increased and/or decreased. It depends on the crystal density and strength of the hydrogen bond synthons. Higher crystal packing leads to increased stability vis-a-vis lower solubility.[54] It was evident from FTIR and Raman spectra study that stronger hydrogen bonding occurred in the case of cocrystal III (CIII), which leads to its lower solubility. Clearly, an enhanced solubility was seen in all the cocrystals as compared to pure drug alone except in CIII.

Determination of Ideal Solubility from Thermal Behavior. Ideal solubility values of cocrystals, derived from the melting enthalpy and temperature of crystals, are listed in Table 3.

Experimental cocrystal aqueous solubility was not well correlated with ideal values derived from the melting enthalpy and temperature of the cocrystals. The ratios of experimental aqueous solubility to ideal solubility are listed in Table 3 to emphasize these deviations. In the case of drug and coformer also, no correlation between ideal and experimental solubility was observed. Therefore, it can be suggested that crystal fusion properties are not sufficient for predicting cocrystal solubility. The solution chemistry of cocrystals appears to be critical for describing solubility behavior.[55] The results further illustrate that melting properties associated with the breaking of the crystal lattice are not sufficiently predictive of cocrystal solubility relations that involve solvent interactions. Ratios of the ideal cocrystal and ideal drug solubilities listed in Table 3 were on a similar order of magnitude to the solution measurements, except in CIII, which showed the highest magnitude.

The thermodynamic ideal solubility seems to more adequately quantify the relative change between cocrystal and drug than absolute solubility values. The cocrystal studied showed that solvent−solute interactions dominate over lattice energies in water.

Dissolution Study. The solubility advantage of cocrystals has been shown to correlate with increased dissolution and bioavailability. Ezetimibe cocrystal solubility was greater than ezetimibe. Therefore, in order to assess whether this solubility advantage correlates with increased dissolution, in vitro release study was performed in biorelevant media at pH 4.5. Table 4 shows the dissolution data of pure ezetimibe and its cocrystals

Table 2. Cocrystal Component Solubilities and Calculated Cocrystal K_{sp} Values, Solubilities, and Solubility Ratios[a]

cocrystal	A:B cocrystal stoichiometry (drug−ligand)	C [drug] (m) (mean ± S.D.)	D [coformer] (m) (mean ± S.D.)	E K_{sp}[b]	F cocrystal solubility (m)[c]	G solubility ratio $[drug]_{Scc}/S_{drug}$
CI	1.35:1	$1.84 \times 10^{-6} \pm 2 \times 10^{-7}$	$1.13 \times 10^{-10} \pm 2 \times 10^{-5}$	1.53×10^{-11}	2.10×10^{-5}	1.78
CII	2.7:1	$2.36 \times 10^{-6} \pm 3 \times 10^{-6}$	$8.04 \times 10^{-12} \pm 4 \times 10^{-4}$	4.17×10^{-18}	8.38×10^{-6}	1.42
CIII	1.0:1	$2.07 \times 10^{-6} \pm 2 \times 10^{-7}$	$2.25 \times 10^{-10} \pm 9 \times 10^{-6}$	2.25×10^{-10}	1.49×10^{-05}	0.94

[a]Solubility of drug was determined experimentally to be $S_{drug} = 1.59 \times 10^{-5}$ (m). [b]K_{sp} units are in m$^{2.35}$, m$^{3.7}$, and m^2 for C I, C II, and C III, respectively. [c]Calculated using eq 1. Indicated values reflect HPLC measurement of dissolved cocrystals. Calculations: E = $[C]^A[D]^E$, F = $[E/(A^A B^B)]^{1/(A+B)}$, G = $(A*F)/S_{drug}$.

Table 3. Melt Temperature and Enthalpy Used in Calculation of Ideal Solubility and Comparison with Experimental Solubility Values

	exp aqueous solubility (m)[a]	ideal solubility (m)[b]	T_m (°C)	ΔH_m^{c} (kJ/mol)	aqueous solubility ratio (exp/ideal)	ideal cocrystal solubility ratio (cocrystal/drug)
EZT	1.59×10^{-05}	15.75	164.36	38.58	1.01×10^{-06}	
MP	1.70×10^{-05}	9.78	127.34	25.29	1.74×10^{-06}	
C I	1.84×10^{-06}	4.51	109.97	28.47	4.08×10^{-07}	0.28
C II	2.36×10^{-06}	3.43	111.27	33.96	6.89×10^{-07}	0.21
C III	2.07×10^{-06}	6.10	109.12	32.92	3.39×10^{-07}	0.39

[a]Measured solubility for anhydrous samples. [b]Ideal solubility calculated from eq 3 using melt temperature and heat of fusion. Mole fractions were converted to molality units in water. [c]The enthalpy of melting for cocrystals is normalized by moles of component molecules(drug + coformer) per mole of cocrystal. All solubility values are expressed in molality units in water.

Table 4. Dissolution Data of Pure Ezetimibe and Its Cocrystals in Acetate Buffer (pH 4.5) at 37 ± 0.5 °C

	%CDR$_{15}$[a] ± SD	%CDR$_{45}$[a] ± SD	%CDR$_{120}$[a] ± SD
ezetimibe	42.55 ± 1.66	61.64 ± 3.35	68.55 ± 3.25
cocrystal I	60.50 ± 1.65[b]	64.93 ± 0.59	76.59 ± 2.98
cocrystal II	69.47 ± 1.66[b]	73.89 ± 0.60[b]	85.56 ± 2.98[b]
cocrystal III	51.53 ± 1.66[b]	61.64 ± 3.34	68.82 ± 3.41

[a]Indicates ± SD, (n = 3); SD: standard deviation; %CDR$_{15}$, %CDR$_{45}$, %CDR$_{120}$: percentage cumulative drug released in 15, 45, and 120 min; [b]Significant difference compared to pure ezetimibe, i.e., significant ($p < 0.05$).

in 0.45% sodium lauryl sulfate (SLS) of acetate buffer (pH 4.5) at 37 ± 0.5 °C. The dissolution curves of pure ezetimibe alone and cocrystals in 500 mL of 0.45% sodium lauryl sulfate (SLS) in 0.05 M acetate buffer (pH 4.5) are shown in Figure 8.
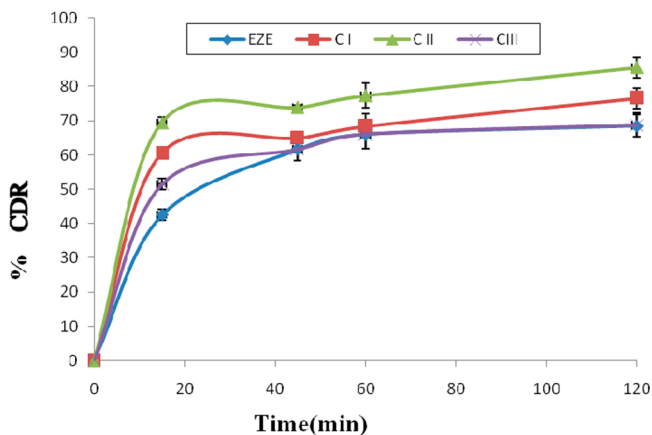

Figure 8. Dissolution curves of ezetimibe and its cocrystals. CI (solution crystallization method); CII (liquid assisted grinding method); CIII (reaction crystallization method).

The dissolution profiles of all cocrystals, with pure ezetimibe as a control, were studied for 2 h in defined biorelevant media. The release data, dissolution efficiency (DE%) (Supporting Information Table S4) at different sampling times of all cocrystals were statistically analyzed using one-way ANOVA followed by Tukey's posthoc analysis at a significance level of 95% ($p < 0.05$). The statistical analysis of %CDR values revealed a significant improvement in dissolution profile of ezetimibe at 15 min (%CDR15) in all three cocrystals ($p < 0.05$). Similarity factor of three cocrystals were calculated with a reference of pure ezetimibe %CDR (Supporting Information Table S4). The cocrystal CII, prepared by liquid assisted

grinding method, showed significant improvement in dissolution at 45 and 120 min, indicating a good dissolution profile. Moreover, CII showed a release of 85.56% drug in 120 min, highest among all. This result is in good agreement with the thermal behavior of CII. From the DSC result, it is clear that CII contains two polymorphic crystals. The peak melting temperature of one polymorph was at about 81.1 °C. Peak melting temperature (T_m) is an indicator of thermostability and generally the higher the value of T_m, the more thermodynamically stable is the molecule and vice versa.[46] The release of pure drug was about 68% in 120 min. CII exhibited enhanced drug release at each time point than CI, despite having less solubility than the latter, thus showing some deviation from the solubility values. CIII, on the other hand, followed a similar pattern of drug release to that of pure drug after 15 min, which might be because of rapid transformation to the original crystal of drug. The faster dissolution of ezetimibe from cocrystals might be accredited to altered crystallinity pattern, size and shape, and crystal habit of the cocrystal, which led to improved solubility of cocrystals in dissolution media. Further, higher association between ezetimibe and coformers also might have contributed for enhanced dissolution of drug from CI and CII.

CONCLUSION

The present study illustrated the formation and characterization of three different cocrystals of ezetimibe using methyl paraben as a coformer, employing three different processes, namely, solution crystallization, liquid assisted grinding and reaction crystallization. DSC results show that the entirely different peak melting temperature was observed in all three cocrystals, indicating the formation of a new solid phase. FTIR and Raman spectroscopy study reveals that the new solid form is the result of weak electrostatic interaction between drug and coformer. From the PXRD study, it is clear that the crystal habit of both the drug and the coformer has been modified. Equilibrium solubility study and dissolution study of the cocrystals reveal that the cocrystals of ezetimibe and methyl paraben can a possible and potential alternative and effective approach for improving its solubility.

ASSOCIATED CONTENT

S Supporting Information

Table S1. Preliminary screening of coformers. Table S2. FTIR spectral band assignment of ezetimibe, methyl paraben, and their cocrystal products. Table S3. Stoichiometric calculation from area under the peak of different cocrystals. Table S4. Dissolution efficiency percent and similarity factor of CI, CII, CIII, and pure ezetimibe. Figure S1. Differential scanning calorimetry of cocrystal II (heating up to 125 °C, then cooling

up to ambient temperature, and again heating up to 250 °C). This material is available free of charge via the Internet at http://pubs.acs.org.

■ AUTHOR INFORMATION

Corresponding Author
*Tel.:+91-9470339587. Fax: +91-6512275290. E-mail: aghosh@bitmesra.ac.in.

Notes
The authors declare no competing financial interest.

■ REFERENCES

(1) Scott L. Childs, S. L.; Hardcastle, K. I. *Cryst. Growth Des.* **2007**, *7*, 1291–1304.
(2) Haleblian, J.; McCrone, W. *J. Pharm. Sci.* **1969**, *58*, 911–929.
(3) *Guidance for Industry, ANDAs: Pharmaceutical Solid Polymorphism*; Food and Drug Administration: Silver Springs, MD, 2007.
(4) Babu, N. J.; Nangia, A. *Cryst. Growth Des.* **2011**, *11*, 2662–2679.
(5) Schultheiss, N.; Newman, A. *Cryst. Growth Des.* **2009**, *9*, 2950–2967.
(6) Maitland, G. C.; Rigby, E. B.; Smith, E. B.; Wakeham, W. A. *Intermolecular Forces: Their Origin and Determination*; Oxford University Press: Oxford, 1981.
(7) Pauling, L. *The Nature of Chemical Bond*; Cornell University Press: New York, 1948.
(8) Pedersen, C. J. *J. Am. Chem. Soc.* **1967**, *89*, 7017–7036.
(9) Cram, D. J.; Dewhirst, K. C. *J. Am. Chem. Soc.* **1959**, *81*, 5963–5971.
(10) Stahl, P. H.; Nakano, M. *Pharmaceutical Aspects of the Drug Salt Form, in Handbook of Pharmaceutical Salts: Properties, Selection, and Use*; Stahl, P. H., Wermuth, C. G., Eds.; Wiley-VCH/VCHA: New York, 2002.
(11) Rxlist homepage, http://www.rxlist.com/top200.htm (accessed Jan 13, 2013).
(12) *The Merck Index*; Merck: Whitehouse Station, NJ, USA; Version 13.4 CD-ROM; 2006.
(13) Walsh, R. D. B.; Bradner, M. W.; Fleischman, S.; Morales, L. A.; Moulton, B.; Rodríguez-Hornedo, N.; Zaworotko, M. J. *Chem. Commun.* **2003**, 186–187.
(14) Fleischman, S. G.; Kuduva, S. S.; McMahon, J. A.; Moulton, B.; Walsh, R. D.B.; Rodríguez-Hornedo, N.; Zaworotko, M. J. *Cryst. Growth Des.* **2003**, *3*, 909–919.
(15) McMahon, J. A.; Bis, J. A.; Vishweshwar, P.; Shattock, T. R.; McLaughlin, O. L.; Zaworotko, M. J. *Z. Kristallogr.* **2005**, *220*, 340–350.
(16) Vishweshwar, P.; McMahon, J. A.; Peterson, M. L.; Hickey, M. B.; Shattock, T. R.; Zaworotko, M. J. *Chem. Commun.* **2005**, 4601–4603.
(17) Childs, S. L.; Chyall, L. J.; Dunlap, J. T.; Smolenskaya, V. N.; Stahly, B. C.; Stahly, G. P. *J. Am. Chem. Soc.* **2004**, *126*, 13335–13342.
(18) Remenar, J. F.; Morissette, S. L.; Peterson, M. L.; Moulton, B.; MacPhee, J. M.; Guzman, H. R.; Almarsson, Ö. *J. Am. Chem. Soc.* **2003**, *125*, 8456–8457.
(19) Scott, C.; Nathan, B.; Reddy, L. S. WO 2012/116349 A2, 2012.
(20) Mulye, P. S.; Jamadar, S. A.; Karekar, P. S. *Powder Technol.* **2012**, *222*, 131–138.

(21) Product monograph: PrEZETROL; Merck Canada Inc.: Canada, 2012. http://www.merckfrosst.ca/assets/en/pdf/products/EZETROL-PM_E.pdf (accessed Nov, 2012).
(22) *Zetia Drug Description RxList.com*; The Internet Drug Index WebMD, Inc.: New York, 2008. http://www.rxlist.com/zetia-drug.htm (accessed Nov, 2012).
(23) Patel, R.; Bhimani, D.; Patel, J.; Patel, D. *J. Incl. Phenom. Macrocycl.* **2008**, *60*, 241–251.
(24) Sancheti, P. P.; Karekar, P.; Vyas, V.; Shah, V. M.; Pore, Y. V. *Pharmazie* **2009**, *64*, 227–231.
(25) Dixit, R. P.; Nagarsenker, M. S. *Eur. J. Pharm. Sci.* **2008**, *35*, 183–192.
(26) U.S. Food and Drug administration approved GRAS list. EAFUS: A Food Additive Database. http://www.cfsan.fda.gov/_dms/eafus.html (accessed November 2013).
(27) Zhang, G. G. Z.; Henry, R. F.; Borchardt, T. B.; Lou, X. *J. Pharm. Sci.* **2007**, *96*, 990–995.
(28) Childs, S. L.; Rodriguez-Hornedo, N.; Reddy, L. S.; Jayasankar, A.; Maheshwari, C.; McCausland, L.; Shipplett, R.; Stahly, B. C. *CrystEngComm* **2008**, *10*, 856–864.
(29) Friščić, T.; Jones, W. *Cryst. Growth Des.* **2009**, *9*, 1621–1637.
(30) Trask, A.; Jones, W. *Top Curr. Chem.* **2005**, *254*, 41–70.
(31) Rodriguez-hornedo, N.; Nehm, S. J.; Seefeldt, K. F.; Pagan, Y.; Falkiewicz, C. J. *Mol. Pharm.* **2006**, *3*, 362–367.
(32) Nehm, S. J.; Rodriguez-Spong, B.; Rodríguez-Hornedo, N. *Cryst. Growth Des.* **2006**, *6*, 592–600.
(33) Goehner, R. P. *Adv. X-ray Anal.* **1982**, *25*, 309–313.
(34) Jayasankar, A.; Reddy, L. S.; Bethune, S. J.; Rodríguez-Hornedo, N. *Cryst. Growth Des.* **2009**, *9*, 889–897.
(35) Childs, S. L.; Rodríguez-Hornedo, N.; Reddy, L. S.; Jayasankar, A.; Maheshwari, C.; McCausland, L.; Shipplett, R.; Stahly, B. C. *CrystEngComm* **2008**, *10*, 856–864.
(36) Jacques, J.; Wilen, S. H. *Enantiomers, Racemates, and Resolution*; Krieger Publishing Company: Malabar, FL, 1991.
(37) Klussmann, M.; White, A. J. P.; Armstrong, A.; Blackmond, D. G. *Angew. Chem., Int. Ed.* **2006**, *45*, 7985–7989.
(38) Glasstone, S. *Textbook of Physical Chemistry*, 2nd ed.; MacMillan: London, 1948.
(39) Grant, D. J. W.; Higuchi, T. *Solubility Behavior of Organic Compounds*; Wiley: New York, 1990.
(40) Bethune, S. J. Thermodynamic and kinetic parameters that explain solubility and crystallization of pharmaceutical cocrystals. Ph.D. Thesis, University of Michigan, Ann Arbor, MI, 2008.
(41) Nehm, S. J.; Jayasankar, A.; Rodríguez-Hornedo, N. *AAPS J.* **2006**; abstract W5205.
(42) Young, P. H.; Schall, C. A. *Thermochim. Acta* **2001**, *367–368*, 387–392.
(43) Schultheiss, N.; Newman, A. *Cryst. Growth. Des.* **2009**, *9*, 2950–2967.
(44) Ghosh, S.; Bag, P. P.; Reddy, C. M. *Cryst. Growth. Des.* **2011**, *11*, 3489–3503.
(45) Bucar, D. K.; Day, G. M.; Halasz, I.; Zhang, G. G. Z.; Sander, J. R. G.; Reid, D. G.; MacGillivary, L. R.; Duer, M. J.; Jones, W. *Chem. Sci.* **2013**, *4*, 4417–4425.
(46) Aitipamula, S.; Chow, P. S.; Tan, R. B. H. *CrystEngComm* **2009**, *11*, 1823–1827.
(47) Adalder, T. K.; Sankolli, R.; Dastidar, P. *Cryst. Growth. Des.* **2012**, *12*, 2533–2542.
(48) Raghavan, K.; Dwivedi, A.; Campbell, G. C.; Johnston, E.; Levorse, D.; McCauley, J.; Hussain, M. *Pharm. Res.* **2003**, *10* (6), 900–904.
(49) Villepin, J.; de Novak, A. *Spectrochim. Acta Part A* **1971**, *34*, 1259–1270.
(50) Mukherjee, K. M.; Misra, T. N. *J. Raman Spectrosc.* **1996**, *27*, 595–600.
(51) Koczon, P.; Dobrowolski, J. C. Z.; Lewandowski, W.; Mazurek, A. P. *J. Mol. Struct.* **2003**, *655*, 89–95.
(52) Sala, O.; Gonc-alves, N. S.; Noda, L. K. *J. Mol. Struct.* **2001**, *565–566*, 411–416.

(53) Ali, H. R. H.; Alhalaweh, A.; Velaga, S. P. *Anal. Chim. Acta* **2008**, *620*, 103−112.

(54) Goud, N. R.; Khan, R. A.; Nangia, A. *CrystEngComm* **2014**, *16*, 5859−5869.

(55) Good, D. J.; Rodríguez-Hornedo, N. *Cryst. Growth. Des.* **2009**, *9*, 2252−2264.

4486

dx.doi.org/10.1021/cg500560w | *Cryst. Growth Des.* 2014, 14, 4475−4486

Research Paper

Co-milling of telmisartan with poly(vinyl alcohol) – An alkalinizer free green approach to ensure its bioavailability

Jinu Isaac, Swastika Ganguly, Animesh Ghosh *

Department of Pharmaceutical Sciences and Technology, Birla Institute of Technology, Mesra, Ranchi, Jharkhand 835215, India

A B S T R A C T

The aim of this study was to enhance the dissolution and bioavailability of telmisartan (TLM), a poorly water soluble drug by co-milling approach. Physical mixtures of TLM and poly(vinyl alcohol) (PVA) were co-milled in a planetary micro mill in a dry condition by varying process parameters such as drug to polymer weight ratio, ball-to-powder weight ratio, and rotational speed. The co-milled products offered cumulative percentage dissolution of TLM above 75% in 30 min (CG 1 and CG2). These samples were characterized using field emission scanning electron microscopy (FE-SEM), powder X-ray diffraction (PXRD), differential scanning calorimetry (DSC) and Raman spectra analysis. Well-dispersed acicular shaped particles of TLM were observed in co-milled products. A mixture of crystalline and amorphous TLM with a particle size less than 1 μm was present in CG1. The particle size of TLM observed in CG2 was less than 2 μm. In addition to crystalline and amorphous form of TLM, defective/disordered crystals of TLM were also present in CG 2. Therefore, CG2 tablets exhibited poor stability. CG 1 tablets were found to be stable under accelerated stability test conditions. The relative bioavailability of TLM of CG 1 containing tablets in comparison with Micardis® was 93.92 ± 12.84% (in rabbits). Thus, co-milling of TLM with PVA proves to be a promising "alkalinizer free green approach" to ensure the dissolution and bioavailability of poorly water soluble TLM.

© 2016 Elsevier B.V. All rights reserved.

1. Introduction

Telmisartan (TLM), an angiotensin II receptor antagonist is widely prescribed for the treatment of hypertension [1,2]. It is crystalline in nature and belongs to biopharmaceutic classification II (poorly soluble and easily permeable) [3–5]. TLM is available in its free acid form and is readily ionizable in an alkaline pH. Thus, incorporation of alkalinizers such as sodium hydroxide, potassium hydroxide, and meglumine, into the dosage form of TLM (tablets), ensures its aqueous solubility and enhances its dissolution [6–8]. Most of these alkalinizers are corrosive in nature and can destroy body tissues on contact [9]. A study conducted by Tran et al. (2011) reported about the gastrointestinal adverse effect of Micardis® (Boehringer Ingelheim Pharmaceuticals, Inc.) on male Sprague-Dawley rats [10]. The results of the study showed that, Micardis® can cause disruption and degeneration of the duodenal and jejunal mucosal tissues, due to the presence of corrosive alkalinizer/s in this formulation. Most of the other techniques reported enhancement of dissolution of TLM are known to utilize organic solvents and therefore, are not environmental friendly [10–23]. Thus, the aim of this work was to enhance the dissolution of TLM and thereby ensure its bioavailability, without the incorporation/use of any of the alkalinizer and/or organic solvents.

One of the simplest environment friendly approaches to improve the dissolution of any drug particle is to reduce its particle size. Particle size reduction increases the surface to volume ratio of the particle and thereby increases the dissolution rate [24–27].

Particle size reduction of TLM was performed using a planetary micro mill. The cumulative percentage release (CPR) of TLM from tablets prepared using milled TLM was 50.11 ± 3.36% at 30 min and achieved saturation point. This was due to the fact that clustering/aggregation of particles of milled TLM results in reduction of effective surface area for dissolution (Supporting information – Preliminary Study 1 and Figs. S1–S4). Hydrophobicity of its surface also contributed to poor wettability. Milled TLM also exhibited poor processing properties (difficult to pour, adhesion to the wall of the jars during processing, etc.). Co-milling of active pharmaceutical ingredient (API) with hydrophilic polymers can be employed to overcome the difficulties associated with particle size reduction of only API and this has been reported for a number of APIs [28–39]. Zhong et al. reported the use of polymers such as polyethylene glycol 6000, polyvinyl pyrrolidone k30, poloxamer 188, hydroxy propyl β-cyclodextrin, microcrystalline cellulose

* Corresponding author. Tel.: +91 9470339587; fax: +91 6512275290.
  E-mail address: aghosh@bitmesra.ac.in (A. Ghosh).

and chitosan for cogrinding with TLM. From the study, it was concluded that only chitosan can solubilize TLM, owing to its ability to create an alkaline micro-environmental pH on the surface of the drug particle [40].

In this study, poly(vinyl alcohol) (PVA), a biocompatible hydrophilic polymer was selected as a co-milling excipient. PVA exhibits better hardness in its solid state and resistant to abrasion [41,42]. It is biodegradable, nontoxic and environmental friendly. The potentiality of PVA as a co-milling excipient for the improvement of the dissolution of poorly water soluble drug/s has not been reported till date.

2. Materials and methods

2.1. Materials

Polymorph A of Telmisartan (TLM), 99.7% pure was provided by Unichem Laboratories Ltd. (Himachal Pradesh, India) as a gift sample. Physicochemical properties of telmisartan (Polymorph A) are enlisted in Supporting Information Table. S1. Poly(vinyl alcohol) (PVA) (87–90% hydrolyzed, average molecular weight 30,000–70,000) was purchased from Sigma–Aldrich Co., USA. All other excipients and chemicals utilized in this study were either of pharmaceutical or of analytical grade and were used as received.

2.2. Methods

2.2.1. Ball milling

Physical mixtures of TLM and PVA were prepared by blending it in specified drug/polymer (D/P) ratios (12.5/87.5 w/w, 25/75 w/w and 50/50 w/w) in a mortar. In each case, 2 g of the physical mixture was loaded into a planetary micro mill (Fritsch GmbH Pulverisette 7, Idar-Oberstein, Germany), equipped with stainless steel jar and balls (weight and diameter of the each ball were 500 mg and 5 mm, respectively). The ball to powder weight ratio (BPR) and rotational speed were varied from 5:1 to 20:1 and 300 to 600 rpm, respectively. The duration of milling was specified in batch process (between 0.5 h and 9 h). In order to avoid possible overheating of the container, pause periods of 10 min were given after every 0.5 h of milling. Milling was performed under normal atmospheric condition. The TLM and PVA powders were also milled separately in the same equipment under the same conditions. All the products were stored in a desiccator until used.

2.2.2. Preparation of tablets

Tablets of TLM, milled TLM, physical mixtures (PMs) and co-milled products (CGs) containing TLM (equivalent to 40 mg) were prepared by blending it with starch (33% w/w) and directly compressible lactose (33% w/w). Then the powder blend was passed through 22 mesh screen. The homogeneity was ensured by blending uniformity study. Tablets were compressed using a rotary tablet compression machine (Cadmach, Ahmadabad, India). The diameter of the punch used was 13 mm. The tablet hardness was adjusted to 4 kg/cm^2. Tablet hardness was measured using Monsanto hardness tester (Campbell electronics, India).

2.2.3. HPLC analysis of TLM

The amount of TLM in the samples was measured by HPLC (Knaur, Germany) method. Analysis was performed by Eurospher 100-5, C-18 column (250 mm × 4.6 mm, 5 µ) at 1.0 mL/min flow rate with a mixture of 10 mM phosphate buffer:methanol (35:65 (v/v)) as mobile phase at 296 nm. The same HPLC method has been developed and validated for the quantitation of TLM (aceclofenac as an internal standard) from rabbit plasma. Plasma calibration curve showed excellent linearity with R^2 = 0.99 over the range of 20–1000 ng/mL.

2.2.4. Dissolution tests

The dissolution rates of tablets containing PMs (12.5/87.5 w/w, 25/75 w/w and 50/50 w/w) and corresponding CGs were investigated using type II USP dissolution test apparatus (TDT-08L Dissolution tester, Electrolab, Mumbai, India), in 900 mL 10 mM phosphate buffer solution (pH 6.8) at 37 ± 0.5 °C with a rotational speed of 75 rpm. The dissolution profile of the final products (CG 1 and CG 2 tablets) was compared to the dissolution profile of the reference product (Micardis®) by model independent mathematical approach as proposed by Moore and Flanner [43]. The similarity factor (f_2) values and dissolution efficiency (DE %) of tablets containing CG 1 and CG 2 in comparison with Micardis® tablets were calculated at 60 min [44]. The dissolution study of CG1 tablet, CG2 tablet and reference product (Micardis®) was also performed in 0.1 N HCl and phosphate buffer pH 4.5 for better understanding of the effect of medium on rate of dissolution.

2.2.5. Characterization of CGs

2.2.5.1. Particle characteristics by field emission scanning electron microscopy (FE-SEM).
The morphology of the TLM, milled TLM, PM 1, CG 1, PM 2 and CG 2 was examined by FE-SEM (Supra 55; Carl Zeiss, Germany) under different magnifications (5 K, 10 K, 20 K, 40 K and 60 K). The samples were coated with platinum to increase the conductivity of the electron beam. The operating conditions were at an accelerating voltage of 4 kV, with a working distance of 5–6 mm at a spot size of 45. In each case, size of 300 particles was measured by using ImageJ software (NIH, USA) [45].

2.2.5.2. Optical contact angle (OCA) and surface free energy (SFE) measurement.
Wettability of TLM, milled TLM, PVA, PM 1, CG 1, PM 2 and CG 2 was determined by contact angle measurement, using a video based contact angle meter OCA 20 (DataPhysics, Germany), attached to a camera. Before measurement, the samples were prepared by making flat surface compacts of powder. Compacts of powder were prepared by using a hydraulic press (Technosearch Instruments, India) at a pressure of 100 kg/cm^2 for a time period of 15 mins. The size of the die used was 13 mm. Millipore® grade distilled water (liquid surface tension (γ_1) = 72.8 mJ/m^2) was used as the wetting liquid. The number of replicates was three. The surface free energy (SFE) was calculated using equation of state, Schultz Method-2, by means of Data Physics SCA20 software (Version 2.01).

2.2.5.3. Phase solubility study.
The phase solubility study of TLM from PM 1, CG 1, PM 2 and CG 2 was performed according to the method described by Higuchi and Connors [46]. Samples were placed in 100 mL volumetric flask containing 25 mL of phosphate buffer pH 6.8. The flasks were placed in a water bath-shaker (Remi Instruments, India) maintained at 37 ± 0.5 °C for 24 h. 5 mL of the supernatant from each flask was withdrawn and filtered through 0.22 µm nylon membrane filter. These filtrates were then diluted suitably and the concentration of TLM in each case was analyzed by HPLC method.

2.2.5.4. Analysis of solid state changes of TLM.
2.2.5.4.1. Powder X-ray diffraction (PXRD).
PXRD pattern of TLM, PVA, PM 1, CG 1, PM 2 and CG 2 (300 mg each) (under size material of 60 mesh) was recorded to determine the crystallinity changes and/or polymorphic transformations if any, by using an X-ray diffractometer (Bruker AXS D8 Advance, Configuration: Vertical, Theta/2 Theta geometry; Rheinstetten, Germany). X-ray source was Cu, wavelength 1.5406 Å, detector: Si (Li) PSD. The diffractograms were recorded at a scanning speed of 2°/min and a chart

speed of 2°/2 cm per 2 theta and the angular range fixed was from 3° to 80°.

2.2.5.4.2. Thermal analysis. Differential scanning calorimetry (DSC) of all the samples was performed using a DSC-60 instrument (Shimadzu). The thermograms were recorded at a heating rate of 10 °C/min in the range of 25 °C to 300 °C in a nitrogen atmosphere (flow rate 20 mL/min) using TA60-WS software (Shimadzu).

Thermo gravimetric analysis (TGA) was performed using a DTG-60 instrument (Shimadzu) at a heating rate of 10 °C/min from 10 °C to 550 °C in a nitrogen atmosphere (flow rate 20 mL/min) using TA60-WS software (Shimadzu).

2.2.5.4.3. Raman spectroscopy. Raman spectra of all the samples were obtained using a Raman microscope (Renishaw plc) with 785 nm stabilized diode excitation. The lower power at the sample was approximately 10 mW. A 50× objective lens was used, giving a laser spot diameter (foot print) of 2 μm at the sample. Spectra were obtained for 10 s exposure of the argon detector in the region 3200–50 cm^{-1}, using an external scanning mode of the instrument.

2.2.5.4.4. Drug–polymer interaction study by Fourier transform infrared (FT-IR) spectroscopy. FT-IR spectra of all the samples were measured using an FTIR-8400S instrument (Shimadzu, Kyoto, Japan). A small amount of each material was triturated with KBr (1 weight% drug content) and placed into a sample holder for analysis. The spectrum was scanned over a range of 400–4000 cm^{-1} at a resolution of 2 cm^{-1} with scan speed of 64 scan/s and was recorded by using IRSolution software (Shimadzu, Kyoto, Japan).

2.2.6. Stability study

The tablets containing CG 1 and CG 2 were subjected to accelerated stability study as per International Conference on Harmonization (ICH) guidelines (Q1E, Step4) at 40 ± 2 °C/75 ± 5% relative humidity in stability chamber (Thermolab Scientific Equipments, India) [47]. The CGs were also subjected to stability studies under the same conditions. The samples were withdrawn after 180 days and evaluated for different parameters viz; appearance, drug content and the *in-vitro* drug release. The DSC study and PXRD study of the CGs were carried out to check physicochemical stability of TLM under stressed condition.

2.2.7. Statistical analysis

Statistical test such as Kruskal–Wallis was applied for comparison among various treatment groups in all cases by GraphPad Prism® software (Version 5.0, GraphPad Inc., USA) [48]. Differences in rank sum of the means of individual groups were performed using Dunn's Multiple Comparison test. A significance level of $p < 0.05$ was denoted in all cases.

2.2.8. In-vivo pharmacokinetic study

A single-dose pharmacokinetic study was conducted on white albino rabbits in accordance with the protocol approved by the Institutional Animal Ethics Committee (CPCSEA approval No: 621/02/ac/CPCSEA) vide a ref. No: BIT/PH/IAEC/38/2011 dated December, 2011 at Department of Pharmaceutical Sciences and Technology, Birla Institute of Technology, Mesra, Ranchi, India. Group-I and Group-II rabbits were administered TLM suspension prepared by marketed formulation (Micardis®) and CG 1 tablets (dose = 1 mg/kg in both cases), respectively by oral gastric intubation. After the administration, 1.0 mL of blood samples was collected from the marginal ear vein at 0, 1, 2, 3, 4, 5, 6, 7, 8, 10, 12 and 24 h into K_2EDTA vial (Mediquip, India). The pharmacokinetic parameters (C_{max}, T_{max}, AUC_{0-t}, $AUC_{0-\infty}$, AUMC, k_{el} and $t_{1/2}$,) were calculated using Microsoft Office Excel 2010® (Microsoft Corporation USA) software application. Paired *t*-test was performed for all pharmacokinetic parameters at a 95% significance level ($P < 0.05$) [49].

3. Results and discussion

3.1. Co-milling

The co-milling of TLM and PVA was carried out as per the scheme given in Fig. 1. The planetary micro mill used here consists of two stainless steel jars (drums) with stainless steel balls in it. Upon working, these jars rotate around the central axis and simultaneously around their own axis in an opposite direction (like the planetary motion around the sun). Such a movement confers high kinetic energy to balls and this aids to exert high impact and pressure to the loaded material. Thus, hard-brittle materials such as TLM and PVA are pulverized better in a planetary type ball mill [50,51].

The primary goal of co-milling of TLM with PVA was to achieve maximum particle size reduction by avoiding agglomeration of micronized particles leading to improve dissolution. A cumulative percent release (CPR) of 75% within 30 min was the target. To achieve this target, we tried to find out maximum D/P ratio and minimum process parameters viz; duration of milling, BPR and rotational speed. The results of the various batches co-milled by varying the D/P ratio, BPR, rotational speed and duration are shown in Table 1. From the results obtained, it was unambiguous that D/P ratio, BPR and rotational speed affect on CPR of TLM. The optimum parameters were found to be BPR 15:1, rotational speed of 600 rpm and duration of milling 3 h for achieving the dissolution of TLM above 75% in 30 min in case of 12.5/87.5 w/w ratio (CG 1). It was also found that with the same process parameters, 5 h milling was optimum for 25/75 w/w ratio (CG 2).

The CPR of TLM at 30 min, from CG 1 tablet, CG 2 tablet and the reference product (Micardis®) was 96.57 ± 2.02, 80.36 ± 5.84, and 91.37 ± 2.07, respectively. The complete release profiles of the final products and the reference product are shown in Fig. 2. The dissolution efficiency is defined as "the area under dissolution curve up to a certain time (*t*), expressed as percentage of area of the rectangle described by 100% dissolution in the same time" [44]. The dissolution efficiencies at 60 min (DE %) of CG 1 tablet, CG 2 tablet and Micardis® were 80.26 ± 3.73, 68.62 ± 3.68 and 73.64 ± 1.51, respectively. The similarity factor (f_2) of CG 1 and CG 2 tablets, to Micardis® was 58.23 and 61.93, respectively. The dissolution profiles of TLM from CG1 tablet, CG2 tablet, and Micardis® in 0.1 N HCl and phosphate buffer pH 4.5 are given in Fig. S5 and Fig. S6, respectively (Supporting information).

3.2. Characterization of CGs

The assay (by HPLC method) value of TLM (%) in CG 1 and CG 2 which were 99.30 ± 0.24 and 98.89 ± 0.09, respectively, revealed that there was no considerable degradation of drug. The optical contact angle (OCA) and the surface free energy (SFE) of PM 1,
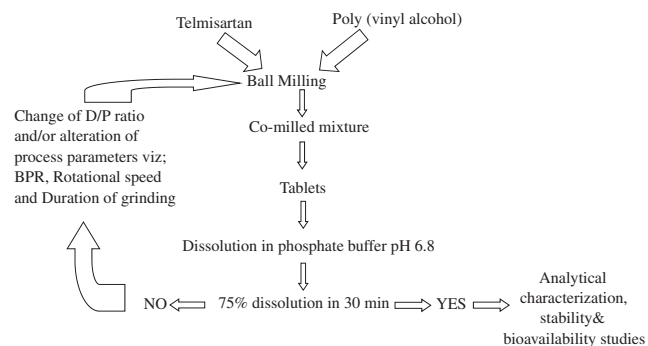

Fig. 1. Flowchart of the co-milling process.

Table 1
Description of D/P ratios, process parameters used for the preparation of co-milled mixtures (CGs) and dissolution pattern from the tablets prepared using each CG.

S. No.	D/P ratio (w/w)	BPR (w/w)	RS (rpm)	Time (h)	Cumulative percentage release (CPR)			
					15 min	30 min	45 min	60 min
a. Preliminary batches and dissolution pattern from them								
1	100/0	–	–	–	5.55 ± 0.99	5.50 ± 0.19	6.07 ± 0.29	6.10 ± 0.05
2	25/75	5:1	300	3	16.86 ± 4.54	23.28 ± 3.43	27.61 ± 5.08	29.80 ± 6.02
3	25/75	10:1	300	3	21.49 ± 1.25	30.57 ± 2.33	40.68 ± 2.48	44.91 ± 2.66
4	25/75	10:1	600	3	43.81 ± 3.81	56.19 ± 5.56	59.92 ± 2.97	61.66 ± 3.03
5	25/75	15:1	600	3	49.52 ± 1.51	59.34 ± 4.21	62.88 ± 2.82	65.59 ± 2.09
6	12.5/87.5	15:1	600	3	77.86 ± 9.32	96.57 ± 2.02[*]	98.20 ± 1.16	96.78 ± 6.40
8	50/50	15:1	600	3	17.83 ± 0.77	22.20 ± 0.69	25.00 ± 0.66	27.10 ± 1.26
b. Effect of reduction in duration of grinding on dissolution of CG 12.5/87.5 w/w								
9	12.5/87.5	15:1	600	2	53.49 ± 12.10	71.45 ± 14.99	75.62 ± 6.57	78.33 ± 5.08
10	12.5/87.5	15:1	600	1	44.92 ± 8.51	56.74 ± 7.85	63.93 ± 5.56	67.97 ± 3.82
11	12.5/87.5	15:1	600	0.5	34.95 ± 4.41	45.19 ± 4.30	50.91 ± 7.52	52.29 ± 6.01
12	12.5/87.5	–	–	0	10.23 ± 1.50	13.10 ± 1.14	16.83 ± 1.88	19.17 ± 1.80
c. Effect of reduction of rotational speed on dissolution of CG 12.5/87.5 w/w								
13	12.5/87.5	15:1	450	3	28.35 ± 5.94	45.35 ± 9.51	55.14 ± 7.15	59.69 ± 5.26
14	12.5/87.5	15:1	300	3	25.86 ± 1.05	36.34 ± 0.22	42.97 ± 0.13	44.98 ± 1.27
d. Effect of BPR on dissolution of CG 12.5/87.5 w/w								
15	12.5/87.5	20:1	600	3	75.66 ± 7.00	85.93 ± 4.67	88.99 ± 3.22	89.44 ± 1.82
16	12.5/87.5	10:1	600	3	45.98 ± 3.61	65.89 ± 6.44	74.75 ± 4.83	80.75 ± 3.59
17	12.5/87.5	5:1	600	3	19.61 ± 1.81	25.18 ± 2.53	27.67 ± 2.60	29.95 ± 2.57
e. Effect of duration of grinding on dissolution of CG 25/75 w/w								
18	25/75	–	–	0	5.12 ± 0.42	7.18 ± 0.52	8.59 ± 1.17	9.00 ± 0.52
19	25/75	15:1	600	3	49.52 ± 1.51	59.34 ± 4.21	62.88 ± 2.82	65.59 ± 2.09
20	25/75	15:1	600	4	46.72 ± 7.02	70.44 ± 14.43	71.21 ± 9.42	76.01 ± 6.79
21	25/75	15:1	600	5	62.49 ± 3.49	80.36 ± 5.84[*]	87.87 ± 3.95	87.49 ± 4.31
22	25/75	15:1	600	7	44.18 ± 9.25	59.22 ± 1.98	70.28 ± 4.55	73.69 ± 1.10
23	25/75	15:1	600	9	46.55 ± 2.85	65.58 ± 0.81	75.29 ± 0.40	83.73 ± 0.70
f. Effect of duration of grinding on dissolution of CG 50/50 w/w								
25	50/50	15:1	600	5	30.83 ± 1.31	37.42 ± 3.49	42.46 ± 6.81	43.09 ± 5.79
26	50/50	15:1	600	7	44.15 ± 5.11	57.74 ± 5.58	64.07 ± 5.65	68.40 ± 5.98
27	50/50	15:1	600	9	30.09 ± 1.89	43.42 ± 3.00	53.30 ± 3.43	62.19 ± 2.53

All values are expressed in mean ± SD, *n* = 3. **D/P ratio** = drug to polymer ratio, **BPR** = ball to powder weight ratio, **RS** = rotational speed.
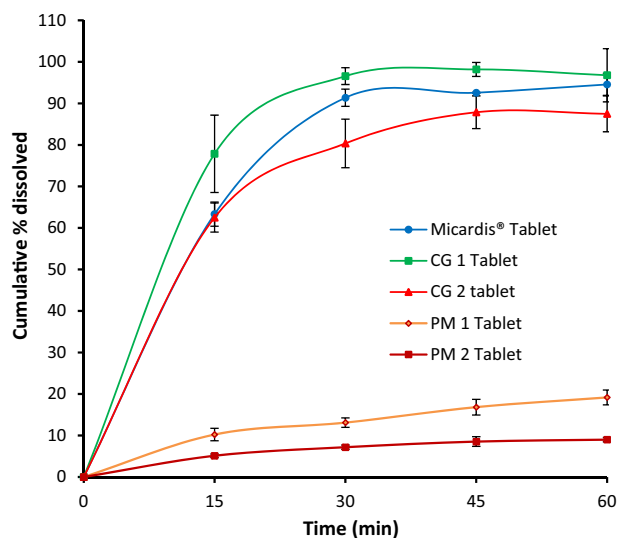[*] Significant ($p < 0.05$).

Fig. 2. Dissolution profile of TLM tablets (Dose = 40 mg) prepared using PM 1, PM 2, CG 1 CG 2 and Micardis® 40 mg tablet.

Table 2
The optical contact angle (OCA) and surface free energy (SFE) of physical mixtures and co-milled products.

Sample	OCA (°)	SFE (mN/m)
PM 1	61.52 ± 1.83	45.15 ± 1.35
CG 1	63.76 ± 0.71	46.87 ± 0.52
PM 2	68.17 ± 1.89	40.75 ± 1.41
CG 2	73.16 ± 1.68	41.11 ± 0.95

All values are expressed in mean ± SD, *n* = 3. **PM 1**: physical mixture of TLM and PVA in D/P ratio of 12.5/87.5 w/w; **CG 1**: PM 1 milled for 3 h at rotational speed of 600 rpm and BPR 15:1; **PM 2**: physical mixture of TLM and PVA in D/P ratio of 25/75 w/w; **CG2**: PM 2 milled for 5 h at rotational speed of 600 rpm and BPR 15:1.

PM 2, CG 1 and CG 2 are given in Table 2 (the representative images of OCA are given in Supporting information – Fig. S7). The difference in the OCA and SFE between the PMs and corresponding CGs was not significant, indicating that the wetting action exerted by PVA in PMs and their corresponding CGs were almost same. The phase solubility of TLM (in phosphate buffer pH 6.8) from PM 1, CG 1, PM 2 and CG 2 was 5.93 ± 0.22 µg/mL, 43.80 ± 7.57 µg/mL, 5.25 ± 0.24 µg/mL and 21.08 ± 0.44 µg/mL, respectively. There were no significant differences in phase solubility of the TLM from PM 1 and PM 2, which indicated that there was no influence of polymer content on phase solubility of TLM. The phase solubility of TLM from CG 1 and CG 2 in phosphate buffer pH 6.8 was higher than that of respective PMs.

FE-SEM images of TLM particles present in CG 1 and CG 2 at 60 K magnification and frequency percentage size distribution are shown in Fig. 3. (FE-SEM images of CG 1 and CG 2 at lower magnifications are given in Supporting information – Fig. S8.)

It was evident from the FE-SEM images that particle size of TLM was decreased and the particles were well-dispersed in the co-milled products. The acicular shape of the TLM crystals (Supporting information – Fig. S1) was retained in both CGs. Owing to the fact that, upon milling the crystals of TLM were cleaved at the weakest lattice plane sides, so along with particle size reduction the shape
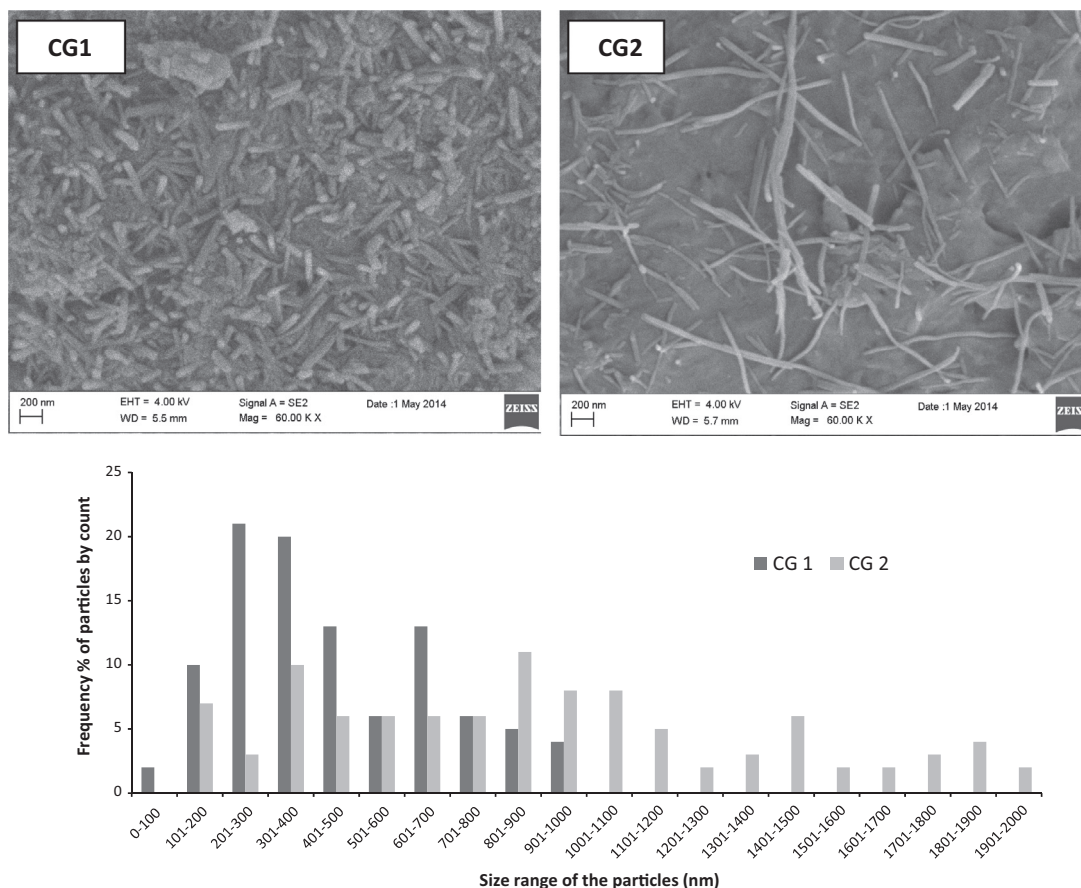
Fig. 3. FE-SEM images of CG 1 and CG 2, and histogram of size distribution of TLM particles in CG 1 and CG 2.

of the crystals was retained [52,53]. The length of the TLM particles found in CG 1 was in submicron level (<1 μm), whereas the length of the particles found in CG 2 was below 2 μm. This difference in the extent of drug particle size reduction was the primary reason for difference in dissolution rate between the tablets of CG 1 and CG 2. There were no shift in IR absorption peaks of either TLM or PVA in FT-IR study in case of both PMs and CGs, indicated the compatibility between drug and polymer (Supporting information – Fig. S9).

The physical changes of TLM, that might have happened during high energy milling process, such as amorphization and polymorphic transformation if any, cannot be ignored because, these changes can contribute to alter its pharmaceutical properties such as dissolution. In order to trace any of such physical changes of TLM as a result of co-milling with PVA, CG 1 and CG 2 were characterized with the help of PXRD, DSC and Raman spectroscopic studies in comparison with corresponding PMs (PM 1 and PM 2, respectively) and pure crystalline TLM. The results of these studies are presented in Figs. 4–6, respectively.

PM 1 and PM 2 showed a similar phenomenon on PXRD, DSC and Raman spectroscopic analyses, which were related to both the crystalline TLM (polymorph A) and semi crystalline PVA. However, the unsurpassed results obtained in case of CG 1 and CG 2 indicated the unique physical changes that have taken place during co-milling.

3.3. Physical changes of TLM in CG 1

In the PXRD of TLM, the signature peaks were observed at 2θ 6.87° and 14.20°. In case of PM 1, the signature peaks of TLM were observed at 2θ 6.85° and 14.22°. The intensity of these signature peaks of TLM in CG1 was very less and was not at all traceable due to high noise level. In order to decrease the noise level, PXRD of CG1 was performed by increasing the counting time per step. It was shown from Fig. S10 (Supporting information) that the peaks of crystalline TLM at the respective 2θ were detectable. The retention of these signature peaks indicated the presence of the crystalline TLM in CG 1.

The onset of melting, transition midpoint (T_m) and melting enthalpy values of TLM derived from DSC thermogram of CG 1 were 214.29 °C, 237.22 °C and 14.22 J/g, respectively. The lower values of all these parameters when compared to pure TLM or PM 1 (Table. 3) indicated the presence of TLM particles with reduced crystallinity and/or particle size in CG1 [53–55]. The significantly reduced enthalpy value of the TLM in CG 1 was attributed to the increased entropy of submicron sized TLM particles (as a result of the increased surface fraction of atoms in it) [53–55]. CG 1 being produced by high energy milling, it is legitimate to have at least some amorphous TLM along with it. However, in the DSC thermogram of CG1, glass transition event corresponding to amorphous TLM ($\sim$128 °C), was not detected [12]. This non-traceability of glass transition temperature (T_g) could have also been due to an excess quantity of PVA in the sample. In order to generate traceable quantity of amorphous TLM in the co-milled product, TLM and PVA in same D/P ratio (12.5/87.5 w/w) were co-milled for a longer period of time (5 h) with same process parameters (BPR 15:1, rotational speed 600 rpm). Upon DSC analysis of this co-milled sample, a glass transition event was noticed with a T_g of 129.64 °C and T_m of crystalline TLM was hardly detected (Supporting information – Fig. S11). This result indicated that the duration
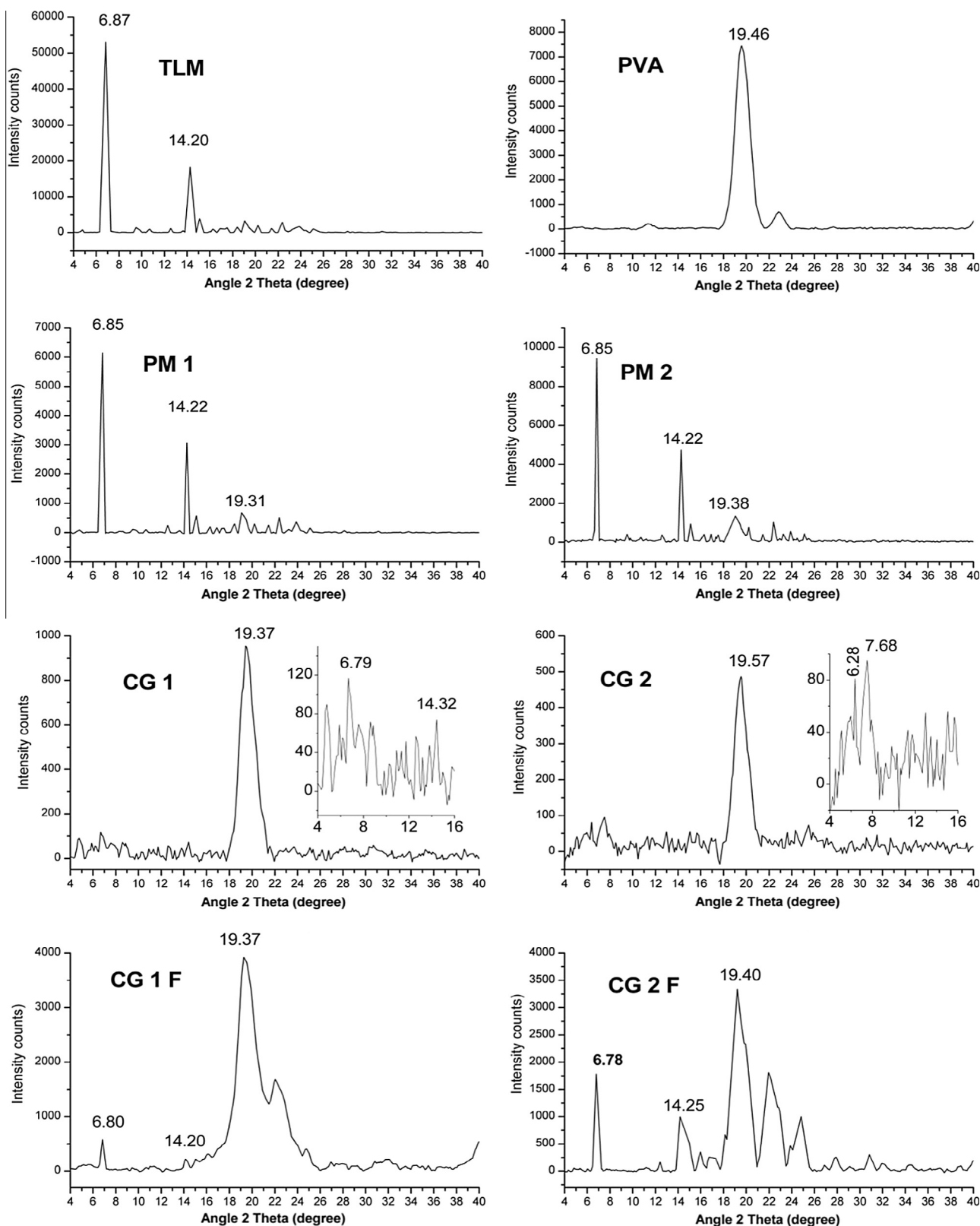
Fig. 4. Powder X-ray diffractograms of tested samples. **TLM**: telmisartan; **PVA**: poly(vinyl alcohol); **PM 1**: physical mixture of TLM and PVA in D/P ratio of 12.5/87.5 w/w; **CG 1**: PM 1 milled for 3 h at rotational speed of 600 rpm and BPR 15:1; **CG 1 F**: CG 1 exposed to high temperature (120 °C) for 24 h; **PM 2**: physical mixture of TLM and PVA in D/P ratio of 25/75 w/w; **CG2**: PM 2 milled for 5 h at rotational speed of 600 rpm and BPR 15:1; **CG 2 F**: CG 2 exposed to high temperature (120 °C) for 24 h.

of co-milling affected the amorphization of TLM. Therefore, the amorphous content in a sample ground for 3 h (i.e. in CG 1) might have been less so as to detect it by DSC techniques.

Raman spectra of PM 1 and CG 1 showed all the characteristic peaks of crystalline TLM. Slight shifts in position of Raman peaks indicated that the average chemical environment in "TLM crystal"
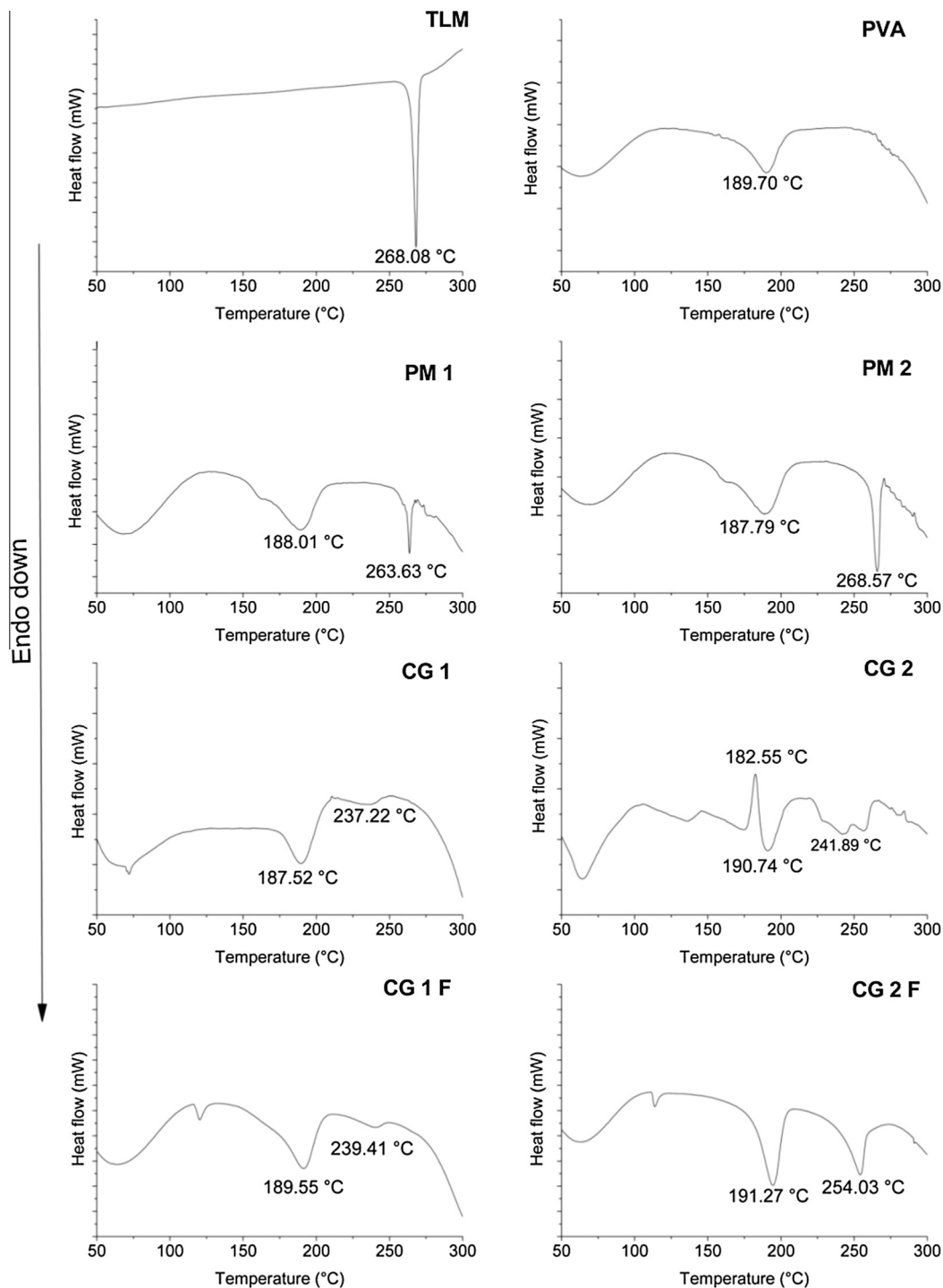
Fig. 5. DSC thermograms of tested samples. **TLM**: telmisartan; **PVA**: poly(vinyl alcohol); **PM 1**: physical mixture of TLM and PVA in D/P ratio of 12.5/87.5 w/w; **CG 1**: PM 1 milled for 3 h at rotational speed of 600 rpm and BPR 15:1; **CG 1 F**: CG 1 exposed to high temperature (120 °C) for 24 h; **PM 2**: physical mixture of TLM and PVA in D/P ratio of 25/75 w/w; **CG2**: PM 2 milled for 5 h at rotational speed of 600 rpm and BPR 15:1; **CG 2 F**: CG 2 exposed to high temperature (120 °C) for 24 h.

was altered due to high energy mechanical processing. Broadening of Raman spectral peaks of the TLM in CG 1 than PM 1, indicated the presence of some amorphous TLM portion also in CG 1 [13,56,57]. All these observations indicated that the CG 1 contained a mixture of crystalline and amorphous TLM.

3.4. Physical changes of TLM in CG 2

In the PXRD of CG 2, peak positions of TLM were observed at 2θ 6.28° and 7.68°, which did not match with the signature peaks of

crystalline TLM (Fig. 4), which indicated the presence of disordered crystals of TLM [58–61].

The onset of melting, transition midpoint (T_m) and melting enthalpy values of the TLM in CG 2 was 223.40 °C, 241.89 °C and 76.67 J/g, respectively. Low values of these parameters of CG 2 in comparison with pure TLM or TLM present in PM 2 (Table 3) indicated the presence of TLM particles of lower size range with reduced crystallinity [53–55]. However, the decrease in enthalpy value was not as drastic as that observed in the case of CG1 vs PM 1. Glass transition of TLM (T_g = 116.15 °C) was also noticed in
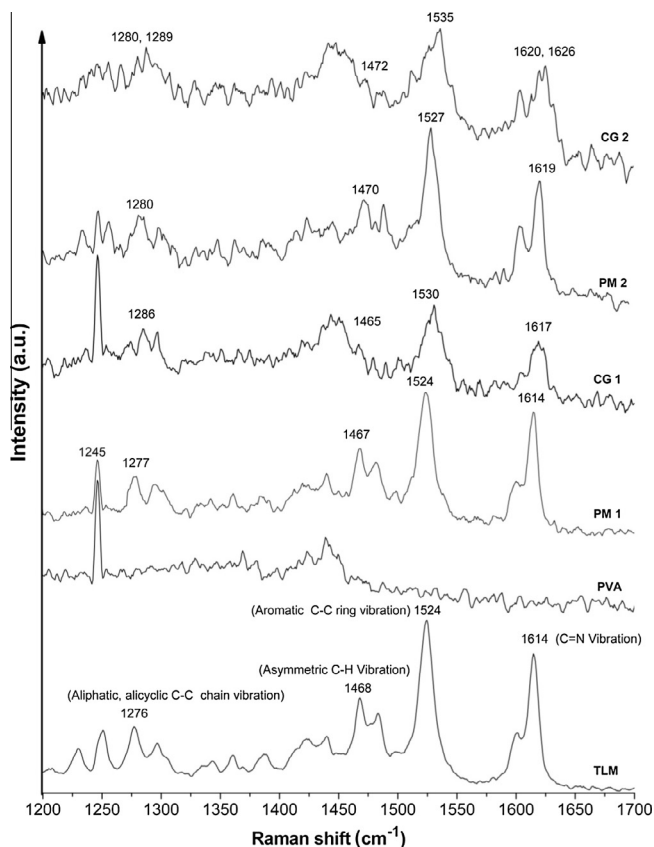
Fig. 6. Raman spectra of tested samples. **TLM**: telmisartan; **PVA**: poly(vinyl alcohol); **PM 1**: physical mixture of TLM and PVA in D/P ratio of 12.5/87.5 w/w; **CG 1**: PM 1 milled for 3 h at rotational speed of 600 rpm and BPR 15:1; **PM 2**: physical mixture of TLM and PVA in D/P ratio of 25/75 w/w; **CG2**: PM 2 milled for 5 h at rotational speed of 600 rpm and BPR 15:1.

Table 3
Endothermic events of telmisartan in the DSC thermogram of tested samples.

Sample	Onset of melting (°C)	T_m (°C)	Enthalpy (J/g)
TLM	264.85	268.08	102.38
PM 1	261.79	263.63	98.85
CG 1	214.29	237.22	14.22
PM 2	261.05	268.57	99.17
CG 2	223.40	241.89	76.67
CG 1 F	224.29	239.41	26.80
CG 2 F	239.45	254.03	88.45

TLM: telmisartan; **PM 1**: physical mixture of TLM and PVA in D/P ratio of 12.5/87.5 w/w; **CG 1**: PM 1 milled for 3 h at rotational speed of 600 rpm and BPR 15:1; **CG 1 F**: CG 1 exposed to high temperature (120 °C) for 24 h; **PM 2**: physical mixture of TLM and PVA in D/P ratio of 25/75 w/w; **CG2**: PM 2 milled for 5 h at rotational speed of 600 rpm and BPR 15:1; **CG 2 F**: CG 2 exposed to high temperature (120 °C) for 24 h.

DSC thermogram of CG 2, which indicated the presence of detectable quantities of the amorphous TLM in this sample. An exothermic event at 182.55 °C was detected in DSC thermogram of CG 2. There was no weight loss at this temperature region upon TGA of CG 2 (Supporting information – Fig. S12), which proved that this exothermic peak in the DSC thermogram of CG 2 was corresponding to recrystallization of disordered crystals or amorphous form of TLM.

Though, the Raman spectral observations of CG 2 indicated the retention of the crystalline nature of TLM, the occurrence of additional peaks at 1289 cm^{-1} (C–C chain vibration) and 1626 cm^{-1} (C=N stretching), further confirmed the presence of disordered crystals of TLM in it. This assumption was drawn on the basis of the fact that, the frequency (in the region of 1200–1700 cm^{-1}) of

lattice phonon vibrations of TLM molecules present in the crystal is very specific and is sensitive to differences in molecular level packing of it in the crystal [56,57]. From these studies, it was concluded that a mixture of crystals, disordered crystals and amorphous form of TLM was present in CG 2.

Further, both CG 1 and CG 2 were subjected to heating at 120 °C for 24 h in a laboratory furnace and cooled at normal atmospheric conditions (coded as CG 1 F and CG 2 F, respectively). This experiment was based on the conviction that defective crystals of TLM if any, in the CGs, shall regain its crystallinity upon exposure to higher temperature for longer period of time. The process of crystal growth by Ostwald ripening, may also take place as a result of exposing it to a higher temperature for a longer period of time [62].

3.5. Thermal behavior, PXRD and dissolution of CG 1 F and CG 2 F

In the DSC thermogram of CG 2 F, no exothermic event was observed. The onset of melting, T_m and enthalpy of the TLM present in CG 2 F were 239.45 °C, 254.03 °C and 88.45 J/g, respectively. These parameters were higher than those of CG 2. In the PXRD of CG 2 F, the signature peaks of TLM were observed at 2θ 6.78° and 14.25° with good intensity. The rate and extent of dissolution of TLM from the tablets containing CG 2 F were less than those of CG 2 (Supporting information – Fig. S13). These results indicated that the defective crystals of TLM presented in CG 2 had regained its crystalline nature to a greater extent, when subjected to heat at elevated temperature for a longer period of time.

In the DSC thermogram of CG 1 F, the onset of melting, T_m and melting enthalpy values of TLM were 224.29 °C, 239.41 °C and 26.80 J/g, respectively. The marker peaks of TLM were observed at 2θ 6.83° and 14.21°. Though, the CPR from the CG 1 F containing tablets was decreased, it was not that drastic as in the case of tablets containing CG 2 F (Supporting information – Fig. S14). These results indicated that the regained crystallinity of the TLM in CG 2 F was greater than CG 1 F. These observations also indicated that the rate of the Ostwald ripening process of TLM was slower in case of CG 1 F in contrast to CG 2 F, where disordered crystals of TLM were present. It may also be attributed to the fact that the submicron sized crystals without crystal disorder are more stable than those of any disordered crystals [61,62]. Thus, CG1 was more stable than CG2 under elevated temperature.

3.6. Stability study

The stability samples (CG 1 and CG 2 and their tablets), showed negligible or no changes in different parameters viz; appearance
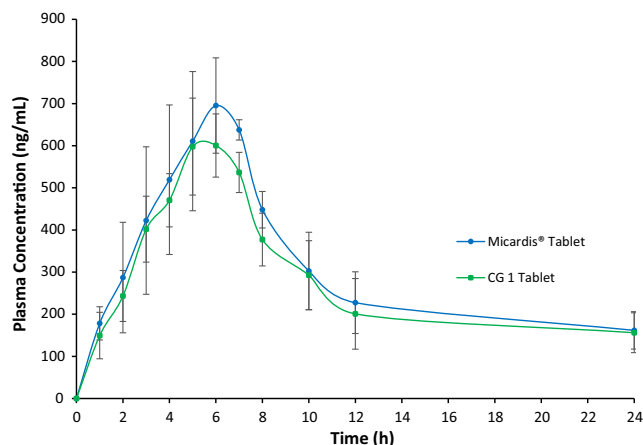

Fig. 7. Mean plasma drug concentration *vs* time profile after administration of Micardis® and CG 1 tablets to white albino rabbits (*n* = 3).

Table 4
Pharmacokinetic parameters after administration of Micardis® and CG 1 tablets to white albino rabbits ($n = 3$).

Formulation		C_{max} (ng/mL)	T_{max} (h)	AUC_{0-t} (ng h/mL)	$AUC_{0-\infty}$ (ng h/mL)	k_{el} (h^{-1})	$t_{1/2}$ (h)	AUMC (ng h^2/mL)	MRT (h)	RBA (%)
Micardis®	Avg	723.01	6.33	7190.95	9478.58	0.08	9.35	69612.39	9.66	–
	±S.D.	70.97	0.58	503.47	1612.34	0.02	2.48	11988.28	1.24	–
	SE	40.97	0.33	290.68	930.88	0.01	1.43	6921.44	0.72	–
	CV%	9.82	9.12	7.00	17.01	23.12	26.55	17.22	12.87	–
CG 1 tablet	Avg	659.72	6.00	6494.11	8906.62	0.07	10.10	63806.01	9.76	93.92
	±S.D.	64.28	1.00	723.12	2023.47	0.02	3.05	14009.58	1.13	12.84
	SE	37.11	0.58	417.49	1168.25	0.01	1.76	8088.44	0.65	7.41
	CV%	9.74	16.67	11.14	22.72	32.39	30.25	21.96	11.58	13.67

All values are expressed in mean ± S.D., $n = 3$.
* Significant ($p < 0.05$).
C_{max} = the maximum observed TLM concentration; T_{max} = the time at which C_{max} was observed; k_{el} = the first order elimination rate constant; $t_{1/2}$ = elimination half-life [$t_{1/2}$ = 0.693/k_{el}]; AUC_{0-t} = the area under plasma concentration time curve from zero to the last measurable plasma concentration at time t; $AUC_{0-\infty}$ = the area was extrapolated to infinity by addition of C_t/k_{el} to AUC_{0-t}, where C_t is the last detectable drug concentration; AUMC = area under first moment curve; MRT = mean residence time [AUMC/AUC]; RBA = relative bioavailability; Avg = Average; ±S.D. = standard deviation; SE = standard error of mean; CV% = coefficient of variation.

and drug content (data not shown). In the case of tablets of CG1 and CG2 subjected to stability study as per ICH guidelines, the CPR observed at 30 min was 81.22 ± 2.15% and 63.98 ± 5.59%, respectively (Supporting information – Fig. S15).

In the PXRD of CG 1, signature peaks of TLM were observed at 2θ 6.80° and 14.20°. The onset of melting and T_m and enthalpy of TLM obtained from the DSC thermogram of CG 1 stability samples were 233.34 °C, 239.65 °C and 24.99 J/g, respectively. In the PXRD of CG 2, the signature peak at 2θ 6.70° appeared with more intensity. The onset of melting, T_m and enthalpy of the TLM in the DSC thermogram of stability sample of CG 2 were 233.94 °C, 253.68 °C and 86.78 J/g. All these observations indicated that, under elevated temperature and humidity the disordered crystals of TLM present in the CG 2 regained its crystallinity to a certain extent, and this was the reason for the decreased CPR from the CG 2 tablets (stability samples). (PXRD and DSC of CG 1 and CG 2 stability samples are given in Supporting information – Figs. S16 and S17.)

Finally, it was concluded that TLM presented in CG 1 was more stable under accelerated stability test conditions due to its submicron crystalline form in contrast to disordered crystals of TLM presented in CG 2.

3.7. In-vivo pharmacokinetic study

The plasma concentrations of TLM after the administration of CG1 tablet and Micardis® were monitored for 24 h and are shown in Fig. 7. The pharmacokinetic parameters in each case were calculated by non-compartmental analysis and the results are enumerated in Table 4. The C_{max}, T_{max}, AUC_{0-t}, $AUC_{0-\infty}$, AUMC, k_{el}, $t_{1/2}$, and mean residence time (MRT) did not significantly differ from each other. The tablet containing CG 1 showed a relative bioavailability (RBA) of 93.92 ± 12.84% in comparison with Micardis®. Thus, the bioavailability of CG 1 tablet in rabbits is comparable to the bioavailability of the reference product (Micardis®).

4. Conclusion

Particle size reduction of TLM by neat milling results in clustering/aggregation of particles. The hydrophobicity of the milled TLM makes it difficult to dissolve effectively in an aqueous environment. Co-milling of TLM with PVA, a hydrophilic polymer resulted in an effective particle size reduction, absence of clustering and improved the wettability of TLM. The physical changes of the co-milling product of TLM were found to depend on D/P ratio and the process parameters used. The dissolution profiles of the final optimized products (CG 1 and CG 2 tablets) were comparable to those of dissolution profile of the reference product (Micardis®). Crystalline and amorphous form of TLM was present in CG1

whereas in CG2 disordered crystals of TLM were present in addition. Therefore, it was unstable under accelerated stability test conditions. The bioavailability of CG 1 tablet in rabbits was comparable to that of the reference product (Micardis®). Absence of use of any of the corrosive chemical agent/s in the formula, ensured the gastro-environmental friendliness of the product. As well as, co-milling being a simple and environment friendly particle engineering feat, this technique has to draw more attention from pharmaceutical formulation scientists from around the world who are striving hard to improve the dissolution of BCS class II drugs by particle engineering.

Declaration of Interest

The authors report no declarations of interest.

Acknowledgments

Appendix A. Supplementary material

Supplementary data associated with this article can be found, in the online version, at http://dx.doi.org/10.1016/j.ejpb.2016.01.016.

References

[1] W. Wienen, M. Entzeroth, J.C. Meel, J. Stangier, U. Busch, T. Ebner, et al., A review on telmisartan: a novel, long-acting angiotensin II-receptor antagonist, Cardiovasc. Drug Rev. 18 (2006) 127–154.

[2] U.J. Ries, G. Mihm, B. Narr, K.M. Hasselbach, H. Wittneben, M. Entzeroth, et al., 6-Substituted benzimidazoles as new nonpeptide angiotensin II receptor antagonists: synthesis, biological activity, and structure–activity relationships, J. Med. Chem. 36 (1993) 4040–4051.

[3] R.E. Dinnebier, P. Sieger, H. Nar, K. Shankland, W.I.F. David, Structural characterization of three crystalline modifications of telmisartan by single

crystal and high-resolution X-ray powder diffraction, J. Pharm. Sci. 89 (2000) 1465–1479.

[4] P. Laad, G. Shete, S.R. Modi, A.K. Bansal, Differential surface properties of commercial crystalline telmisartan samples, Eur. J. Pharm. Sci. 49 (2013) 109–116.

[5] J. Kausalya, K. Suresh, S. Padmapriya, B. Senthilnathan, Solubility and dissolution enhancement profile of telmisartan using various techniques, Int. J. PharmTech Res. 3 (2011) 1737–1749.

[6] N. Marasini, T.H. Tran, B.K. Poudel, H.J. Chou, Y.K. Choi, S.C. Chi, H.G. Choi, C.S. Yong, J.O. Kim, Fabrication and evaluation of pH-modulated solid dispersion for telmisartan by spray-drying technique, Int. J. Pharm. 441 (2013) 424–432.

[7] P.H.L. Tran, T.T.D. Tran, S.A. Lee, V.H. Nho, S.C. Chi, B.J. Lee, Roles of MgO release from polyethylene glycol 6000-based solid dispersions on microenvironmental pH, enhanced dissolution and reduced gastrointestinal damage of telmisartan, Arch. Pharm. Res. 34 (2011) 747–755.

[8] New Drug Application-20850, Centre for Drug Evaluation and Research USFDA, 1998.

[9] K. Ramasamy, V.V. Gumast, Corrosive ingestion in adults, J. Clin. Gastroentrol. 37 (2003) 119–124.

[10] L. Antoncic, A. Copar, Salt From of Telmisartan, US20090012140A1, 2005.

[11] H. Schneider, Polymorphs of Telmisartan, US 20020094997A1, 2002.

[12] P. Lepek, W. Sawicki, K. Wlodarski, Z. Wojnarowska, M. Paluch, L. Guzik, Effect of amorphization method on telmisartan solubility and the tableting process, Eur. J. Pharm. Biopharm. 83 (2013) 114–121.

[13] R. Dukeck, P. Sieger, P. Karmwar, Investigation and correlation of physical stability, dissolution behaviour and interaction parameter of amorphous solid dispersions of telmisartan: a drug development perspective, Eur. J. Pharm. Sci. 49 (2013) 723–731.

[14] A.R. Lekkala, K. Golla, S.R. Ganji, Amorphous Telmisartan, US 20060111417A1, 2006.

[15] F. Thomas, S. Gottfried, Method for the Preparation of Amorphous Telmisartan, EP1 854 454 B1, 2002.

[16] Y. Zhang, Z. Zhi, T. Jiang, J. Zhang, Z. Wang, S. Wang, Spherical mesoporous silica nanoparticles for loading and release of the poorly water-soluble drug telmisartan, J. Controlled Release 145 (2010) 257–263.

[17] J. Patel, K. Kevin, A. Patel, M. Raval, N. Sheth, Design and development of a self-nanoemulsifying drug delivery system for telmisartan for oral drug delivery, Int. J. Pharm. Investig. 1 (2011) 112–118.

[18] A. Bajaj, M.R.P. Rao, A. Pardeshi, D. Sali, Nanocrystallization by evaporative antisolvent technique for solubility and bioavailability enhancement of telmisartan, AAPS PharmSciTech 13 (2012) 1331–1340.

[19] P.A.A. Borba, M. Pinotti, C.E. Maduro de Campos, B.R. Pezzini, H.K. Stulzer, Sodium alginate as a potential carrier in solid dispersion formulations to enhance dissolution rate and apparent water solubility of BCS II drugs, Carbohydr. Polym. 137 (2016) 350–359.

[20] P.A.A. Borba, M. Pinotti, G.R.S. Andrade, N. Bezerra da Costa Jr., L.R. Olchanheski Junior, D. Fernandes, C.E. Maduro de Campos, H.K. Stulzer, The effect of mechanical grinding on the formation, crystalline changes and dissolution behaviour of the inclusion complex of telmisartan and β-cyclodextrins, Carbohydr. Polym. 133 (2015) 373–383.

[21] S. Jamadar, Y. Pore, F. Sayyad, Formation of amorphous telmisartan polymeric microparticles for improvement of physicochemical characteristics, Part. Sci. Technol. 32 (2014) 512–519.

[22] Hetal Patel, Hiral Patel, M. Gohel, S. Tiwari, Dissolution rate improvement of telmisartan through modified MCC pellets using 3^2 full factorial design, Saudi Pharm. J. (2015), http://dx.doi.org/10.1016/j.jsps.2015.03.007.

[23] Y. Zhang, J. Wang, X. Bai, T. Jiang, Q. Zhang, S. Wang, Mesoporous silica nanoparticles for increasing the oral bioavailability and permeation of poorly water soluble drugs, Mol. Pharm. 9 (2012) 505–513.

[24] J.H. Fincher, Particle size of drugs and its relationship to absorption and activity, J. Pharm. Sci. 57 (1968) 1825–1835.

[25] D. Hörter, J.B. Dressman, Influence of physicochemical properties on dissolution of drugs in the gastrointestinal tract, Adv. Drug Deliv. Rev. 46 (2001) 75–87.

[26] I. Colombo, G. Grassi, M. Grassi, Drug mechanochemical activation, J. Pharm. Sci. 98 (2009) 3961–3986.

[27] E.L. Parrott, Milling of pharmaceutical solids, J. Pharm. Sci. 63 (1974) 813–829.

[28] X. Han, C. Ghoroi, D. To, Y. Chen, R. Davé, Simultaneous micronization and surface modification for improvement of flow and dissolution of drug particles, Int. J. Pharm. 415 (2011) 185–195.

[29] M.K. Riekes, G. Kuminek, G.S. Rauber, C.E.M. de Campos, A.J. Bortoluzzi, H.K. Stulzer, HPMC as a potential enhancer of nimodipine biopharmaceutical properties via ball-milled solid dispersions, Carbohydr. Polym. 99 (2014) 474–482.

[30] K. Wlodarski, W. Sawicki, K.J. Paluch, L. Tajber, M. Grembecka, L. Hawelel, Z. Wojnarowska, K. Grzybowska, E. Talik, M. Paluch, The influence of amorphization methods on the apparent solubility and dissolution rate of tadalafil, Eur. J. Pharm. Sci. 62 (2014) 132–140.

[31] R.T.Y. Lim, W.K. Ng, R.B.H. Tan, Dissolution enhancement of indomethacin via amorphization using co-milling and supercritical coprecipitation processing, Powder Technol. 240 (2013) 79–87.

[32] T. Szunyogh, R. Ambrus, P. Szabó-révész, Nanonization of niflumic acid by co-grinding, Adv. Nanopart. 2 (2013) 329–335.

[33] Y. Inoue, T. Yamazoe, S. Watanabe, I. Murata, I. Kanamoto, Examination of intermolecular interaction as a result of cogrinding actarit and β-cyclodextrin, J. Incl. Phenom. Macrocycl. Chem. 78 (2013) 457–464.

[34] W. Limwikrant, M. Osada, K. Higashi, Y. Tozuka, Unique indomethacin nanoparticles formation by cogrinding with dextrin under defined moisture conditions, Powder Technol. 221 (2012) 213–219.

[35] V. Caron, L. Tajber, O.I. Corrigan, A.M. Healy, A comparison of spray drying and milling in the production of amorphous dispersions of sulfathiazole/polyvinylpyrrolidone and sulfadimidine/polyvinylpyrrolidone, Mol. Pharm. 8 (2011) 532–542.

[36] L. Kürti, Á. Kukovecz, G. Kozma, R. Ambrus, M.a. Deli, P. Szabó-Révész, Study of the parameters influencing the cogrinding process for the production of meloxicam nanoparticles, Powder Technol. 212 (2011) 210–217.

[37] M. Barzegar-jalali, H. Valizadeh, M.S. Shadbad, K. Adibkia, Cogrinding as an approach to enhance dissolution rate of a poorly water-soluble drug (gliclazide), Powder Technol. 197 (2010) 150–158.

[38] M. Vogt, K. Kunath, J.B. Dressman, Dissolution enhancement of fenofibrate by micronization, cogrinding and spray-drying: comparison with commercial preparations, Eur. J. Pharm. Biopharm. 68 (2008) 283–288.

[39] M. Vogt, K. Kunath, J.B. Dressman, Dissolution improvement of four poorly water soluble drugs by cogrinding with commonly used excipients, Eur. J. Pharm. Biopharm. 68 (2008) 330–337.

[40] L. Zhong, X. Zhu, X. Luo, W. Su, Dissolution properties and physical characterization of telmisartan-chitosan solid dispersions prepared by mechanochemical activation, AAPS PharmSciTech 14 (2013) 541–550.

[41] H.G. Brittain, Analytical Profiles of Drug Substances and Excipients, vol. 28, Academic Press, San Diego, 1998, pp. 397–431.

[42] R.C. Rowe, P.J. Sheskey, M.E. Quinn, Hand Book of Pharmaceutical Excipients, sixth ed., Pharmaceutical Press, London, 2009.

[43] J.W. Moore, H.H. Flanner, Mathematical comparison of dissolution profiles, Pharm. Technol. 20 (1996) 64–74.

[44] K.A. Khan, The concept of dissolution efficiency, J. Pharm. Pharmacol. 27 (1975) 48–49.

[45] C.A. Schneider, W.S. Rasband, K.W. Eliceiri, NIH Image to ImageJ: 25 years of image analysis, Nat. Methods 9 (2012) 671–675.

[46] T. Higuchi, K.A. Connors, Phase solubility techniques, Adv. Anal. Chem. Instrum. 4 (1965) 117–212.

[47] International conference on harmonization of technical requirements for registration of pharmaceuticals for human use, ICH harmonized tripartite guideline evaluation for stability data Q1E, current step 4 version, dated 6 February 2003.

[48] Graphpad Prism, Prism 5 for Windows, Version 5.0. (Trial). <http://www.Graphpad.Com> (last accessed on 29-07-2014).

[49] L. Shargel, S. Wu-Pong, A.B.C. Yu, Applied Biopharmaceutics and Pharmacokinetics, fifth ed., McGraw Hill Companies, Inc., New York, 2005.

[50] P. Balaz, Mechanochemistry in Nanoscience and Minerals Engineering, Springer-Verlag, Berlin, Heidelberg, 2008.

[51] L. Sheng-Yong, M. Qiong-Jing, P. Zheng, L. Xiao-Dong, Y. Jian-Hua, Simulation and energy transfer in a planetary ball mill, Chin. Phys. B 21 (2012). 078201-1–078201-9.

[52] L. Peltonen, J. Hirvonen, Pharmaceutical nanocrystals by nanomilling: critical process parameters, particle fracturing and stabilization methods, J. Pharm. Pharmacol. 62 (2010) 1569–1579.

[53] J.Y.Y. Heng, F. Thielmann, D.R. Williams, The effects of milling on the surface properties of form I paracetamol crystals, Pharm. Res. 23 (2006) 1918–1927.

[54] D. Hasa, D. Voinovich, B. Perissutti, G. Grassi, S. Fiorentino, R. Farra, M. Abrami, I. Colombo, M. Grassi, Reduction of melting temperature and enthalpy of drug crystals: theoretical aspects, Eur. J. Pharm. Sci. 50 (2013) 17–28.

[55] Q. Jiang, C.C. Yang, J.C. Li, Melting enthalpy depression of nanocrystals, Mater. Lett. 56 (2002) 1019–1021.

[56] A. Brillante, I. Bilotti, R.G. Della Valle, E. Venuti, A. Girlando, Probing polymorphs of organic semiconductors by lattice phonon Raman microscopy, CrystEngComm 10 (2008) 937–946.

[57] G. Gouadec, P. Colomban, Raman spectroscopy of nanomaterials: how spectra relate to disorder, particle size and mechanical properties, Prog. Cryst. Growth Charact. Mater. 53 (2007) 1–56.

[58] B. Fultz, J.M. Howe, Transmission Electron Microscopy and Diffractometry of Materials, Springer Science & Business Media, New York, 2007, pp. 1–59.

[59] J.D. Makinson, J.S. Lee, S.H. Magner, R.J. De Angelis, W.N. Weins, A.S. Hieronymus, X-ray diffraction-signatures of defects in nanocrystalline materials, JCPDS – Int. Centre Diffract. Data Adv. X-ray Anal. 42 (2000) 407–411.

[60] A. Guiner, X-ray Diffraction in Crystals, Imperfect Crystals and Amorphous Solids, General Publishing Company Ltd., Toronto, 1994.

[61] T. Feng, R. Pinal, M.T. Carvajal, Process induced disorder in crystalline materials: differentiating defective crystals from the amorphous form of griseofulvin, J. Pharm. Sci. 97 (2008) 3207–3221.

[62] G. Madras, B.J. McCoy, Temperature effects during Ostwald ripening, J. Chem. Phys. 119 (2003) 1683–1693.

REPORT OF THE WORK DONE

Objective: To enhance the solubility of ezetimibe by cocrystal engineering technique.

Abstract:

The present study illustrates the formation and characterization of three different cocrystals of ezetimibe using methyl paraben as a coformer, employing three different processes, namely solution crystallization, liquid assisted grinding and reaction crystallisation. Thermal analysis by DSC and TGA were used as a primary analytical tool, followed by spectroscopic and crystallographic study as a confirmatory analytical tool. Equilibrium aqueous solubility studies were performed for all cocrystals taking ezetimibe as control. The ideal solubility of drug and cocrystals were also calculated using data obtained from DSC (heat of fusion, ΔH and transition melting temperature, T_m). The equilibrium aqueous solubility of ezetimibe was enhanced by about two fold in case of cocrystal that prepared by solution crystallization. Cocrystals prepared via reaction crystallization showed solubility was almost same as that of pure ezetimibe. The dissolution profile of all cocrystals, with pure ezetimibe as a control was studied for 2 hours in defined biorelevant media. Cocrystal II, prepared by liquid assisted grinding method showed significant improvement in solubility at 45 and 120 min, indicating a good dissolution profile. The study demonstrates that pharmaceutical cocrystallization of ezetimibe with methyl paraben can be a possible and potential alternative and effective approach for improving its solubility.

Introduction:

The efficacy of the active pharmaceutical ingredients (API) dramatically depends on the physical properties of their solid form. Dissolution rate, solubility, hygroscopic nature, and chemical stability are some of the most important factors that must be considered.[1] API can be polymorphic,[2] meaning that it can exist in two or more crystallographic forms. This may include solvation or hydration products (also known as pseudo polymorphs) and amorphous forms.[3] Cocrystals are like polymorphic solids, crystalline in nature and composed of two or more compounds in the same crystal lattice. Nevertheless, cocrystallisation influences the same before mentioned properties, just like for different polymorphs.[4-5] A large range of intermolecular interactions including electrostatic interactions (ion-ion, ion-dipole and dipole-dipole interactions), coordinate bonding (metal-ligand), hydrogen bonding, halogen bonding, π-π stacking and Van der Waals forces can be resposible when cocrystallization occurs.[6]

While the intramolecular interactions bond the atoms in a molecule, the intermolecular forces minimize the energy of the molecules in the crystal and are primarily responsible for the formation of organic crystals.[7] The major attractive interactions in most pharmaceutical crystals are hydrogen bonds and van der Waals interactions.[8] The arrangement of molecules in a crystal determines its physical properties and in some cases, its chemical properties also.[9] The physicochemical properties of the solid drug can affect its performance. Thus, an understanding of the crystalline state leads to an understanding of the drug properties, which is crucial for preformulation and formulation in the pharmaceutical industry.

This class of pharmaceutical cocrystals have gained large interest over the past few years since they offer the potential to eliminate undesirable physicochemical properties without covalent modification of the API. Moreover, unlike salt forms of API's, cocrystal formation is not restricted to an ionizable (acidic or basic) centre on the API and can simultaneously address multiple functional groups on the API. A relatively large number of non-toxic compounds with hydrogen bonding functionalities exist on the GRAS (generally regarded as safe) list that may act as cocrystal formers in comparison to the limited number of salt forming counter-ions in use.[10]

The presence of multiple functional groups inherent to APIs affords the opportunity for the design of pharmaceutical cocrystals. In fact an analysis of the top 100 prescription drugs, [11] reveal that 39% of pharmaceutically active ingredients contains at least one alcohol and 30% contain at least one carboxylic acid, this is also consistent with the percentage alcohol and carboxylic acid moieties in the Merck Index.[12] Consequently addressing the ability of these functional groups to form supramolecular synthons would be of great interest. The crystal engineering approach for APIs based upon the use of reliable supramolecular heterosynthons is exemplified by several series of cocrystal involving carbamazepine (CBZ),[13,14] ibuprofen,[15] iracetam,[16] fluoxetine hydrochloride,[17] and itraconazole.[18]

Ezetimibe (EZE) is a modern hypocholesterolemic drug used both as monotherapy and adjunctive therapy to diet for the reduction of elevated total cholesterol (total-C), Low density lipoprotein cholesterol (LDL-C), and Apoprotein B (Apo B) in patients with primary hypercholesterolemia (heterozygous familial and non-familial).[19] However, this API as per Biopharmaceutics Classification System, class II drug, [20] has poor water solubility (0.012 mg/mL at 25 °C), [21] which leads to its limited dissolution resulting in poor bioavailability (35-65%).[22]

Several researchers have reported the improvement in solubility/dissolution properties of ezetimibe by complexation with cyclodextrin, [23] solid dispersion, [24] and preparing liquid-solid compacts.[25] From the literature, it has been found that cocrystal technique is an alternative approach to manipulate the physicochemical properties of the drug such as solubility, dissolution rate, stability and compressibility and to improve overall performance of APIs without affecting the pharmacological properties. Ezetimibe has rarely been investigated for its cocrystallization tendencies. This motivated us to explore the potential of ezetimibe to cocrystallize in order to improve its solubility.

The present study is aimed to enhance the solubility of ezetimibe by cocrystal engineering technique. After selecting the suitable coformer, the cocrystals of EZE was prepared by solution crystallization method (CI), liquid assisted grinding (LAG) method (CII) and reaction crystallization method (CIII). The product thereof was characterized by differential scanning calorimetry (DSC), thermo gravimetric analysis (TGA), Fourier transform infrared spectroscopy (FTIR), Raman spectroscopy and powder X-ray diffraction (PXRD). After that the cocrystals were subjected for solubility and dissolution study.

Experimental Section

Materials: Ezetimibe was obtained as a gift sample from Dr. Reddy's Laboratory Ltd. Hyderabad, India. Methyl paraben (99%) was purchased from CDH, New Delhi, India and the solvents used for crystallization including methanol were of HPLC grade (Rankem, India). Analytical chemicals like acetonitrile and potassium dihydrogen ortho phosphate were purchased from Rankem, India. All of these were used as received.

Sample preparation:

Selection of coformers: Various coformers such as benzoic acid, salicylic acid, L-proline, valine, glycine and methyl paraben were selected from the GRAS list generated by the U.S. FDA (generally regarded as safe additive chemicals by the Food and Drug Administration)[26]

Cocrystal preparation and preliminary screening: Solution crystallization,[27,28] and slurry[29] methods were opted to prepare cocrystals. The first hand information about the existence of new solid phases was obtained by melting point, as it is a fundamental physical property of a compound. Digital melting point apparatus (OPTIMELT, SRS, Germany) was used to determine the melting points of pure API, coformer and the solid phase obtained.

Following three methods were used to prepare cocrystal of ezetimibe with the selected coformer (from the preliminary screening based on melting point).

Solution crystallization method (CI): This is the simplest technique for air stable samples. Solution crystallisation can yield large, well-formed single crystals, from which one may easily evaluate crystal habit and surface features. Analysis of the diffraction pattern of a single crystal is typically the best means of obtaining an absolute crystal structure determination.[30] A molar ratio of 1:1 mixture of ezetimibe (204.7 mg, 0.5 mmol) and methyl paraben (76.075 mg, 0.5 mmol) was dissolved in a 10 mL solution of methanol in a 20 mL conical flask. The resulting solution was placed at water bath (REMI RSB-12) maintained at a temperature of 35°C for slow evaporation. After two days, white, very fine needle-shaped crystals were recovered, filtered, and air-dried.[27,28] The crystal size was not sufficient for single crystal X-ray diffraction analysis.

Liquid assisted grinding (LAG) method (CII): This is a solvent-free solid state grinding method where the relative solubility of ingoing component in a particular solvent is not a concern unlike in the case of solution crystallization method. Further, the absence of solvent makes this an inherently 'green' approach to form cocrystals by eliminating large volumes of solvent waste; the minimization of excess crystallisation solvent could help achieve corporate green chemistry targets.[30] A mixture of 1:1 molar ratio of ezetimibe and methyl paraben at a total of 1 g was placed in the grinding jar (45 mL) in a planetary micro mill (Fritsch, Germany) with 10 stainless steel balls (5 mm dia). 50 μL of methanol was added in the mixture and milled for 30 min at an operating frequency of 600 rpm.[31]

Reaction crystallization method (CIII): This is a method for rapid generation of cocrystals at microscopic and macroscopic scale at ambient temperature, where nucleation and cocrystallization are initiated by the effect of the cocrystal components on reducing the solubility of the molecular complex to be crystallized.[31] The saturated solution of the lesser soluble component (drug) was made in 10 mL methanol, filtered, and then the more soluble component (methyl paraben) was added in amount just under its solubility limit. The goal was not to have any excess drug or coformer in the starting solutions that could be confused as a cocrystal. Furthermore, by not exceeding the solubility limits of the components, the cocrystal that precipitated out of solution was pure. Solution concentrations were monitored by HPLC throughout the crystallization process to evaluate whether the solid observed appeared to be a complex of the reactants (cocrystals). The solid precipitate was also

collected and analyzed by HPLC to determine the stochiometry of the complex. If the solid appeared to be a cocrystal based on the HPLC results; it was further characterized by DSC, TGA and PXRD.[32]

Differential scanning calorimetry (DSC)

DSC of all the samples were conducted using DSC Q10 (TA Instruments, USA) which was calibrated for temperature and enthalpy using indium. Samples (3-5mg) were crimped in non-hermetic aluminum pans and scanned from 25°C to 200°C at a heating rate 10°C/min under a continuously purged dry nitrogen atmosphere (flow rate 50 mL/min).The data were managed by TA Explorer software.

Thermo gravimetric analysis (TGA)

TGA was performed by a DTG-60 (Shimadzu, Japan) analyser. The samples (approximately 5 mg) were placed into aluminium pans and heated from 25°C to 500°C at the rate of 10 °C/min under nitrogen purge at flow rate of 50 mL/min. The data were managed by TA-60WS acquisition software.

Fourier transform infrared spectroscopy (FTIR)

A FTIR- 8400 S spectrophotometer (Shimadzu, Japan) was employed to collect the infrared spectrum of drug, coformer and cocrystals. The IR absorption spectra of samples were measured over the range of 4000-600 cm^{-1}. A few milligrams of sample was mixed with 10 times of its weight of potassium bromide (KBr) and pressed to form a pellet. The data were analysed using IR solution software.

Raman spectroscopy

Raman spectra of pure drug, coformer and cocrystals were obtained using a Raman spectrometer (Renishaw plc.) with 514 nm stabilized diode laser excitation. The laser power at the sample was approximately 10 mW. A 50 x objective lens was used, giving a laser spot diameter (footprint) of 2µm at the sample. Spectra were obtained for a 10 s exposure of the argon detector in the region 3200-100 cm^{-1} using the extended scanning mode of the instrument.

Powder X-ray diffraction (PXRD)

PXRD patterns were collected on Bruker AXS D8 Advance Diffractometer system with a Cu Kα radiation (1.5406 Å). The tube voltage and current were set at 40 kV and 35 mA respectively. Each sample was placed on an aluminum sample holder and measured by a continuous scan between 3 and 80° in 2θ with a step size of 0.020° and step time 31.2 s. The experimental PXRD patterns were refined using Diffrac plus software.

Scanning electron microscopy (SEM)

The surface morphology and topography of all three cocrystals were evaluated by scanning electron microscope (JSM-6390LV, Jeol, Japan). Before examination, the samples were mounted onto stubs using double-sided dried adhesive carbon tape and vacuum coated with gold palladium film (thickness 2 nm) by sputter coater (Edward S-150, U.K.) to make them electrically conductive. Representative sections were photographed.

Solubility studies

Determination of cocrystal stochiometry

Stochiometry via PXRD: The stochiometry of ezetimibe and methyl paraben were calculated from the X-ray diffractograms of CI, CII and CIII. The peaks with highest intensity of ezetimibe and methyl paraben were identified. Peaks of cocrystals were fitted with Gaussian line shapes and the area under the peak at their respective 2θ value (highest peak intensity of the virgin crystals) was calculated by integration.[33]

Stochiometry via HPLC results in case of CIII: In case of cocrystal prepared through reaction crystallization method (RCM), the stochiometry was calculated through analysis of the solid precipitate left after attainment of equilibrium position [transition concentration (C_{tr})] in the RCM experiment.

Determination of transition concentration (C_{tr}): Transition concentration (C_{tr}) is the solution concentrations ($[drug]_{tr}$ and $[ligand]_{tr}$) which separates the region where either the solid cocrystal or drug are thermodynamically stable.[34-39]
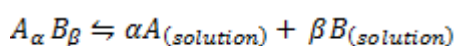
The measurement of cocrystal C_{tr} values were performed by precipitating cocrystal as a result of stirring excess solid coformer in a presaturated drug solution wherein cocrystal occurs though RCM .

A saturated solution of drug (ezetimibe) was prepared in methanol and to it a known excess amount of coformer (methyl paraben) was added to it. The amount of coformer added was based on its solubility limit in methanol. The solution was stirred on a water bath shaker, maintained at a temperature of 25°C, for 24 h and checked for precipitation of cocrystals. The solid precipitate so obtained were separated and dried.

Stochiometry calculation: For calculating, the stochiometry, a known concentration (5μg/mL) of the solid was prepared in methanol and the concentration of both the drug and the coformer was measured by HPLC. The concentrations were determined in molality units and their ratio gave the stochiometry of the cocrystal. The whole process was performed in triplicate.

Theoretical Calculations

For cocrystal $A_\alpha B_\beta$, where A is drug and B is ligand, solubility is described by the chemical equilibrium of solid cocrystal with solution and the corresponding equilibrium constant given by.[40,41]

$$A_\alpha B_\beta \leftrightharpoons \alpha A_{(solution)} + \beta B_{(solution)}$$

$$K = \frac{a^\alpha_{A(solution)} a^\beta_{B(solution)}}{a_{A_\alpha B_\beta(s)}}$$

Defining solid cocrystal activity as unity ($a_{A_\alpha B_\beta(s)}= 1$) and assuming the activity coefficients

(γ) of A and B equal unity for low solute levels, the above equation reduces to

$$K_{sp} = [A]^\alpha [B]^\beta \qquad (1)$$

where, K_{sp} is the solubility product of the cocrystal. The cocrystal solubility ($S_{A_\alpha B_\beta}$) is given

as

$$S_{A_\alpha B_\beta} = \sqrt[\alpha+\beta]{K_{sp}\Big/\alpha^\alpha \beta^\beta} \qquad (2)$$

The saturation solubility of pure drug (ezetimibe), CI, CII, and CIII in water were determined by suspending excess amount of material in water. The solutions were shaken on a water bath shaker at a temperature of 25 ± 2°C for approximately 24 h. Samples were then filtered using a 0.2 μm nylon filter (AXIVA) and analyzed by HPLC. If necessary, samples were diluted in methanol prior to analysis. Ezetimibe and methyl paraben solubility was also measured as a control. The solubility of the cocrystals was calculated using equation 1 and 2.

High performance liquid chromatography (HPLC)

Solution concentration of ezetimibe and methyl paraben was analysed by HPLC (Waters USA) equipped with a UV/vis detector. A C18 Nova-Pak® column 4μm, 4.6 x 150 mm (Waters, USA) at ambient temperature with a flow rate of 1 mL/min was used to separate ezetimibe and methyl paraben. An isocratic method with water (pH 3.0) and acetonitrile mixed in a ratio of 55:45(v/v), respectively was opted for quantitative determination of ezetimibe and methyl paraben, at an optimum wavelength of 248 nm. Sample injection volume was 20 μL. Empower software from Waters was used to collect and process the data. All concentrations are reported in molality.

Determination of ideal solubility from thermal behaviour

For an ideal solution, the solute solubility, x (mole fraction), is a function of the heat of fusion ($\Delta Hm \ or \Delta H_s^{ideal}$), melt temperature ($Tm$), solution temperature (T) and universal gas constant (R). It is expressed by the following equation[42]

$$\ln\chi_{solute}^{ideal} = \frac{-\Delta Hm}{R}\frac{(Tm-T)}{(TmT)} \qquad (3)$$

Where $\Delta Hm \cong \Delta H_s^{ideal}$

Melting temperature and enthalpy of all the samples including drug and coformer were obtained from DSC data and put into the above equation to get the ideal solubility value. To determine the ideal solubility of cocrystals using the same equation, the melting enthalpy was first normalized by the cocrystal stochiometry. The enthalpy of melting of the cocrystals was the measured value divided by the number of moles of reactant per mole of cocrystal.

Dissolution study

The dissolution studies were conducted in 500 mL of 0.45% sodium lauryl sulphate (SLS) in 0.05 M acetate buffer (pH 4.5) in a USP type II dissolution apparatus (Electrolab, India). Paddle rotation speed was 50 rpm. 10 mg of drug or its equivalent amount of cocrystal was added to the dissolution medium. Time points were collected for 2 h and the concentrations of ezetimibe were analyzed by HPLC. The dissolution profile of the cocrystals were then statistically analysed by applying one way ANOVA followed by Tuckey's post hoc test.

Result and Discussions

Cocrystal preparation

The detailed methodology opted for preparing cocrystals of ezetimibe using selected coformers, along with the results obtained is presented in supplementary information (Table S1).

A total of nine formulations were prepared, using seven coformers. It was observed that the melting point of multicomponent solid form of ezetimibe prepared with methyl paraben was 109.97°C indicating a lower melting point than either ezetimibe or methyl paraben. The chemical structure of ezetimibe and methyl paraben is given in figure 1. The multicomponent solid form of ezetimibe with L-proline displayed a melting point of 173.1°C which was in agreement with the findings of Scott et al. (2012).[19] These observations clearly indicated the formation of stable interaction between ezetimibe and the coformer. After an analysis of 50 cocrystalline samples, it has been documented earlier that 51% cocrystals had melting points between the API and coformer, 39% were lower than either the API or coformer, 6% were higher, and 4% had the same melting point as either the API or coformer.[43] The altered melting points in multicomponent solid forms might be attributed to noncovalent bonding interaction between API and coformers, altered packing arrangements and change in crystallinity of molecules in the cocrystals. Therefore, methyl paraben was selected as a coformer for preparing cocrystal of ezetimibe by different methods.
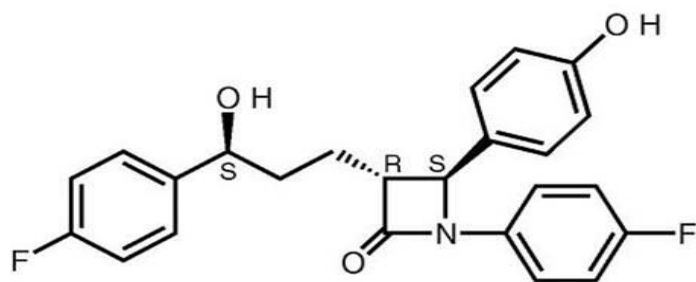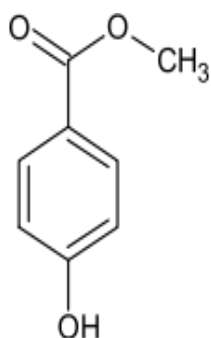
Ezetimibe

Methyl paraben

Figure 1. Chemical structure of ezetimibe and methyl paraben

Ezetimibe cocrystal preparation with methyl paraben as a coformer

The melting point of CI, CII and CIII prepared by solution crystallization; liquid assisted grinding and reaction crystallization were 109.97°C, 111.27°C and 109.12°C, respectively. In all the three cases, a melting point lower than that of pure ezetimibe or methyl paraben was obtained. Ghosh et al., reported that the cocrystals of sulfamethazine/3,4-dichlorobenzoic acid (1:1), sulfamethazine/fumaric acid/acetonitrile (2:1:1), sulfamethazine/1-hydroxy-2-napthoic acid (1:1) and sulfamethazine/3-hydroxy-2-napthoic acid (1:1) was having melting point lower than the melting point of pure drug and respective coformers.[44] In another recent report, Bucar et al., obtained different cocrystals of caffeine having lower melting point than that of pure drug and respective coformers.[45]

Thermal analysis (DSC & TGA)

Thermal analysis by DSC and TGA are the primary analytical tools for getting first hand information about the existence of new solid phase. The DSC thermograms of pure

ezetimibe, methyl paraben and the cocrystals (CI, CII & CIII) are shown in Figure 2. The corresponding TGA patterns of the same are depicted in Figure 3.

The DSC thermograms of pure ezetimibe and methyl paraben showed single melting endotherm (T_m) at 164.36°C and 127.34°C, respectively. In all the three cocrystals, melting endotherm was lower than that of either drug or cocrystal. From TGA study of methyl paraben it was observed that a negligible mass loss (2.66%) was obtained in the range of 25 - 130°C, followed by a major mass loss of (96.99%) in the range of 130 - 200°C. This major mass loss was due to its degradation.

CI showed a single and sharp melting endotherm at a temperature of 109.97°C. Further, negligible mass loss (3.51%) was observed in the TGA scan of CI in the range of 25 - 130°C, suggesting that there was no degradation rather it was only phase transformation. So it may be concluded that it is an anhydrous and pure cocrystal phase.

CII showed two melting endotherm at 81.1 °C and 111.27 °C, where first peak was broadened with very less intensity. From TGA study, a negligible mass loss (2.70%) in the range of 30 - 100 °C does not correspond to mass loss due to solvent. Another negligible mass loss (1.84%) seen in the range of 100 - 130°C does not correspond to any degradation of cocrystal suggesting phase transformation. To check whether two endotherms correspond to two different polymorphic crystals, the cocrystal (CII) was heated at 10 °C/min up to 125 °C and then cooled at 10 °C/min up to ambient temperature then again reheated up to 250 °C at a same heating rate as shown in supplementary information (Figure S1). One exothermic peak corresponding to recrystallization was observed at 72.73 °C during cooling cycle. However in the reheating cycle, the first endotherm disappeared (81.1°C) but the second endothermic peak appeared at the same temperature. It is clear that the exothermic peak observed at 72.73 °C is not due to the recrystallization of the polymorphic form I rather it is due to the recrystallization of polymorphic form II. Upon heating polymorphic form I transforms to polymorphic form II as confirmed by the endothermic peak during reheating cycle. Similar findings were reported in case of sulfamethazine/hydroxy benzoic acid cocrystal and ethenzamide/gentisic acid cocrystal (solvent system was toluene-acetonitrile 1:1) by Ghosh et al., and Aitipamula et al., respectively.[44,46]

CIII showed a single and sharp melting endotherm at 109.12°C free of any eutectic melting, thus establishing the existence of pure cocrystal phase. A very negligible mass loss confirmed the phase transformation of cocrystal.

The heat of fusion (ΔH) of all cocrystals (Fig.2) were less than that of pure ezetimibe as well as methyl paraben which indicates the probability of increased entropy and subsequent higher solubility of all cocrystals compared to pure ezetimibe. The mass loss occurred in all cocrystals in two stages. The first mass loss at a range of 130 - 200 °C was 19.69%, 22.06% and 16.24% for CI, CII and CIII, respectively which is similar to mass loss pattern of methyl paraben. The second mass loss at a range of 250 - 380 °C was, 54.86 %, 54.59 % and 24.90 % for CI, CII and CIII, respectively which is also similar to mass loss pattern of ezetimibe. So, it is clear that the amount of ezetimibe present in CIII is less as compared to other cocrystals which may be reflected in stoichiometric ratio calculation by PXRD.
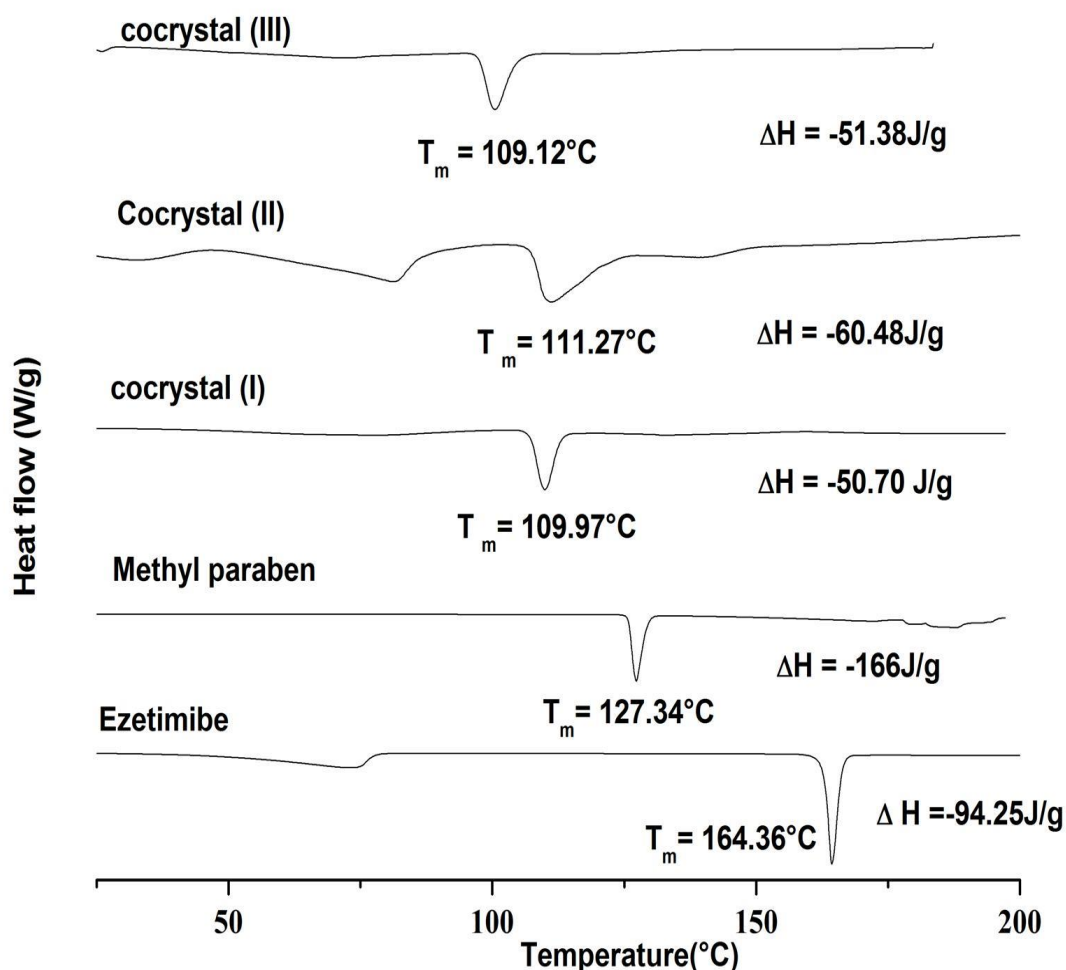

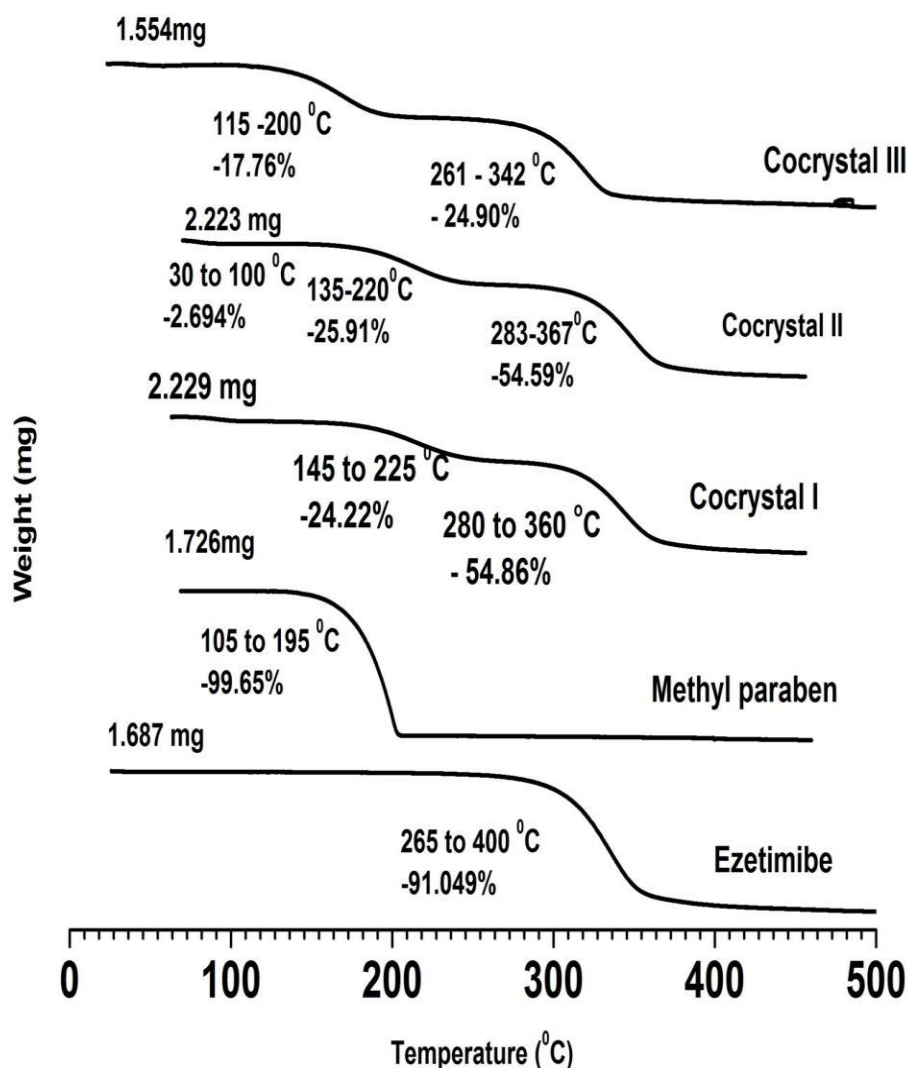**Figure 2.** DSC scans of ezetimibe, methyl paraben, cocrystal I, cocrystal II and cocrystal III.

Figure 3. TGA curve ezetimibe, methyl paraben, cocrystal I, cocrystal II and cocrystal III

Fourier Transform Infrared Spectroscopy (FTIR)

Vibrational spectroscopy is an excellent technique to characterize and study cocrystallization. The characteristic peaks and their shift of pure ezetimibe, methyl paraben, CI, CII and CIII are tabulated in supplementary file (Table S2). The FTIR spectra of ezetimibe, methyl paraben, CI, CII and CIII in the regions of 3900 to 1500 and 1500 to 600 cm^{-1} are presented in Figure 4a & Figure 4b, respectively.

A comparison of spectra reveals that there were several band shifts occurring between the starting components and CI. The FTIR spectra for pure ezetimibe and methyl paraben in the starting material have bands at 3261.74 and 3292.00 cm^{-1} corresponding to υ(O-H), respectively. The bands at 1716.70 and 1678.13 cm^{-1}, corresponding to υ(C=O) was for ezetimibe and methyl paraben, respectively. In case of CI, bands corresponding to υ (O-H) of both molecules, shifted to 3275.24 cm^{-1}. The band corresponding to υ(C=O) of methyl paraben shifted to 1681.98 cm^{-1} indicating the formation of hydrogen bond between phenolic hydroxyl group and carbonyl group (lactum) of ezetimibe with *p*-hydroxy group of methyl paraben.[47] The peak at 1435.09 cm^{-1} (υ (C-O) enolic) of methyl paraben and peak at 1444.73 cm^{-1} of ezetimibe shifted and then merged with the peak at 1448.73 cm^{-1} of CI with a relatively higher intensity. The peak at 1444.73 cm^{-1} [υ (C-N)] of ezetimibe shifted to 1448.59 cm^{-1} which is likely due to charge transfer interaction between tertiary nitrogen of ezetimibe with methyl paraben molecule. These peak shifts, strongly indicated the formation of hydrogen bond and other weak interaction between ezetimibe and methyl paraben.

During formation of ezetimibe-methyl paraben cocrystal via liquid assisted grinding method (CII), the OH band of ezetimibe and methyl paraben shifted to a higher wave number by 47 cm^{-1} and 16 cm^{-1}, respectively which was a very significant shift clearly depicting participation of OH group of both molecules in hydrogen bond formation. This peak was found to be sharper than the pure ezetimibe peak. Further, the band at 1354.07 cm^{-1}, corresponding to β(O-H) of pure ezetimibe shifted to 1361.79 cm^{-1}. The FTIR spectrum of pure ezetimibe has strong bands at 1716.70 cm^{-1}, which correspond to υ(C=O) lactam. During crystallization, its intensity was drastically reduced. In CII, the C-F stretching band shifted to a higher wave number by 13 cm^{-1}, which indicates that the fluorine (F) atom might be also engage in formation of hydrogen bond.

The cocrystal (CIII) of ezetimibe and methyl paraben prepared by reaction crystallization process showed the maximum number of significant changes in FTIR spectrum. The FTIR spectrum of pure ezetimibe showed a broad peak at 3261.74 cm^{-1} of strong intensity, corresponding to stretching of OH group. This peak became narrow and weak in intensity with a shift towards higher wavenumber by 18 cm^{-1}. Further, the carbonyl group (lactam) of ezetimibe and the carbonyl group of methyl paraben showed a shift to higher wavenumber by 14 and 5 cm^{-1}, respectively. It indicates that there is a electrostatic repulsion between the lone pair of electrons present in carbonyl group of both the drug and coformer. In this cocrystal

(CIII) only, the band at 1444.73 cm^{-1} corresponding to υ (C-N) got shifted to 1448.59 cm^{-1}, which is similar to CI.
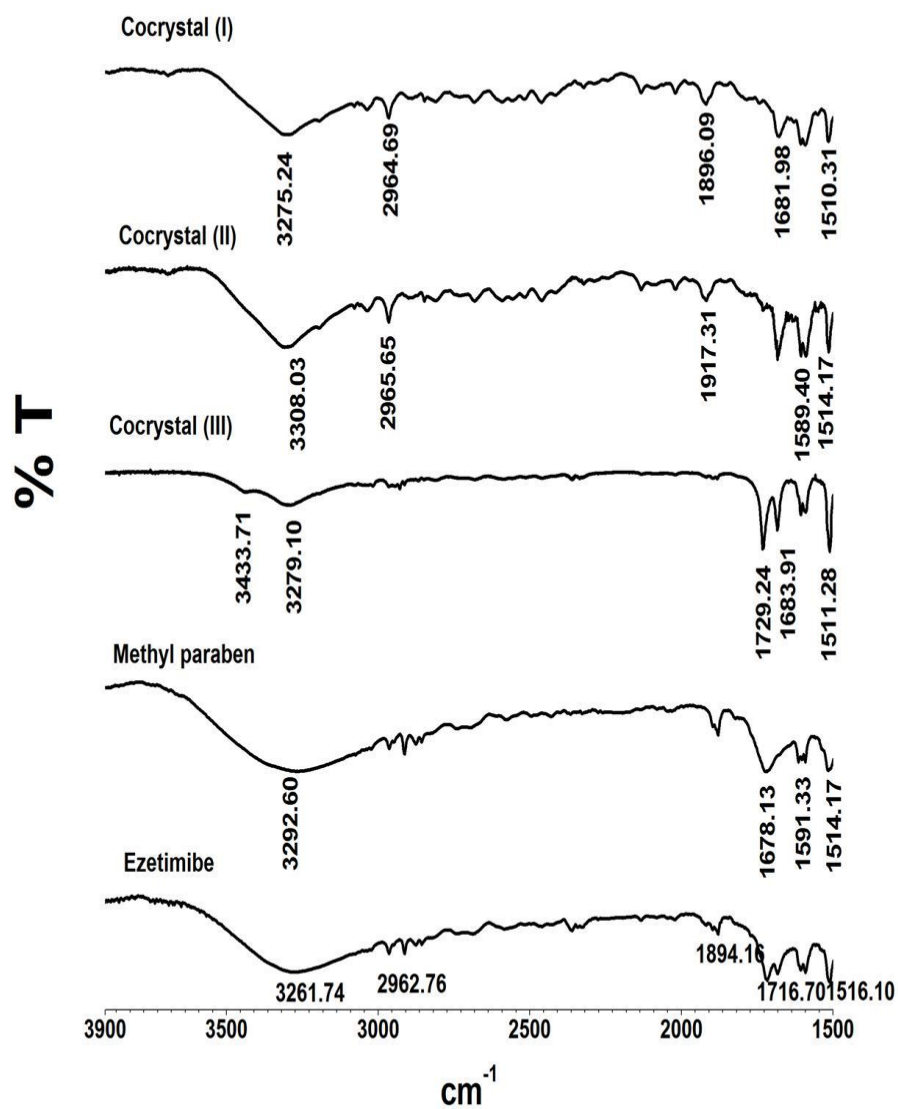

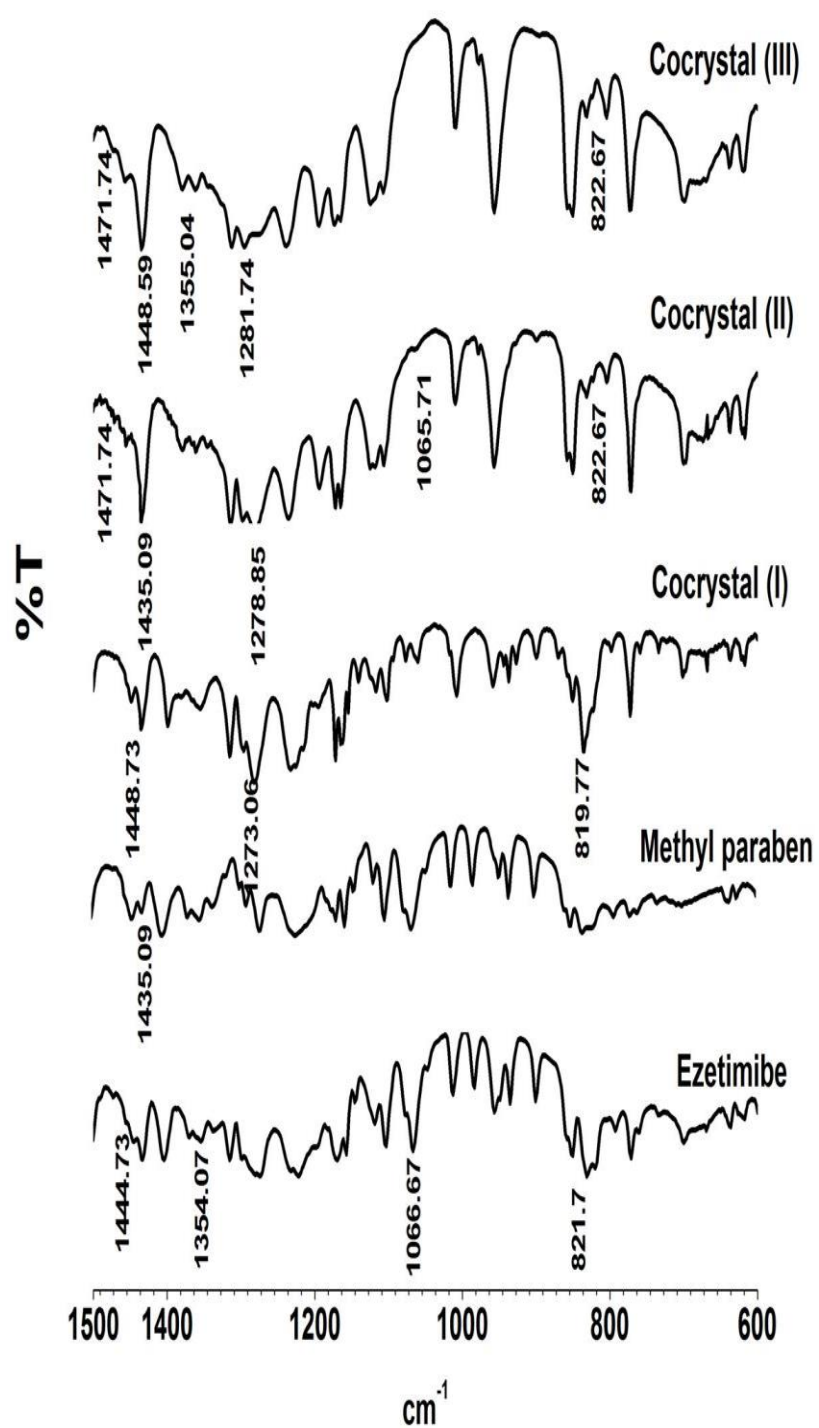**Figure 4a.** FTIR spectra (1500 - 3900 cm^{-1}) obtained for ezetimibe, methyl paraben and cocrystals.

Figure 4b. FTIR spectra (600 - 1500 cm^{-1}) obtained for ezetimibe, methyl paraben and cocrystals.

Raman Spectroscopy

FTIR and Raman spectroscopy are complementary techniques for characterizing of solid forms of drugs[43]. Solid samples isolated from screening experiments can be mixtures and have poor crystal quality. Relying only on one technique may not provide enough evidence to confirm a potential hit. However, by comparing data for the screening samples from spectroscopic tools, a more informed determination may be achieved. These spectroscopic techniques can provide evidence for cocrystal formation by evaluating the intermolecular interactions. Additionally, Raman spectroscopy may be used in the identification of polymorphism, since different vibration modes can be associated to modifications in molecular packing in crystalline solids.[43] These differences are observed mainly in low-frequency, which may arise due to lattice vibration that is more sensitive to structural changes in solid state.[48] The assignment for the most prominent vibrational bands of ezetimibe, methyl paraben, CI, CII, and CIII are listed in Table 1 presented in Figure 5a and 5b.

The molecular interaction between ezetimibe and methyl paraben was examined by Raman spectroscopy, and the vibrational wavenumbers and assignments are listed in Table 1. The Raman spectra of pure ezetimibe in the starting material have bands at 1760.22, 1716.28, and 1431.84 cm^{-1}, corresponding to υ(C=O) lactam, υ(C=O) lactam, and υ(C-N), respectively. During the cocrystallization of ezetimibe and methyl paraben, these bands in the cocrystal (CI) were shifted to 1761.43, 1715.45 and 1432.72 cm^{-1}. A significant decrease in the intensity was observed in υ(C-N). Similarly, intensity of υ(C=O) lactam also decreased. Further, the peak of carbonyl stretching in methyl paraben also shifted, suggesting that C=O is participating in hydrogen bonding. The hydroxyl group also seemed to be participating in hydrogen bonding. The band for β(O-H) of pure ezetimibe showed a shift to a lower wave number by 4 cm^{-1}.

A comparison of the spectra reveals that there are several band shifts occurring between the individual components and the cocrystal (CII). During the formation of cocrystals, the bands at 1341.11 and 1234.12, cm^{-1} depicting β(O-H) and υ(C-O)h shifted to 1342.94 & 1232.15 cm^{-1}, respectively with decreased intensity. It depicts that the hydroxyl group is engaged in hydrogen bonding.

CIII, prepared by reaction crystallization showed the maximum number of band shifts as compared to other two cocrystals. It is in agreement with the FTIR results, thereby giving

strong evidence of formation of new supramolecular synthon in cocrystal. The Raman spectra of pure ezetimibe showed band at 1431.84 cm^{-1} of strong intensity corresponding to stretching of C-N of lactam ring. This band showed a shift of 3 cm^{-1} with a significant decrease in its intensity, indicating possible Coulombic interaction between nitrogen atom\of ezetimibe and oxygen atom of methyl paraben. The band corresponding to stretching of C-F in ezetimibe got shifted to higher wave number by 2 cm^{-1}. The peak obtained was very weak, as compared to strong intense peak in pure ezetimibe indicating that fluorine is also participating in hydrogen bonding.

Table 1. Assignments of major bands of Raman spectra of ezetimibe, methyl paraben and their cocrystal products.

Ezetimibe	Methyl paraben	cocrystal I	Cocrystal II	Cocrystal III	Assignment[48-52]
1760.22m		1761.43m	1761vw	1761.38vw	υ(C=O) lactam
1716.28m		1715.45w	1716.7vw	1716.38vw	υ(C=O) lactam
	1676.15	1675.31	1675.47	1675.47	υ(C=O)
1613.64s	1606.83s	**1611.09s**	**1611.63vs**	**1610.61s**	υ(CC)ar chain vibrations
	1588.92s	1588.92s	1587.16m	1588.18s	υ(C=C)
1510.56m	1517.7m	**1510.56m**	**1510.12m**	**1509.09w**	υ (C-O) phenolic
1431.84s		1432.72vw	1431.2m	**1434.33vvw**	υ (C-N)
1403.55w		1404.43s	1402.95s	1402.95vvw	δ(CH2)
1370.64w		1369.75	1370.37	1369.32	(O-H) i.p. bend
1341.11w		**1338.42vvw**	1342.94vw	1341.88vw	β(O-H)
1316.83m	1311.42m	**1311.42w**	**1312.22w**	**1311.16m**	υ (C-O)c
1292.43m			1292.02	**1287.76**	(CC)ar
	1281.54s	1281.54vvw	1281.36w	1282.43m	υ (C-O)
1272.46w			1272.83w	1272.83w	υ (C-O)
	1234.12w	**1232.29w**	**1232.15w**	1234.3w	υ (C-O)
1214.85s		1214.85w	1214.96s	**1216.03vw**	υ (C-F)
1183.49w		1182.56w			υ C-O (H)
1168.66		1167.74			
1158.45s	1159.38s	1159.38s	1159.87s	1159.87s	υ(CC)ar chain vib.
	1121.13w	**1118.32vvw**	1121.83vvw	1121.83vw	υ(C-O-C) asym
948.913m		948.913w	947.62w	949.851vw	β(C-H)
860.186s	856.252s	**857.236m**	**857.839m**	860.097m	υ (C-C)
838.515s		**836.54vw**	838.622m	837.49vvw	υ (C-C)
821.709w		821.709w	821.626m	822.76vvw	υ(= (C-H))
	829.624w	828.63w		829.562w	
734.886w		734.886vw	737.214vw	734.92vw	CH2 rock
699.565m		700.578	700..421	700.421	υ(CC) al. chain vib.
635.413m		636.437m	636.167m	636.167w	
397.95m		397.95	397.199	397.199	δ(CC) aliphatic chains

 s ,strong; m, medium; w, weak; vw, very weak; vvw, very very weak; υ, stretching; β, in plane deformation; δ,bending; φ,phenyl; i.p.,in plane; ar,aromatic; asym,asymmetric; vib, vibration; def, deformation.

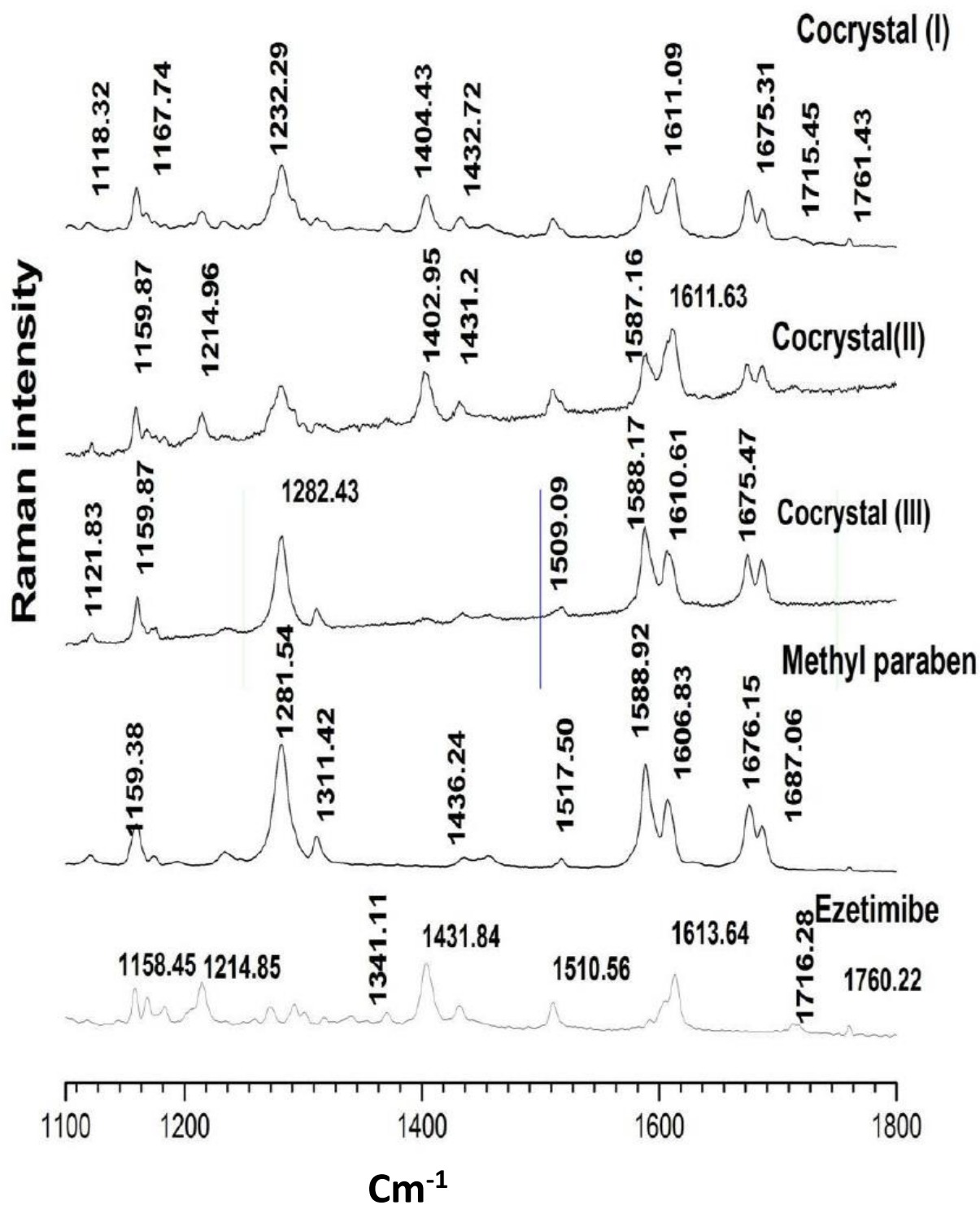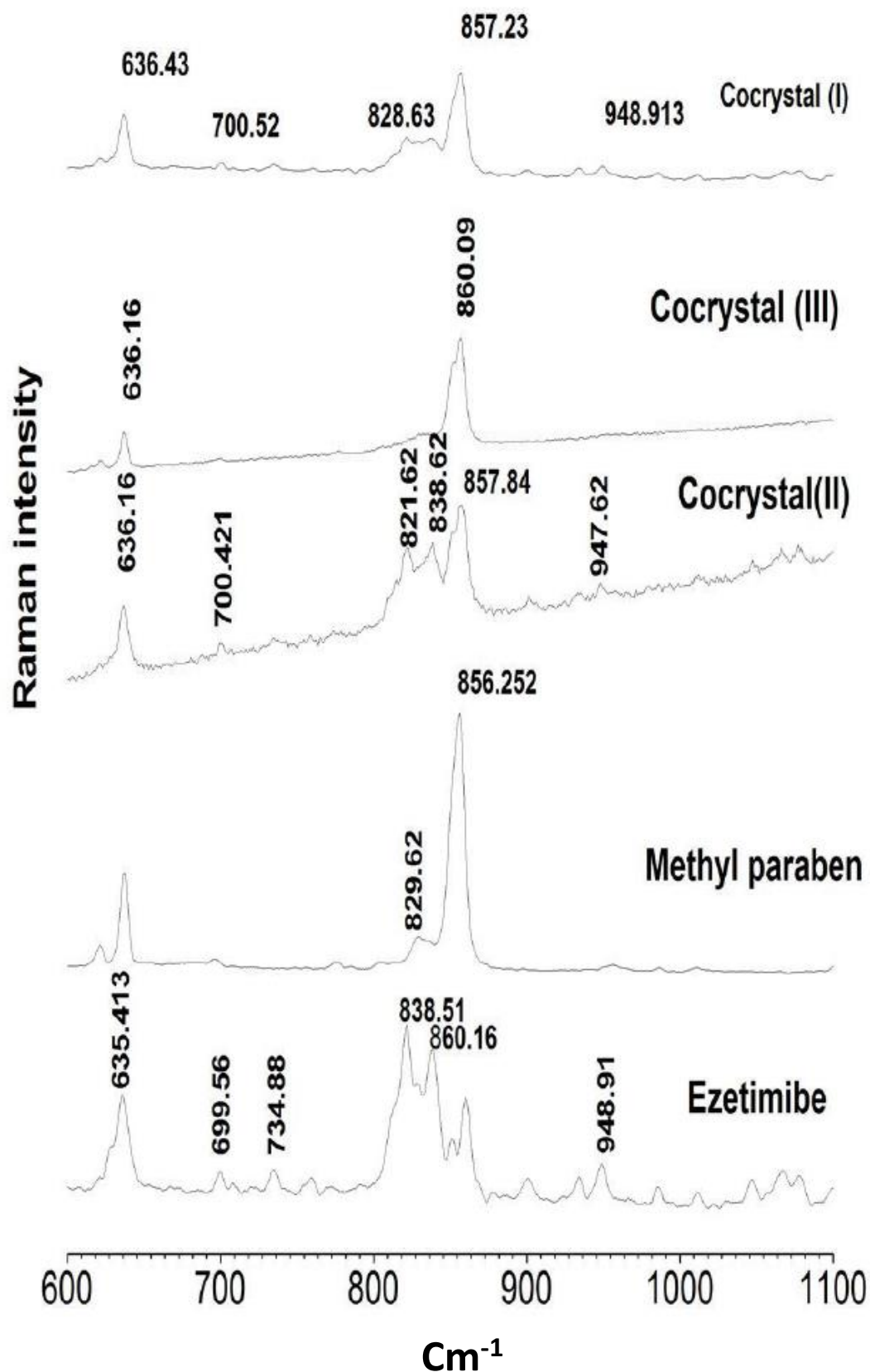**Figure 5a.** Raman spectra (1100 - 1800 cm^{-1}) obtained for ezetimibe, methyl paraben and cocrystals.

Figure 5b. Raman spectra (600 - 1100 cm^{-1}) obtained for ezetimibe, methyl paraben and cocrystals

Powder X-Ray Diffraction (PXRD)

Powder X-ray diffraction is a fingerprint characterization method for cocrystals. If the resulting PXRD of the solid product obtained after cocrystallization experiment is different from that of the reactants, then it may be inferred that a new solid phase has formed. PXRD is a powerful technique for determining the presence of polymorphs, crystal habit modifications in drug crystals and/or generation of new crystal form during cocrystallization process.[53]

The PXRD pattern of ezetimibe exhibited characteristic reflections at about 2θ 15.70°, 17.11°, 18.56°, 19.24°, 21.63°, 22.67°, 23.24°, 24.19°, 25.10°, 28.04°, and 32.76°. Similarly, the PXRD pattern of methyl paraben exhibited characteristic reflections at about 2θ 21.228°, 23.23°, 25.08°, and 36.56°. The major peak with 100% intensity had reflections at 2θ of 19.24° and 25.08° in ezetimibe and methyl paraben, respectively. As shown in Figure 6, unique PXRD patterns of the cocrystals distinguishable from the host (drug) and the guest (coformer) were noted.

The PXRD pattern of CI exhibited characteristic reflections at about 2θ 13.91°,15.77°,17.11°,18.60°,19.34°,20.74°,21.66°,22.77°,23.44°,24.50°,26.25°,27.71°,28.15° ,29.78°,31.18°,33.4°, and 36.28°. The most intense peak was at reflection 2θ 19.34°. These peaks were significantly different from the parent components, which indicated that CI is a unique with respect to pure ezetimibe. Major peaks at 25.11°, and 32.76° of pure ezetimibe were missing in the cocrystal phase, whereas, peaks at 31.18° and 39.31° were observed.

The PXRD pattern of CII exhibited characteristic reflections at about 2θ 18.99°,19.33°,19.79°,19.8°,20.63°,21.04°,22.6° and 24.97°, which were significantly different from either of ezetimibe or methyl paraben. The absence of peaks, characteristic of pure ezetimibe and methyl paraben in the PXRD pattern of CII implies it to be pure and homogenous cocrystal sample. Newer peaks, with significant intensities were observed at 18.99° and 20.639°. The most intense peak was obtained at 19.8°.

The PXRD pattern of CIII exhibited characteristic reflections at about 2θ 13.70°, 16.50°, 19.15°, 21.14°, 22.71°, 24.90°,25.92°,26.86°,34.90°,36.115°,41.387°, and 53.45°. The PXRD pattern so obtained was very unique compared to the two earlier cocrystals. The intensities of all the peaks were reduced drastically. No major peaks were seen except the most intense peak at 36.115°. The absence of characteristics peaks of ezetimibe and methyl paraben clearly indicates the cocrystal's uniqueness and purity.

It can be seen that the cocrystals exhibited spectra with different peak positions (patterns) from their respective host and guest crystals possessing different crystallographic structures with significant habit modification. Further, the relative intensities of their PXRD peaks were modified which might be attributed to the different crystal habits[14] and arrangement of molecules indicating formation of new crystal forms. This was also strongly supported by the melting points observed for the cocrystals, which were completely different from their respective host and guest crystals as discussed earlier.
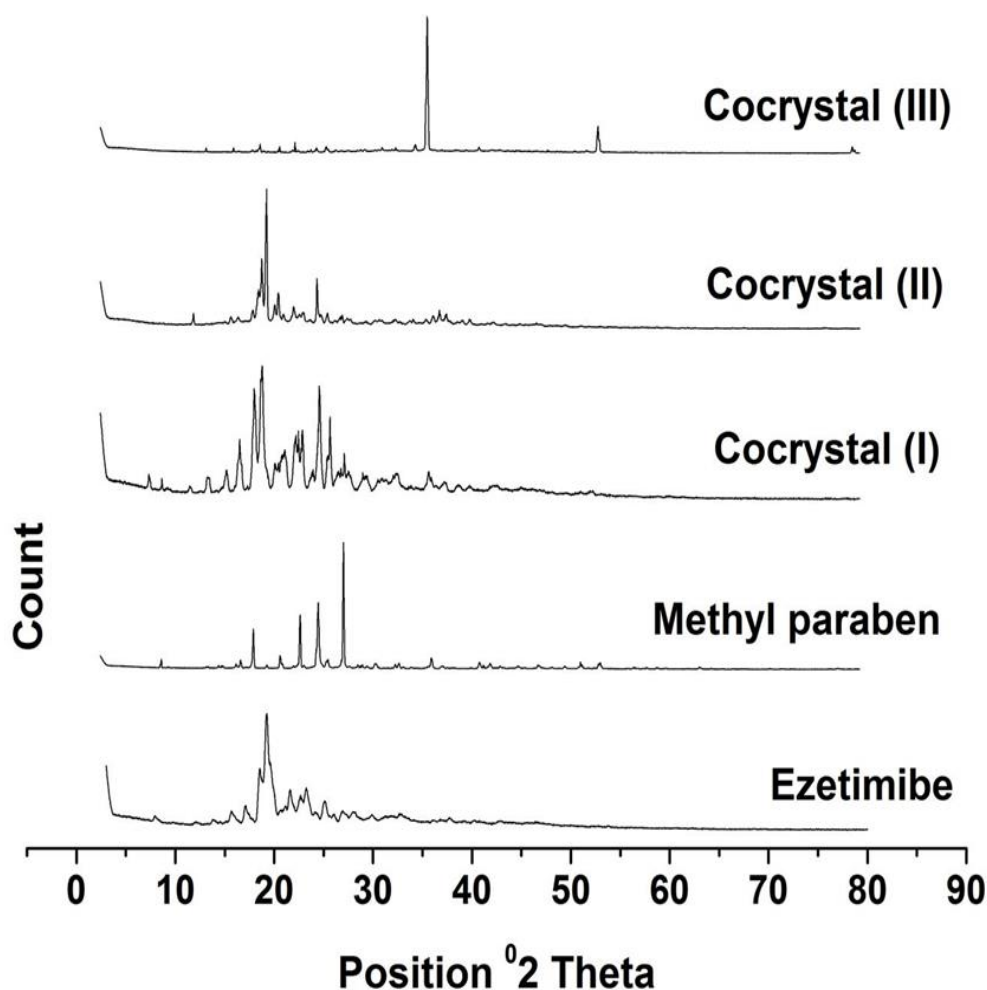

Figure 6. The PXRD patterns of ezetimibe, methyl paraben and cocrystals.

Scanning electron microscopy (SEM)

Figure 7 (a), (b) and (c) show the SEM overview of all the three cocrystal samples CI, CII and CIII. The particles of sample CI appear to be mainly tetragonal and rod-shaped. The

particles of CII on the other hand have no fixed geometry although it is clear that the average particle size of the sample CII is quite less than that of CI. An important point worth noting here is that particles of both the samples CI and CII have non-spherical geometries hence a larger surface compared to spherical particles. This may be because sample CII was prepared by high energy ball milling which is a very high entropy synthesis route hence particles formed are mostly non spherical and quite small. The particles of sample CIII are much bigger in size with average size of about 12 μm. The particle sizes and shapes seen in the electron micrographs completely compliment the results of our dissolution study. We have obtained in our dissolution study that the rate of dissolution for sample CII is highest and for the sample CIII, it is lowest. This can be easily understood by examining the electron micrographs of CII. The particle size of CII is the smallest among the all three cocrystals. Further due to non-sphericity, the surface to volume ratio is much higher than the sample CIII. Both these factors add up in increasing its dissolution rate. Further, due to larger particle size of the sample CIII, its dissolution rate is lowest among the three cocrystals.
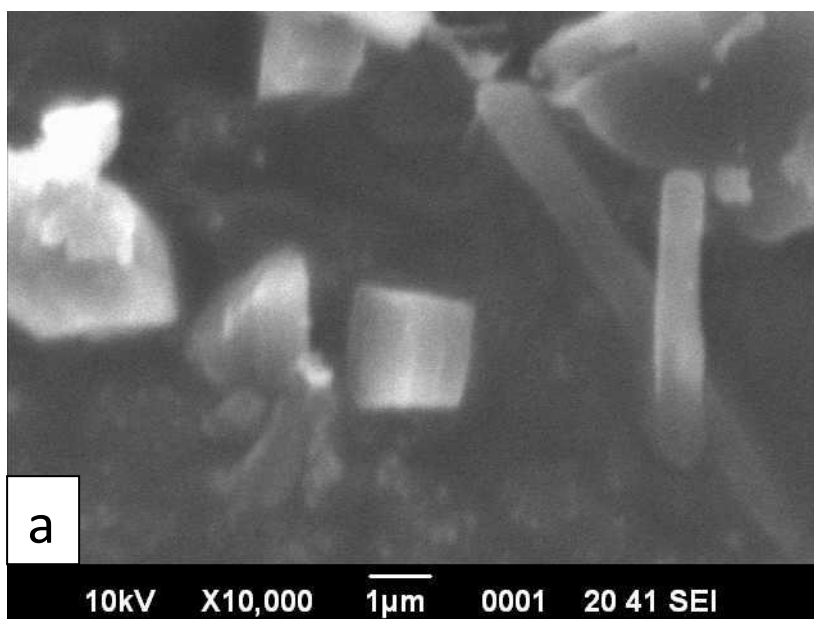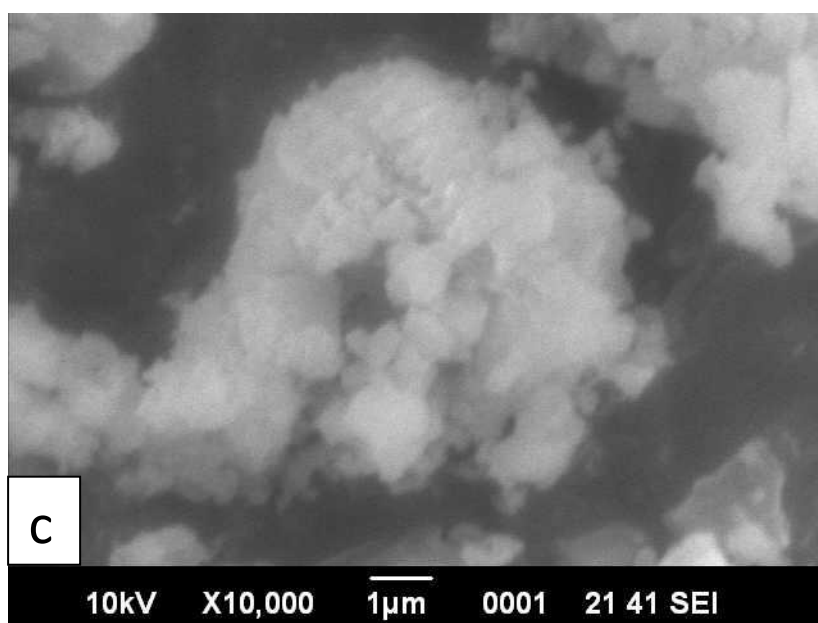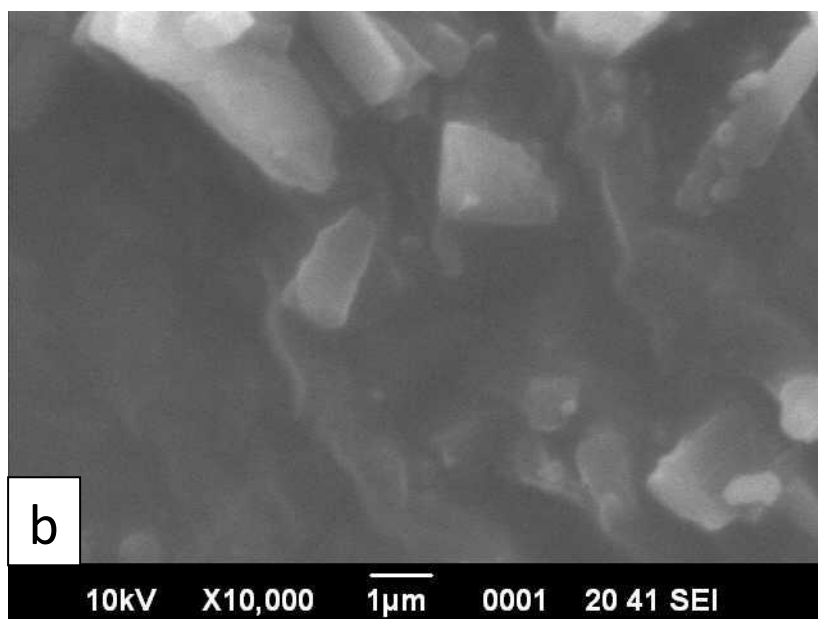
Figure 7. Scanning electron microscopy images of (a) cocrystal I (CI), (b) cocrystal II (CII) and (c) cocrystal III (CIII).

Solubility Studies

Determination of cocrystal stochiometry

Stochiometry of cocrystals via PXRD

The stochiometry of ezetimibe and methyl paraben were calculated from the X-ray diffractograms of CI, CII and CIII. The most intense peak of ezetimibe and methyl paraben was obtained at a reflection of 2θ, 19.24 and 25.08, respectively. Stoichiometric (ezetimibe : methyl paraben) ratio were 1.35, 2.70 and 1.0 for CI, CII and CIII, respectively as given in supplementary information (Table S3). The amount of ezetimibe present in CIII is less as compared to other two cocrystals. It may be confirmed from the mass loss data (24.90%) of CIII in the range of 250 - 380 °C which is corresponding to the mass loss of ezetimibe as shown in TGA data (figure 3).

Stochiometry via HPLC results in case of CIII

The transition concentration values of drug and the coformer measured at the invariant point where two solid phases (drug and cocrystal) are in equilibrium with organic solution. The stoichiometric ratio of ezetimibe and methyl paraben in cocrystal III was 0.97:1. This result was found to be in good agreement with the stochiometry obtained from PXRD quantification.

Measurement of equilibrium cocrystal solubility

The equilibrium solubility ($[drug]_{Scc}/S_{drug}$) values of ezetimibe and its cocrystals is shown in Table 2. Solubility product of cocrystal (K_{sp}), and equilibrium solubility values of cocrystals, that represent nonionized drug and coformer in solution, was calculated according to eq. 1 & 2, respectively. Solubility of cocrystals were multiplied by the stoichiometric coefficient to provide the associated drug concentration and normalized with the relevant stable crystalline drug solubility to provide solubility ratios $[drug]_{Scc}/S_{drug..}$ Solubility ratios emphasize the magnitude of change in solubility achieved by various cocrystals and facilitate comparisons between different cocrystals.

The cocrystals of ezetimibe and methyl paraben studied, showed a maximum of about two fold increase. The solubility ratios were 1.78, 1.42, and 0.941 for CI, CII and CIII, respectively. The solubility of the cocrystals may be increased and/or decreased. It depends

on the crystal density and strength of the hydrogen bond synthons. Higher crystal packing leads to increased stability *vis-a-vis* lower solubility.[54] It was evident from FTIR and Raman spectra study that stronger hydrogen bonding occurred in case of cocrystal III (CIII) which leads to its lower solubility. Clearly, an enhanced solubility was seen in all the cocrystals as compared to pure drug alone except in CIII.

Table 2. Cocrystal component solubilities and calculated cocrystal K_{sp} values, solubilities, and solubility ratios.

Cocrystal	A:B cocrystal stochiometry (drug-ligand)	C [drug] (m) (mean ±S.D.)	D [coformer](m) (mean ± S.D.)	E K_{sp}^{a}	F Cocrystal solubility (m)[b]	G Solubility ratio $[drug]_{Scc}/S_{drug}$
C I	1.35:1	1.84 E-06 ± 2 E-07	1.13E-10 ± 2 E-05	1.53 E-11	2.10 E-05	1.78
C II	2.7:1	2.36E-06 ± 3 E-06	8.04 E-12 ± 4 E-04	4.17 E-18	8.38 E-06	1.42
C III	1.0:1	2.07 E-06 ± 2 E-07	2.25 E-10 ± 9 E-06	2.25 E-10	1.49 E-05	0.941

Solubility of drug was determined experimentally to be S_{drug} = 1.59E-05 (m). [a] K_{sp} units are in $m^{2.35}$, $m^{3.7}$, and m^2 for C I , C II, and C III, respectively. [b] calculated using eq 1. Indicated values reflect HPLC measurement of dissolved cocrystals. Calculations: $E = [C]^A[D]^B$, $F = [E/(A^A B^B)]^{1/A+B}$, $G = (A * F)/S_{drug}$.

Determination of ideal solubility from thermal behaviour

Ideal solubility values of cocrystals, derived from the melting enthalpy and temperature of crystals are listed in Table 3.

Experimental cocrystal aqueous solubility was not well correlated with ideal values derived from the melting enthalpy and temperature of the cocrystals. The ratios of experimental aqueous solubility to ideal solubility are listed in Table 3 to emphasize these deviations. In case of drug and coformer also, no correlation between ideal and experimental solubility was observed. Therefore, it can be suggested that crystal fusion properties are not sufficient for predicting cocrystal solubility. The solution chemistry of cocrystals appears to be critical for describing solubility behaviour.[55] The results further illustrate that melting properties associated with the breaking of the crystal lattice are not sufficiently predictive of cocrystal solubility relations that involve solvent interactions. Ratios of the ideal cocrystal and ideal drug solubilities listed in Table 3 were on a similar order of magnitude to the solution measurements, except in CIII, which showed the highest magnitude.

The thermodynamic ideal solubility seems to more adequately quantify the relative change between cocrystal and drug than absolute solubility values. The cocrystal studied showed that solvent-solute interactions dominate over lattice energies in water.

Table 3. Melt temperature and enthalpy used in calculation of ideal solubility and comparison with experimental solubility values

	Exp aqueous solubility (m)[a]	Ideal Solubility (m)[b]	T_m(°C)	$\Delta H_m{}^c$ (KJ/mol)	Aqueous solubility ratio (exp/ideal)	Ideal cocrystal solubility ratio (cocrystal/drug)
EZT	1.59E-05	15.75	164.36	38.58	1.01E-06	
MP	1.70 E-05	9.78	127.34	25.29	1.74E-06	
C I	1.84 E-06	4.51	109.97	28.47	4.08 E-07	0.28
C II	2.36E-06	3.43	111.27	33.96	6.89 E-07	0.21
C III	2.07 E-06	6.10	109.12	32.92	3.39 E-07	0.39

[a] Measured solubility for anhydrous samples. [b] Ideal solubility calculated from eq 3 using melt temperature and heat of fusion. Mole fractions were converted to molality units in water. [c] The enthalpy of melting for cocrystals is normalized by moles of component molecules(drug + coformer) per mole of cocrystal. All solubility values are expressed in molality units in water.

Dissolution study

The solubility advantage of cocrystals has been shown to correlate with increased dissolution and bioavailability. Ezetimibe cocrystal solubility was greater than ezetimibe. Therefore, in order to assess whether this solubility advantage correlates with increased dissolution, invitro release study was performed in biorelevant media at pH 4.5. Table 4 shows the dissolution data of pure ezetimibe and its cocrystals in 0.45% sodium lauryl sulphate (SLS) of acetate buffer (pH 4.5) at 37 ± 0.5 °C. The dissolution curves of pure ezetimibe alone and cocrystals in 500 mL of 0.45% sodium lauryl sulphate (SLS) in 0.05 M acetate buffer (pH 4.5) are shown in Figure 8.

Table 4. The dissolution data of pure ezetimibe and its cocrystals in acetate buffer (Ph 4.5) at 37 ± 0.5°C.

	%CDR_{15}[a] $\pm$ S.D.	%CDR_{45}[a] $\pm$ S.D.	%CDR_{120}[a] $\pm$ S.D.
Ezetimibe	42.55 ± 1.66	61.64 ± 3.35	68.55 ± 3.25
Cocrystal I	60.50 ± 1.65[b]	64.93 ± 0.59	76.59 ± 2.98
Cocrystal II	69.47 ± 1.66[b]	73.89 ± 0.60[b]	85.56 ± 2.98[b]
Cocrystal III	51.53 ± 1.66[b]	61.64 ± 3.34	68.82 ± 3.41

[a] Indicates $\pm$ S.D., (n=3); S.D.: standard deviation; %CDR_{15}, %CDR_{45} , %CDR_{120}: percentage cumulative drug released in 15 min, 45 min and 120 min; [b] Significant difference compared to pure ezetimibe i.e. significant (p<0.05).
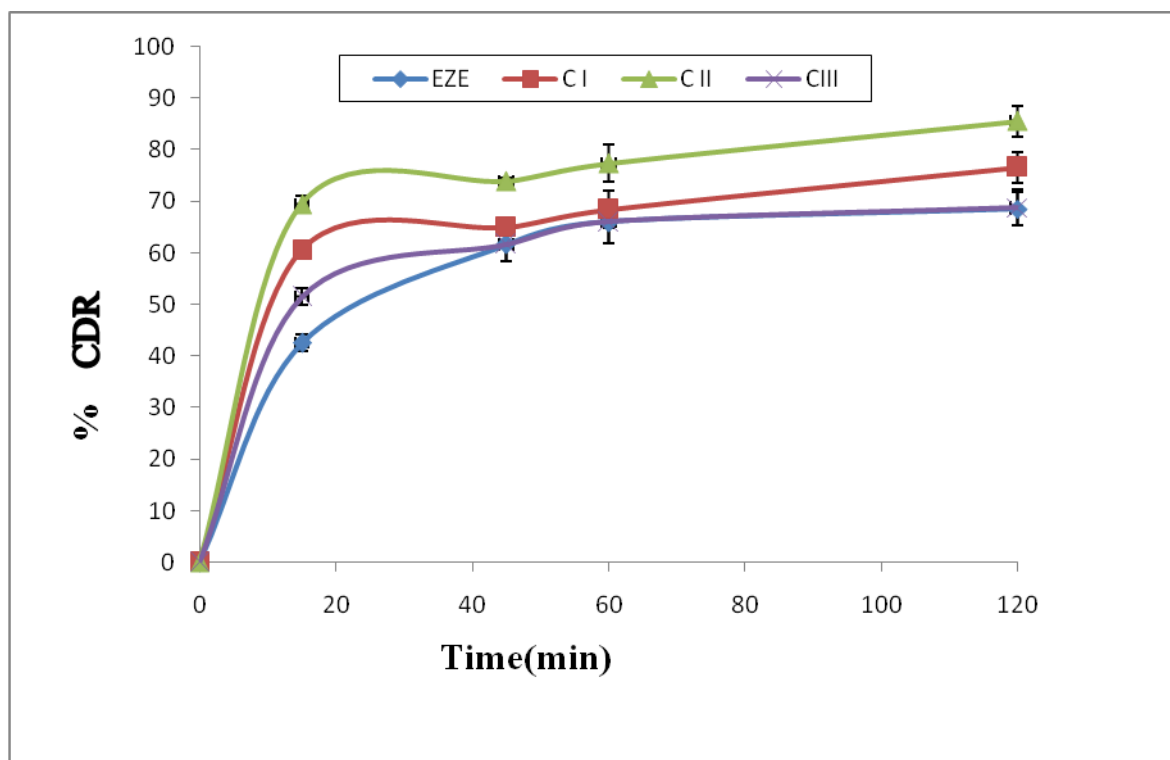
Figure 8. Dissolution curves of ezetimibe and its cocrystals. CI (solution crystallization method); CII (liquid assisted grinding method); CIII (reaction crystallization method)

The dissolution profiles of all cocrystals, with pure ezetimibe as a control were studied for 2 hours in defined biorelevant media. The release data, dissolution efficiency (DE%) (supplementary information table S4) at different sampling time of all cocrystals were statistically analysed using one way ANOVA followed by Tuckey's post-hoc analysis at a significance level of 95% ($p<0.05$). The statistical analysis of %CDR values revealed a significant improvement in dissolution profile of ezetimibe at 15 min (%CDR15) in all the three cocrystals ($p<0.05$). Similarity factor of three cocrystals were calculated with a reference of pure ezetimibe %CDR (supplementary information table S4). The cocrystal CII, prepared by liquid assisted grinding method showed significant improvement in dissolution at 45 and 120 min, indicating a good dissolution profile. Moreover, CII showed a release of 85.56% drug in 120 min, highest among all. This result is in good agreement with the thermal behaviour of CII. From DSC result it is clear that CII contains two polymorphic crystals. The peak melting temperature of one polymorph was at about 81.1 °C. Peak melting temperature (Tm) is an indicator of thermostability and generally the higher the value of Tm, the more thermodynamically stable is the molecule and vice versa.[46] The release of pure drug was about 68% in 120 min. CII exhibited enhanced drug release at each time point, than CI,

despite having lesser solubility than the latter, thus showing some deviation from the solubility values. CIII on the other hand, followed similar pattern of drug release to that of pure drug after 15 min which might be because of rapid transformation to original crystal of drug. The faster dissolution of ezetimibe from cocrystals might be accredited to altered crystallinity pattern, size and shape and crystal habit of cocrystal, which led to improved solubility of cocrystals in dissolution media. Further, higher association between ezetimibe and coformers also might have contributed for enhanced dissolution of drug from CI and CII.

Conclusion:

The present study illustrated the formation and characterization of three different cocrystals of ezetimibe using methyl paraben as a coformer, employing three different processes, namely solution crystallization, liquid assisted grinding and reaction crystallisation. DSC result shows that the entirely different peak melting temperature was observed in all three cocrystals indicating the formation of new solid phase. FTIR and Raman spectroscopy study reveals that the new solid form is the result of weak electrostatic interaction between drug and coformer. From PXRD study, it is clear that the crystal habit of both the drug and the coformer has been modified. Equilibrium solubility study and dissolution study of the cocrystals reveals that the cocrystals of ezetimibe and methyl paraben can a possible and potential alternative and effective approach for improving its solubility.

References:

1. Scott L. Childs, S. L. ; Hardcastle, K. I. *Cryst. Growth Des.***2007,** 7, 1291-1304.
2. Haleblian, J.; McCrone, W. *J. Pharm. Sci*. **1969**, 58, 911-929.
3. *Guidance for Industry, ANDAs: Pharmaceutical Solid Polymorphism*; Food and Drug Administration: Silver Spring, 2007.
4. N. J. Babu and A. Nangia, Cryst. Growth Des. 2011, 11, 2662–2679.
5. N. Schultheiss and A. Newman, Cryst. Growth Des. 2009, 9, 2950–2967.
6. Maitland, G. C.; Rigby, E. B.; Smith, E. B.; Wakeham, W. A. *Intermolecular Forces: Their Origin and Determination*; Oxford University Press: Oxford, 1981.
7. Pauling, L. *The Nature of Chemical Bond*; Cornell University Press: New York, 1948.
8. Pedersen, C. J. *J. Am. Chem. Soc*. **1967**, *89*, 7017-7036.
9. Cram, D. J.; Dewhirst, K. C. *J. Am. Chem. Soc*., **1959**, *81*, 5963-5971.

10. Stahl, P. H.; Nakano, M. *Pharmaceutical Aspects of the Drug Salt Form, in Handbook of Pharmaceutical Salts: Properties, Selection, and Use*; Stahl, P.H., Wermuth, C. G., Eds.; Wiley-VCH/VCHA: New York, 2002.

11. Rxlist homepage. http://www.rxlist.com/top200.htm. (accessed Jan 13, 2013).

12. *The Merck Index.*; U.S. publication; Whitehouse Station, N.J.: USA;13, 4.

13. Walsh, R. D. B.; Bradner, M. W.; Fleischman, S.; Morales, L. A.; Moulton, B.; Rodríguez-Hornedo, N.; Zaworotko, M. J. *Chem. Commun.* **2003**, 186-187.

14. Fleischman, S. G.; Kuduva, S. S.; McMahon, J. A.; Moulton, B.; Walsh, R. D.B.; Rodríguez-Hornedo, N.; Zaworotko, M. J. *Cryst. Growth Des.* **2003**, *3*, 909-919.

15. McMahon, J. A.; Bis, J. A.; Vishweshwar, P.; Shattock, T. R.; McLaughlin, O. L.;Zaworotko, M. J. *Z. Kristallogr.* **2005**, *220*, 340-350.

16. Vishweshwar, P.; McMahon, J. A.; Peterson, M. L.; Hickey, M. B.; Shattock, T.R.; Zaworotko, M. J. *Chem. Commun*., **2005**, 4601-4603.

17. Childs S. L.; Chyall L. J.; Dunlap J. T.; Smolenskaya V. N.; Stahly B. C.; Stahly G. P. *J. Am. Chem. Soc.* **2004**, *126*, 13335-13342.

18. Remenar, J. F.; Morissette, S. L.; Peterson, M. L.; Moulton, B.; MacPhee, J. M.;Guzman, H. R.; Almarsson, Ö. *J. Am. Chem. Soc.* **2003**, *125*, 8456-8457.

19. Scott, C.; Nathan, B.; Reddy, L.S. WO 2012/116349 A2 , 2012.

20. Mulye, P. S.; Jamadar, S. A.; Karekar, P. S. *Powder Technology* **2012**, 222,131-138.

21. Product monograph: [Pr]EZETROL®.; Merck Canada Inc.: Canada, 2012. http://www.merckfrosst.ca/assets/en/pdf/products/EZETROL-PM_E.pdf
 (accessed Nov, 2012).

22. Zetia Drug Description RxList.com.; The Internet Drug Index WebMD ,Inc.: New York, 2008. http://www.rxlist.com/zetia-drug.htm. (accessed Nov, 2012).

23. Patel, R.; Bhimani, D.; Patel, J.; Patel, D. *J. Inclu. Phenom. Macro*. **2008**, 60, 241-251.

24. Sancheti, P. P.; Karekar, P.; Vyas, V.; Shah, V. M.; Pore, Y. V. *Pharmazie.* **2009**, 64, 227-231.

25. Dixit, R. P.; Nagarsenker, M. S. *Eu. J. Pharm. Sci*. **2008**, 35, 183-192.

26. U.S. Food and Drug administration approved GRAS list. EAFUS: A Food Additive Database. http://www.cfsan.fda.gov/_dms/eafus.html. (accessed Nov, 2013).

27. Zhang, G. G. Z.; Henry, R. F.; Borchardt, T. B.; Lou, X. *J. Pharmac. Sci.* **2007**, 96, 990-995.

28. Childs, S. L.; Rodriguez-Hornedo, N.; Reddy, L. S.; Jayasankar, A.; Maheshwari, C.; McCausland, L.; Shipplett, R.; Stahly, B. C. *Cryst. Eng. Comm.* **2008**, 10, 856-864.

29. Frisˇcˇic, T.; Jones, W. *Cryst Growth Des.* **2009**, 9, 1621-1637.

30. Trask, A.; Jones, W. *Top Curr Chem.* 2005, 254, 41-70.

31. Rodriguez-hornedo, N.; Nehm, S. J.; Seefeldt, K. F.; Pagan, Y.; Falkiewicz, C. J. *Mol Pharm.* **2006**, 3, 362-367.

32. Nehm, S. J.; Rodriguez-Spong, B.; Rodrı´guez-Hornedo, N. *Cryst.Growth Des.* **2006**, *6*, 592-600.

33. Goehner, R. P. *Advances in X-Ray Analysis.* **1982**, 25, 309-313.

34. Jayasankar, A.; Reddy, L. S.; Bethune, S. J. ; Rodrı´guez-Hornedo, N. *Cryst. Growth Des.* **2009**, 9, 889-897.

35. Childs, S. L.; Rodrı´guez-Hornedo, N.; Reddy, L. S.; Jayasankar, A.; Maheshwari, C.; McCausland, L.; Shipplett, R.; Stahly, B. C. *Cryst.Eng. Comm.* **2008**, *10*, 856-864.

36. Jacques, J.; Wilen, S. H. *Enantiomers, Racemates, and Resolution.*; Krieger Publishing Company: Malabar, FL, 1991.

37. Klussmann, M.; White, A. J. P.; Armstrong, A.; Blackmond, D. G.*Angew. Chem., Int. Ed.* **2006**, *45*, 7985-7989.

38. Glasstone, S., *Textbook of Physical Chemistry*, 2nd ed.; MacMillan: London, 1948.

39. Grant, D. J. W.; Higuchi, T., *Solubility Behavior of Organic Compounds*; Wiley: New York, 1990; liii.

40. Bethune, S. J. Thermodynamic and kinetic parameters that explain solubility and crystallization of pharmaceutical cocrystals. Ph.D. Thesis, University of Michigan, Ann Arbor, MI, 2008.

41. Nehm, S. J.; Jayasankar, A.; Rodrı´guez-Hornedo, N. *AAPS J.* **2006** ; abstract W5205.

42. Young, P. H.; Schall, C. A. *Thermochimica. acta.* **2001**, 367-368, 387-392.

43. Schultheiss, N.; Newman, A. *Cryst. Growth. Des.* **2009**, 9, 2950-2967.

44. Ghosh, S.; Bag, P. P.; Reddy, C. M. *Cryst. Growth. Des.***2011,** 11, 3489-3503.

45. Bucar, D. K.; Day, G. M.; Halasz, I.; Zhang, G. G. Z.; Sander, J. R. G.; Reid, D. G.; MacGillivary, L. R.; Duer, M. J.; Jones. W. C*hem. Sci*. **2013**, 4, 4417-4425.

46. Aitipamula, S.; Chow, P. S.; Tan, R. B. H. *CrystEngComm.* **2009,** 11, 1823-1827.

47. Adalder, T. K.; Sankolli, R.; Dastidar, P. *Cryst. Growth. Des.* **2012,** 12, 2533-2542.

48. Raghavan, K.; Dwivedi, A.; Campbell, G.C.; Johnston, E.; Levorse, D.; McCauley, J.; Hussain, M. *Pharm. Res***. 2003**, 10, 6, 900-904.

49. Villepin, J.; de Novak, *A. Spectrochim. Acta Part A* .**1971**, 34, 1259-1270.

50. Mukherjee, K. M.; Misra, T. N. *J. Raman Spectrosc.* **1996**, 27, 595-600.

51. Koczon, P.; Dobrowolski, J. C. Z.; Lewandowski, W.; Mazurek, A. P. *J. Mol. Struct.* **2003**, 655, 89-95.

52. Sala, O.; Gonc-alves, N. S.; Noda, L. K. *J. Mol. Struct*. **2001**, 565-566, 411-416.

53. Ali, H. R. H.; Alhalaweh, A.; Velaga, S. P. *Anal. Chim. Acta.* **2008**, 620, 103-112.

54. Goud, N. R.; Khan, R. A.; Nangia, A. *CrystEngComm.* **2014,** 16, 5859-5869.

55. Good, D. J.; Rodrı´guez-Hornedo, N. *Cryst. Growth. Des.* **2009,** 9, 2252-2264.

Objective: To ensure the bioavailability of telmisartan without using any alkalinizer.

Abstract of literature review

The poor dissolution characteristics of relatively insoluble drugs have been a problem to the pharmaceutical industry. When an insoluble or sparingly soluble drug is administered orally, the rate and extent of absorption are controlled by the dissolution rate in the gastrointestinal fluids[1]. Among various techniques emerged to address bioavailability problem co grinding approach (usually with water soluble polymers as carriers) is less frequently reported [2]. Cogrinding techniques is effective in increasing the solubility of insoluble drugs and is economically desirable and environment friendly as it does not require any organic solvents/toxic solvents or any sophisticated equipment [3-4].Various investigators reported that the ratio of the drug to carrier and the type of carriers play a major role to control the dissolution rate from co-ground sample [5-8].The undesirable effects on APIs upon milling such as aggregation of fine particles, induction of electrostatic charges, mechanochemical transformation, APIs degradation and solid state reactivity has been initiated the utilization of co-milling techniques of drug with additives and has successfully applied which also increased the milling efficiency[9-13].

2. Objectives

Improvement of dissolution and bioavailability of Telmisartan (TLM) (a BCS class II drug) by cogrinding with poly (vinyl alcohol) (PVA).

- To formulate tablet dosage form using suitable co grinded mixtures and compare the dissolution profile with reference product.
- To study the effect of various parameters that affect co-grinding process *viz;* ball to powder ratio (BPR), rotational speed and duration of grinding on dissolution profile of the TLM.
- To characterize the various co-grinded mixtures using FTIR, DSC, PXRD and SEM
- To conduct accelerated stability studies on the formulations.
- To conduct bioavailability studies in rabbits for the optimized formulation.

3. Materials and Method

3.1. Materials

TLM (Assay HPLC 99.7%) was provided by Unichem Laborotories Ltd. (Himachal Pradesh, India). PVA 87-90% hydrolyzed, average Mol weight 30,000 to 70,000 (Sigma- Aldrich Co. USA), were used.

3.2. Ball milling

The physical mixtures of drug: carrier was prepared by simply blending the TLM powder and PVA powder in different ratio and co-milled using Fritsch Pulverisette 5 (Fritsch GmbH Pulverisette 5, Idar-Oberstein, Germany), a planetary ball mill equipped with stainless steel jar and balls (diameter 5 mm). The mass ratio of ball to sample was varied between 5:1 to 20:1. The rotation speed was set at 300 and 600 rev min^{-1} at specified milling duration. For comparison purposes the TLM and PVA powders were also ground alone in the ball mill under the same conditions used to prepare the cogrinds. The co-milled powder was characterized immediately after harvesting the sample from the milling jars at the end of the milling process.

3.3. Preparation of tablets

Tablets containing 20 mg TLM were prepared by direct compression method. Starch (not less than 33% w/w), lactose (not less than 33 % w/w), were blended with PM or cogrinds equivalent to 20 mg of TLM and was passed through 22 # mesh. The homogeneity was ensured by mixing index determination and the tablets were compressed using a rotary tablet machine with 7 mm or 13 mm punch diameter (Cadmach, Ahmadabad, India). The tablet hardness was setted to 4 kg/cm^2, measured using Monsanto hardness tester (Campbell electronics, India).

3.4. Dissolution tests

The dissolution rates of TLM from tablets were investigated using by USP dissolution test apparatus, Type II (TDT-08L dissolution tester Electrolab, Mumbai, India), at a rotation speed of 75 rpm in 900 mL phosphate buffer solution (pH 6.8) at 37±0.5°C. 5 mL of aliquots were withdrawn at predetermined interval, replaced with same volume of fresh solution. The samples were filtered through nylon membrane filter (0.22 μm). Then, the concentration of TLM was analyzed by UV- Visible spectroscopy (model UV 1800, Shimadzu, Tokyo, Japan.) at a UV detection wavelength of 296 nm.

3.5. Powder X-ray diffraction

The powder X-ray diffractograms (PXRDs) of TLM, PVA, PMs and cogrinds (under size material of 60 # mesh) were recorded to determine the polymorphic transformations occurring during the process, by using an X-ray diffractometer (Bruker AXS D8 Advance, Configuration: Vertical, Theta/2 Theta geometry; Rheinstetten, Germany,) X-ray source was Cu, wavelength 1.5406 Å, detector: Si (Li) PSD. The diffractograms were recorded at a scanning speed of 2°/min and a chart speed of 2°/2 cm per 2q and the angular range fixed was from 3° to 80°.

3.6. Differential scanning calorimetry

Differential scanning calorimetry (DSC) thermograms of TLM, PVA, PMs and cogrinds (2mg of each) were obtained using a DSC-60 instrument (Shimadzu), which was calibrated with indium. The thermograms were recorded at a heating rate of 10°C/min from 10°C to 300°C in nitrogen atmosphere (flow rate 20 ml/min) using TA60-WS software (Shimadzu).

3.7. Fourier transform infrared spectroscopy

Fourier transform infrared spectroscopy (FTIR) spectra of TLM, PVA, PMs and cogrinds were obtained using an FTIR-8400S instrument (Shimadzu, Kyoto, Japan).A small amount of each material was triturated with KBr (1weight % drug content) and placed into sample holder for analysis. The spectrum was scanned in the range of 400– 4000/cm at a resolution of 2/cm with scan speed of 64 scan/s and was recorded by using IRSolution software (Shimadzu).

3.8 Scanning electron microscopy

The morphology of the TLM, PVA, PMs and cogrinds were examined by scanning electron microscopy (SEM) (JSM-6390; JEOL, Tokyo, Japan). The samples were coated using platinum to increase the conductivity of the electron beam. The operating conditions were an accelerating voltage of 10 kV, with a working distance of 12 mm at a spot size of 45.

3.9. Stability study

Cogrinds were subjected to accelerated stability studies as per ICH (International Conference on Harmonization) guidelines (Q1E, Step4) at 40°C±2°C/75±5% relative humidity. The samples were withdrawn periodically (0, 15, 30, 60, 90 and 180 days) and evaluated for different parameters viz; appearance, drug content and in-vitro release studies. After 180 days, FTIR and PXRD study of the samples were carried out to check physicochemical stability of TLM in stressed condition.

4. Results

4.1. Optimization of the process

The goal of the study was to improve the dissolution of the TLM to > 75% at 45 mins. The experiment was preceded as per the flow chart (fig.1). The preliminary results obtained were shown as in table.1
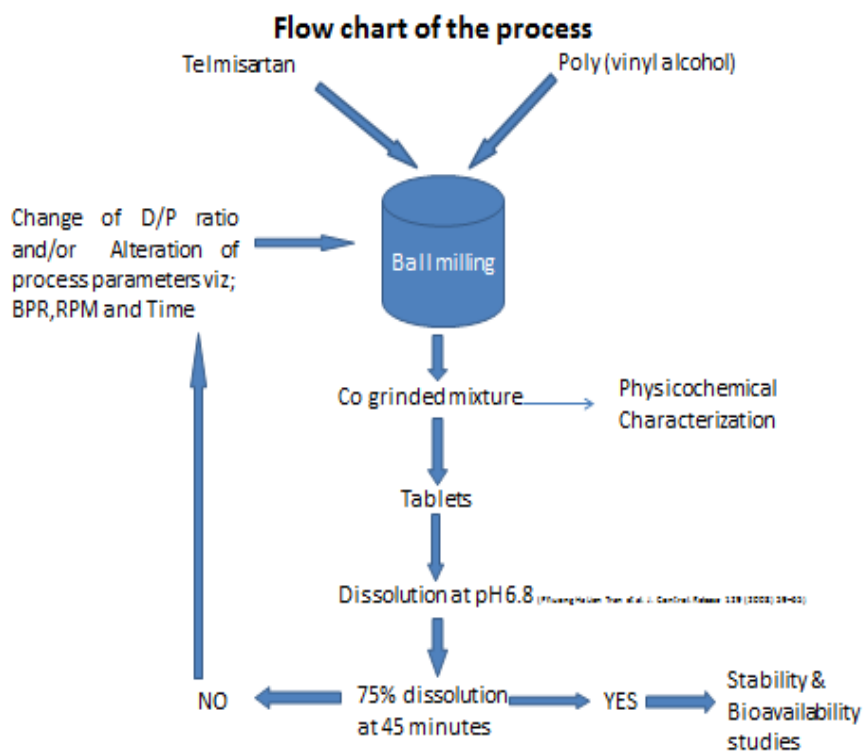

Figure 1: Flow chart of the process

Table 1. Process description of preliminary batches and dissolution pattern

NO.	D/P ratio	BPR	RPM	Time (hrs)	Tablet Dissolution (Cumulative %)			
					15 mins	*30 mins*	*45 mins*	*60 mins*
1	100/0	0	0	0	5.55 ±0.99	5.50±0.19	6.07±0.29	6.10±0.05
2	50/50	5:1	300	3	17.18±1.93	18.57±2.89	20.61±2.46	20.65±2.40
3	25/75	5:1	300	3	16.86±4.54	23.28±3.43	27.61±5.08	29.80±6.02
4	25/75	10:1	300	3	21.49±1.25	30.57±2.33	40.68±2.48	44.91±2.66
5	25/75	10:1	600	3	43.81±3.81	56.19±5.56	59.92±2.97	61.66±3.03
6	25/75	15:1	600	3	49.52±1.51	59.34±4.21	62.88±2.82	65.59±2.09
7	12.5/87.5	15:1	600	3	77.86±9.32	96.57±2.02	98.20±1.16	96.78±6.40
8	100/00	15:1	600	3	44.83±3.42	50.11±0.36	52.00±0.62	54.10±2.75

The batch no 7 showed the desired result and there is significance enhancement of dissolution when compare to the previous batches studied (batch 1 -6). Further to study the effect of various parameters on the optimized batch (batch 7 were studied).

Table 2. Effect of drug to polymer ratio on dissolution

No.	D/P ratio	BPR	RPM	Time (hrs)	Tablet Dissolution (Cumulative %)			
					15 mins	*30 mins*	*45 mins*	*60 mins*
1	50/50	15:1	600	3	17.83±0.77	22.20±0.69	25.00±0.96	27.10±1.26
2	25/75	15:1	600	3	49.52±1.51	59.34±4.21	62.88±2.82	65.59±2.09
3	12.5/87.5	15:1	600	3	77.86±9.32	96.57±2.02	98.20±1.16	96.78±6.40
4	100/00	15:1	600	3	44.83±3.42	50.11±0.36	52.00±0.62	54.10±2.75

Table 3. Effect of duration of grinding on dissolution

No	D/P ratio	BPR	RPM	Time (hrs)	Tablet Dissolution (Cumulative %)			
					15 mins	*30 mins*	*45 mins*	*60 mins*
1	12.5/87.5	15:1	600	3	77.86 ±9.32	96.57±2.02	98.20±1.16	96.78±6.40
2	12.5/87.5	15:1	600	2	53.49±12.10	71.45±14.99	75.62±6.57	78.33±5.08
3	12.5/87.5	15:1	600	1	44.92±8.51	56.74±7.85	63.93±5.56	67.97±3.82
4	12.5/87.5	15:1	600	0.5	34.95±4.41	45.19±4.30	50.91±7.52	52.29±6.01
5	12.5/87.5	-	-	0	10.23±1.50	13.10±1.14	16.83±1.88	19.17±1.80

Table 4. Effect of RPM on dissolution

No	D/P ratio	BPR	RPM	Time(hrs)	Tablet Dissolution (Cumulative %)			
					15 mins	*30 mins*	*45 mins*	*60 mins*
1	12.5/87.5	15:1	300	3	25.86±1.05	36.34±0.22	42.97±0.13	44.98±1.27
2	12.5/87.5	15:1	450	3	28.35±5.94	45.35±9.51	55.14±7.15	59.69±5.26
3	12.5/87.5	15:1	600	3	77.86±9.32	96.57±2.02	98.20±1.16	96.78±6.40

Table 5. Effect of Ball to powder ratio (BPR) on dissolution

No.	D/P ratio	BPR	RPM	Time(hrs)	Tablet Dissolution (Cumulative %)			
					15 mins	*30 mins*	*45 mins*	*60 mins*
1	12.5/87.5	20:1	600	3	75.66±7.00	85.93±4.67	88.99±3.22	89.44±1.82
2	12.5/87.5	15:1	600	3	77.86±9.32	96.57±2.02	98.20±1.16	99.00±2.40
3	12.5/87.5	10:1	600	3	45.98±3.61	65.89±6.44	74.75±4.83	80.75±3.59
4	12.5/87.5	5:1	600	3	19.61±1.81	25.18±2.53	27.67±2.60	29.95±2.57
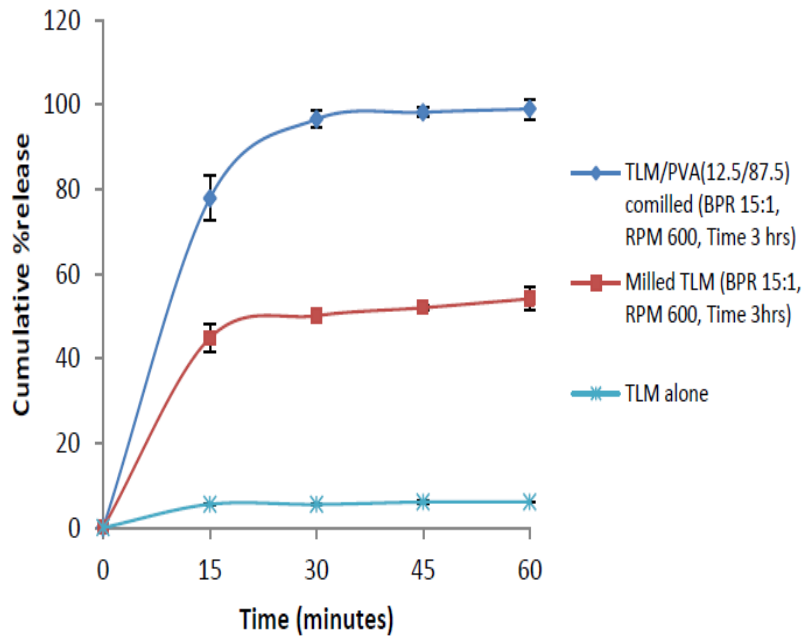
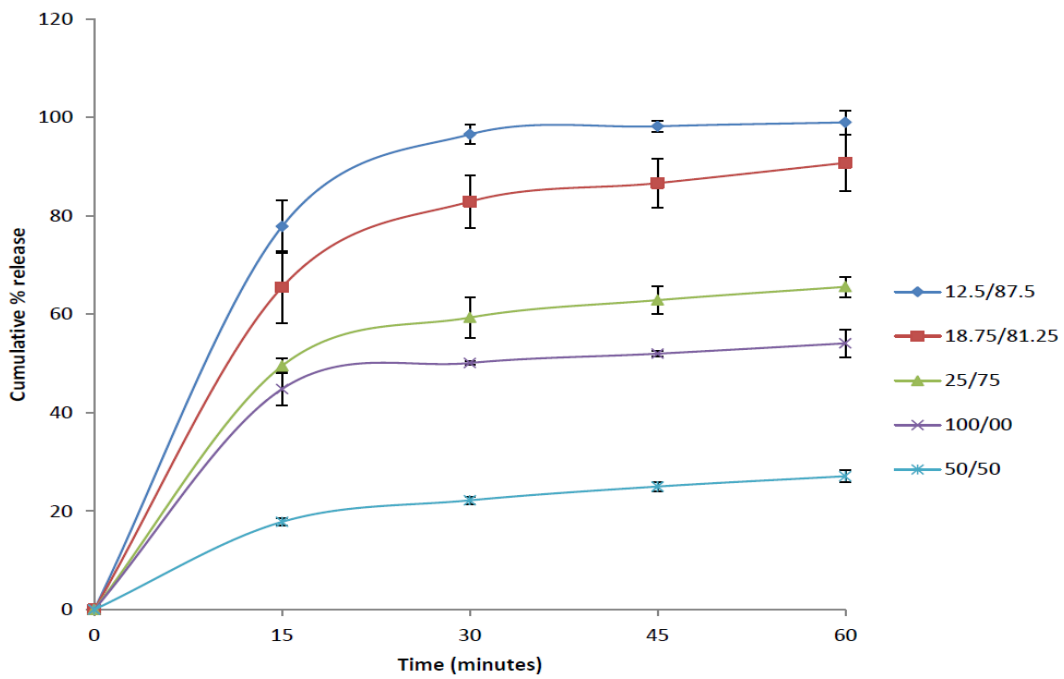**Fig.2:** Effect of milling and comilling with PVA on dissolution of TLM

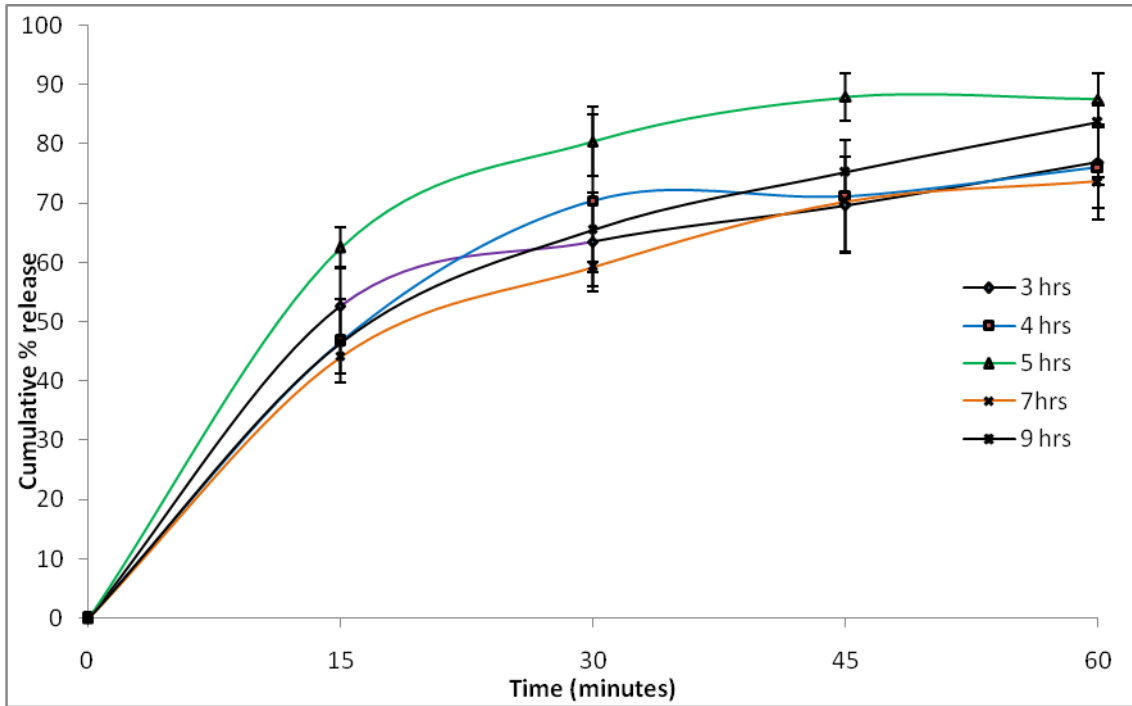**Fig. 3:** Effect of TLM /PVA ratio on drug release (BPR 15:1, RPM 600, Time 3hrs)

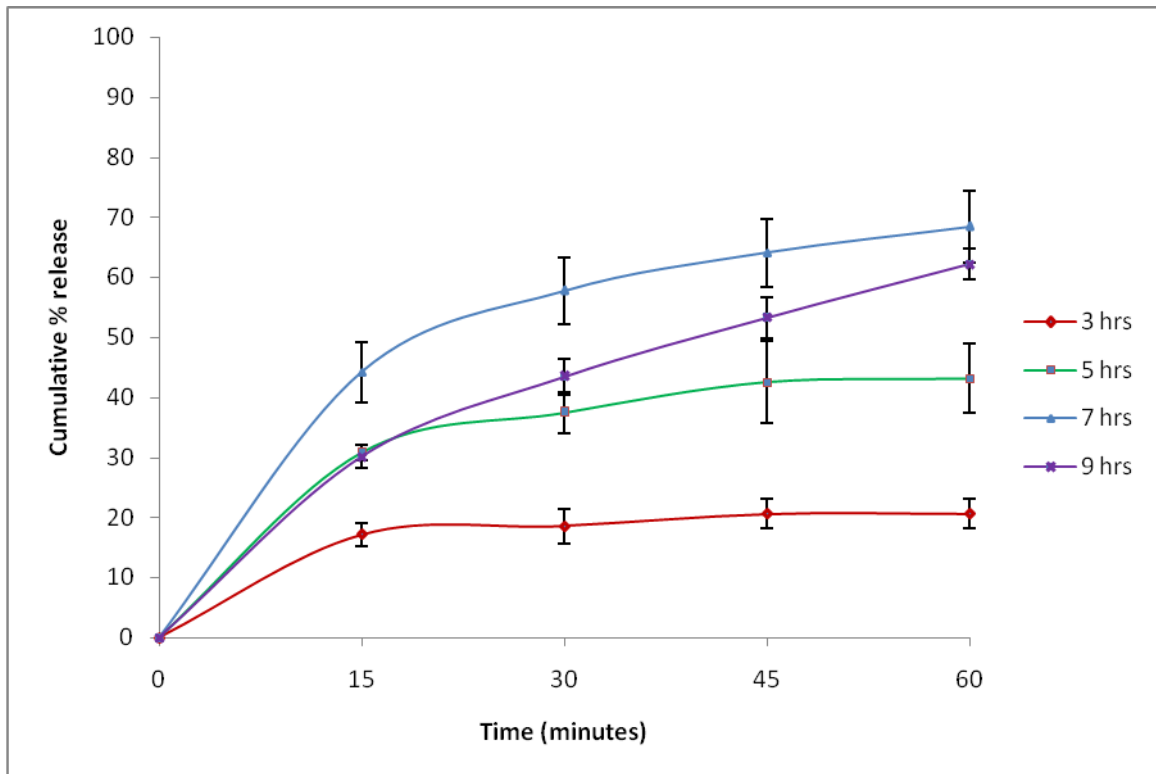**Fig.4**: Effect duration of grinding on drug release (D/P ratio (25/75), BPR 15:1, RPM 600)

Fig.5: Effect duration of grinding on drug release (D/P ratio (50/50), BPR 15:1, RPM 600)

4.2. Powder X-ray diffraction

In this experiment, the crystallinity of the drug was remarkably decreased and amorphous form was formed by the mechanical stress during grinding, which is depicted by a halo pattern in the PXRD of grinded sample Fig.2.b. In the cogrinded sample resulted extremely small sizes of crystallite or micro-assemblies of the molecules, and these small particles surrounded by additives did not clearly show the diffraction peaks on the X-ray diffractogram. The solid state of the drug in the CG might be consisted as the amorphous and/or fine crystallite of the drug.
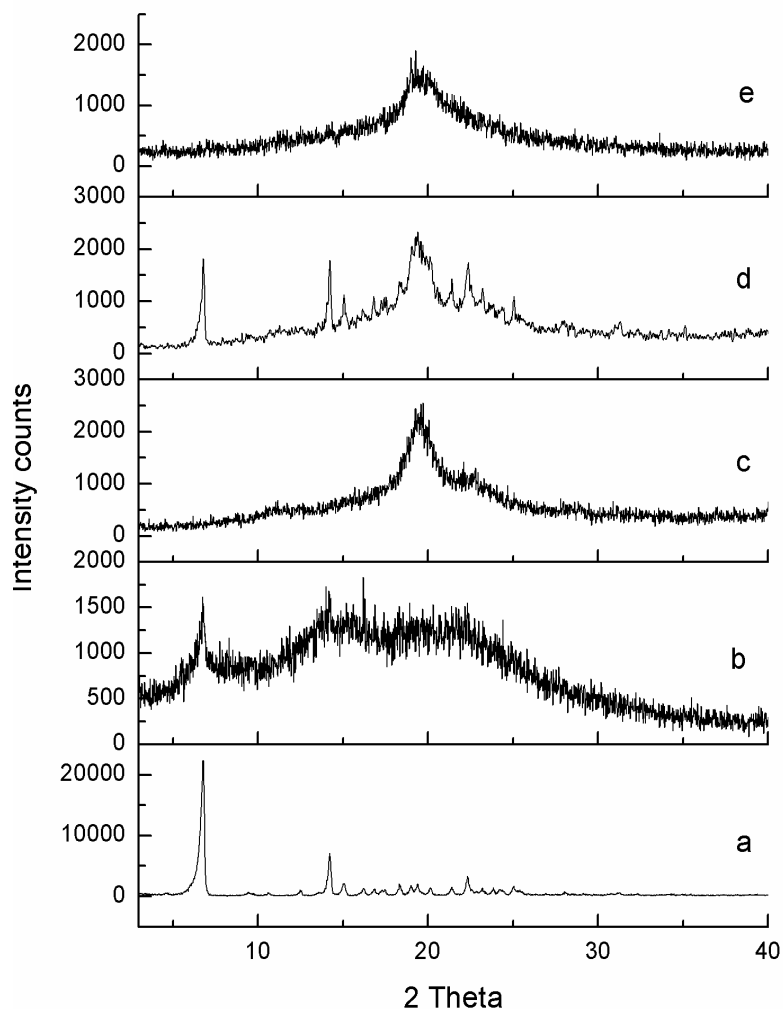

Fig. 6: PXRD pattern of TLM (a) Milled TLM (b), PVA (c), Physical mixture of TLM/PVA (d) and Co grinded mixture (e)
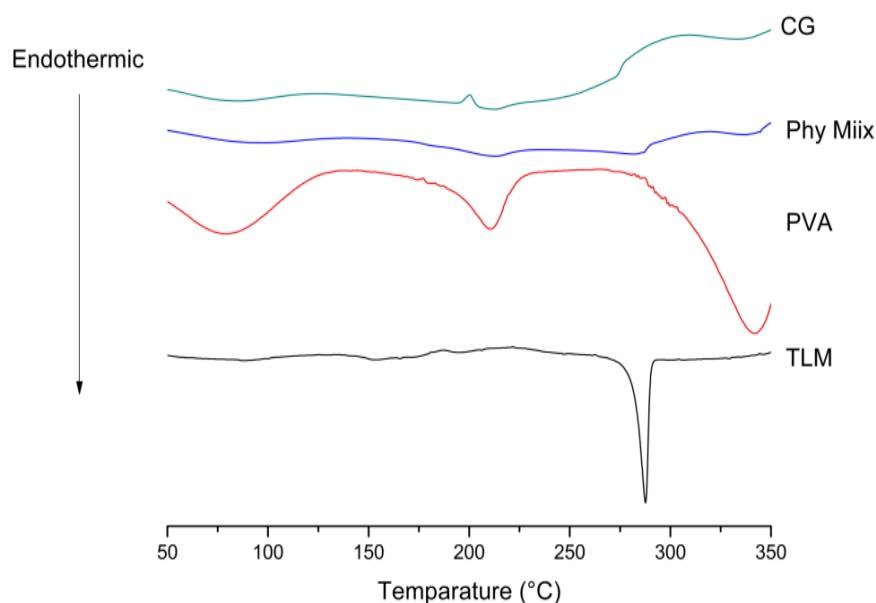
4.3 Differential scanning calorimetry

Fig. 7: DSC pattern of TLM, PVA ,Physical mixture of TLM/PVA and Co grinded mixture

A depression in melting peak (270 to 267) of TLM upon milling indicates particle size reduction. This depression may be also due to the defective crystals of TLM upon milling. PVA (partially hydrolyzed) exhibited a T_m around 190 °C. In PM the lower value (Tm 267) than pure TLM (Tm 270) attest only weaker interaction between TLM and PVA.

4.4. Fourier transform infrared spectroscopy

The structure of TLM involves two benzimidazole rings (proton acceptor N atom) and one biphenyl rings with a carboxylic acid (proton donor) group. These groups on the surface are responsible for forming hydrogen bond with neighboring components and thus are responsible for polarity of the surface.TLM possesses hydrophobic (phenyl ring) as well as hydrophilic regions [carbonyl (C=O) and imine (C=N)] in its structure. It can be seen from Fig. 8 that, the nitrogen and oxygen are associated with hydrophilic moieties while benzene ring of benzimidazole and phenyl ring is associated with hydro-phobic moieties.

The FTIR spectrum of TLM shows characteristics peaks at 3060 cm⁻¹ (O-H stretching), 2959 cm⁻¹ (aliphatic C-H stretching), 2903 cm⁻¹ (aromatic C-H stretching), 1696 cm⁻¹ (C=O stretching), 1599 cm⁻¹ (C=N) stretching), 1521 cm⁻¹ ,1459 cm⁻¹ ,1412 (aromatic C=C stretching), 1127 cm ⁻¹(O-H bending of –COOH) and 757& 748 cm⁻¹ (ring vibration of 1,2 substituted benzene).

The PVA (partially hydrolyzed shows very intense and broad peaks centered at 3252 cm$^{-1.}$ this band is attributed to a wide distribution of hydrogen bonded hydroxyl groups (self-association. Since we used a partially hydrolyzed PVA, we would attribute the bands at 1740, 1256, 1028 and 946 cm-1 to the presence of acetates monomer units. The spectrum of PVA (87-90% hydrolyzed) presents a strong absorption at 1735 cm^{-1} (free carbonyl groups) with a shoulder peak (1716 cm^{-}1) at lower wave number side due to hydrogen bonded carbonyl groups. There are some other bands that should be shifted due to hydrogen bond interactions. For example C-O-C stretching region of acetate units is observed at 1247cm^{-1} but not shifted significantly indicated the absence of hydrogen bong interaction between acetate units of PVA and TLM.
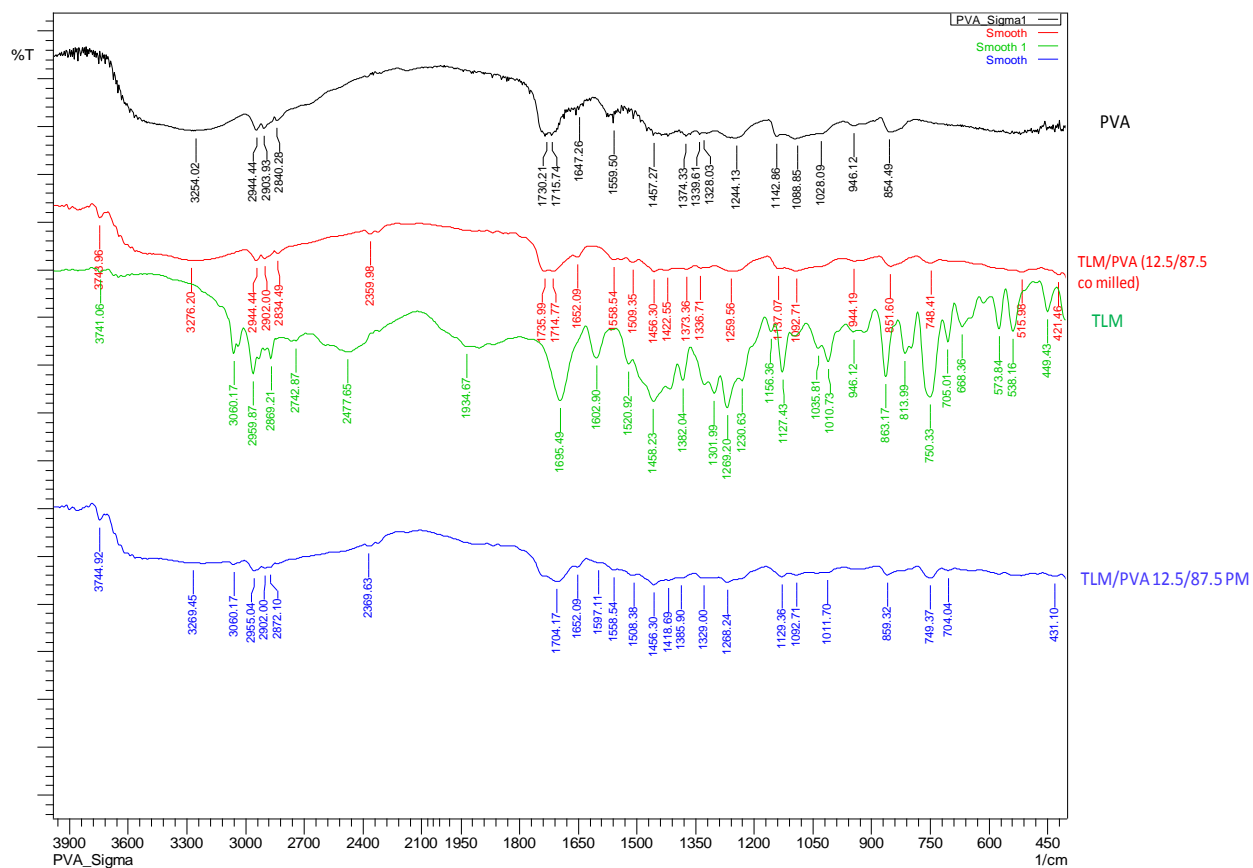
Fig. 8 FTIR spectra of TLM, PVA, Physical mixture of TLM/PVA and Co grinded mixture

Key findings from the completed work

The cogrinding of TLM with PVA showed higher rate of drug dissolution than "TLM alone" grinding. Tablets prepared from grinded mixture of TLM/PVA in a weight ratio of 12.5/87.5 (BPR 15:1, RPM 600, and Time 3hrs) and 25/75 (BPR 15:1, RPM 600, and Time 5hrs) showed improved dissolution (>75% in 45 minutes) of TLM in phosphate buffer pH 6.8 (37°C, RPM 75).

References

1. Shargel L. *Applied Biopharmaceutics and Pharmacokinetics*, 5th edn. Newyork: McGraw Hill, 2005

2. Amidon GL, Lennernäs H, Shah VP, Crison JR.A theoretical basis for a biopharmaceutic drug classification: the correlation of in vitro drug product dissolution and in vivo bioavailability. *Pharm Res.* 1995 12(3):413-20.

3. Pius Fasinu, Viness Pillay,Valence M. K. Ndesendo, Lisa C. du Toit, and Yahya E. Choonara, Diverse approaches for the enhancement of oral drug bioavailability, *Biopharm. Drug Dispos.* (2011)32: 185–209.

4. Martin. A, Micromeritics, *Physical Pharmacy*, Baltimore,MD; Lippincott, Williams and Wilkins; 2001Edtn-4th: 423-454.

5. G.G. Liversidge, K.C. Cundy, Particle size reduction for improvement of oral bioavailability of hydrophobic drugs: absolute oral bioavailability of nanocrystalline danazol in beagle dogs, *Int. J. Pharm.,* 125 (1995), pp. 91–97.

6. A. Jounela, P. Pentikainen, A. Sothmann,Effect of particle size on the bioavailability of digoxin*, Eur. J. Clin. Pharmacol*., 8 (1975), pp. 365–370.

7. A.G Baily,Electrostatic phenomena during powder handling, *Powder Technol*. 37 (1984) 71-85.

8. Barzegar-Jalali M, Valizadeh H, Shadbad MS, Adibkia K, Mohammadi G, Farahani A, et al. Cogrinding as an approach to enhance dissolution rate of a poorly water-soluble drug(gliclazide). *Powder Technol.* 2010; 197:150–8.

9. Colombo I, Grassi G, Grass M. Drug mechanochemical activation. *J Pharm Sci.* 2009; 98(11):3961–86. doi:10.1002/jps.21733.

10. Gibaldi, M. & Feldman, S. , *J Pharm Sci. 59*, 579–589 (1970).

11. Corti G, Capasso G, Maestrelli F, Cirri M, Mura P. Physical–chemical characterization of binary systems of metformin hydrochloride with triacetyl-β-cyclodextrin. *J Pharm Biomed Anal.*2007; 45:480–6. doi:10.1016/j.jpba.2007.07.018.

12. D.Bahl, J Hudak, R.H Bogner, Comparison of ability of various pharmaceutical silicates to amorphize and enhance dissolution of indomethacin upon co-grinding, *Pharmaceutical Development and Technology*. 13 (2008) 255-269.

13. L.Zhong, X. Zhu, X. Luo, W.Su, Dissolution properties and physical characterization of TLM-chitosan solid dispersions prepared by mechanochemical activation, *AAPS Pharm SciTech,* 2013 doi:10.1208/s12249-013-9937-1

14. M. Barzegar-Jalali, H. Valizadeh, M.S. Shadbad, K.Adibkia, G. Mohammadi, A. Farahani, Z. Arash, A. Nokhodchi, Cogrinding as an approach to enhance dissolution rate of a poorly water-soluble drug (gliclazide), *Powder Technol.* 197 (2010) 150-158.

15. A.G Baily,Electrostatic phenomena during powder handling, Powder Technol. 37 (1984) 71-85.

16. Colombo I, Grassi G, Grass M. Drug mechanochemical activation. *J Pharm Sci.* 2009; 98(11):3961–86. doi:10.1002/jps.21733.

17. Corti G, Capasso G, Maestrelli F, Cirri M, Mura P. Physical–chemical characterization of binary systems of metformin hydrochloride with triacetyl-β-cyclodextrin. *J Pharm Biomed Anal.*2007; 45:480–6. doi:10.1016/j.jpba.2007.07.018.

18. D.Bahl, J Hudak, R.H Bogner, Comparison of ability of various pharmaceutical silicates to amorphize and enhance dissolution of indomethacin upon co-grinding, *Pharmaceutical Development and Technology.* 13 (2008) 255-269.

19. Dushkin AV. Mechanochemical synthesis of organic compounds and rapidly-soluble materials. High-energy ball milling: mechanochemical processing of nanopowders. Cambridge, UK: Woodhead Publishing Limited; 2010. p. 224–47.

20. L.Zhong, X. Zhu, X. Luo, W.Su, Dissolution properties and physical characterization of TLM-chitosan solid dispersions prepared by mechanochemical activation, *AAPS Pharm SciTech*, 2013 doi:10.1208/s12249-013-9937-1

21. M. Barzegar-Jalali, H. Valizadeh, M.S. Shadbad, K.Adibkia, G. Mohammadi, A. Farahani, Z. Arash, A. Nokhodchi, Cogrinding as an approach to enhance dissolution rate of a poorly water-soluble drug (gliclazide), *Powder Technol*. 197 (2010) 150-158.

22. J.C. Chaumeil,Micronization: a method of improving the bioavailability of poorly soluble drugs , *Exp. Clin. Pharmacol*, 20 (1998), pp. 211–215

23. Klaus Kunath b, Jennifer B. Dressmana, Dissolution enhancement of fenofibrate by micronization, cogrinding, *European Journal of Pharmaceutics and Biopharmaceutics* 68 (2008) 283–288.

WHETHER OBJECTIVES WERE ACHIEVED (GIVE DETAILS)

The objectives were achieved as proposed in project proposal.

The objective was to improve the rate of dissolution of poorly water soluble drug molecules to achieve improved bioavailability.

Two methods were applied to achieve the objective namely corytallization and co-milling. Both methods were environmental friendly and the scale up is also easy. The choice of drugs were ezetimibe and telmisartan. Both drugs are under the BCS II group of drugs. They have low solubility and high permeability. Therefore, rate limiting step of their bioavailability is in-vivo dissolution. Ultimately, for both drugs the rate of dissolution *viz.* bioavailability was improved with reference to the conventional dosage form.

SUMMARY OF THE FINDINGS (IN 500 WORDS)

The present study illustrated the formation and characterization of three different cocrystals of ezetimibe using methyl paraben as a coformer, employing three different processes, namely solution crystallization, liquid assisted grinding and reaction crystallisation. DSC result shows that the entirely different peak melting temperature was observed in all three cocrystals indicating the formation of new solid phase. FTIR and Raman spectroscopy study reveals that the new solid form is the result of weak electrostatic interaction between drug and coformer. From PXRD study, it is clear that the crystal habit of both the drug and the coformer has been modified. Equilibrium solubility study and dissolution study of the cocrystals reveals that the cocrystals of ezetimibe and methyl paraben can a possible and potential alternative and effective approach for improving its solubility.

Particle size reduction of TLM by neat milling results in clustering/aggregation of particles. The hydrophobicity of the milled TLM makes it difficult to dissolve effectively in an aqueous environment. Co-milling of TLM with PVA, a hydrophilic polymer resulted in an effective particle size reduction, absence of clustering and improved the wettability of TLM. The physical changes of the comilling product of TLM were found to depend on D/P ratio and the process parameters used. The dissolution profiles of the final optimized products (CG 1 and CG 2 tablets) were comparable to those of dissolution profile of the reference product (Micardis). Crystalline and amorphous form of TLM was present in CG1 whereas in CG2 disordered crystals of TLM were present in addition. Therefore, it was unstable under accelerated stability test conditions. The bioavailability of CG 1 tablet in rabbits was comparable to that of the reference product (Micardis)). Absence of use of any of the corrosive chemical agent/s in the formula, ensured the gastro-environmental friendliness of the product. As well as, comilling being a simple and environment friendly particle engineering feat, this technique has to draw more attention from pharmaceutical formulation scientists from around the world who are striving hard to improve the dissolution of BCS class II drugs by particle engineering.

CONTRIBUTION TO THE SOCIETY (GIVE DETAILS)

Most of new drug molecules are showing poor water solubility. Hence to achieve the therapeutic concentration there is a need to administer high dose which definitely cause dose related toxicity. Therefore, total medication cost will be high. By increasing the water solubility, required therapeutic concentration may be achieved by administering low dose which ultimately reduce total medication cost which is the ultimate contribution to the society.

PLANETARY MICRO MILL

MODEL: PULVERISETTE 7

MAKE: FRITSCH, GERMANY

Dissolution tester USP

Model: TDT-08L

Make: Electrolab, Mumbai, India